STRUCTURE-PROPERTY CORRELATION ON SIMILAR AND DISSIMILAR FRICTION STIR WELDED MAGNESIUM-BASED ALLOYS

A dissertation work

Submitted in partial fulfilment of the requirements

for

the award of the degree of

DOCTOR OF PHILOSOPHY

in

METALLURGICAL AND MATERIALS ENGINEERING

by

KADIGITHALA. N. B. KUMAR
(Roll No.701251)

Under the guidance of

Dr. C. Vanitha
Associate Professor

DEPARTMENT OF METALLURGICAL AND MATERIALS ENGINEERING
NATIONAL INSTITUTE OF TECHNOLOGY WARANGAL
WARANGAL-506 004 (T.S) INDIA

OCTOBER – 2020

THESIS APPROVAL FOR Ph.D.

This thesis entitled **"Structure- property correlation on similar and dissimilar friction stir welded magnesium-based alloys"** by **Kadigithala. N. B. Kumar (Roll No.701251),** is approved for the degree of Doctor of Philosophy.

Examiner

(Prof. S.P. Kumaresh babu)
Department of Metallurgical and Materials Engineering
National Institute of Technology, Tiruchirappalli.

Supervisor

Dr. C. Vanitha
Associate Professor,
Department of Metallurgical and Materials Engineering,
NIT Warangal

Chairman

Dr. Asit Kumar Khanra
Associate Professor,
Head of the Department,
Department of Metallurgical and Materials Engineering,
NIT Warangal

Date: 28th April 2021.

DEPARTEMENT OF METALLURGICAL AND MATERIALS ENGINEERING

NATIONAL INSTITUTE OF TECHNOLOGY,

WARANGAL, TS, INDIA – 506004

CERTIFICATE

This is to certify that the dissertation work entitled **"Structure- property correlation on similar and dissimilar friction stir welded magnesium-based alloys"** which is being submitted by **Mr. Kadigithala. N. B. Kumar (Roll No.701251)**, is a bonafide work submitted to the Department of Metallurgical and Materials Engineering., National Institute of Technology, Warangal in partial fulfillment of the requirement for the award of the degree of **Doctor of Philosophy** in **Metallurgical and Materials Engineering**.

To the best of our knowledge, the work incorporated in this thesis has not been submitted elsewhere for the award of any degree.

Dr. C. Vanitha
Associate Professor and Thesis Supervisor
Department of Metallurgical and Materials Engineering
National Institute of Technology
Warangal- 506004

Dr. Asit Kumar Khanra
Head, Department of Metallurgical and Materials Engineering
National Institute of Technology
Warangal-506004

DECLARATION

I hereby declare that the work described in this thesis, entitled **"Structure- property correlation on similar and dissimilar friction stir welded magnesium-based alloys"**, which is submitted by me in partial fulfillment for the award of **Doctor of Philosophy (Ph.D.)** in the Department of Metallurgical and Materials Engineering, National Institute of Technology, Warangal (T.S) – 506004, is the result of investigation carried out by me under the guidance of **Dr. C. Vanitha**, Associate Professor in the Department of Metallurgical and Materials Engineering, National Institute of Technology, Warangal. The work is original and has not been submitted for the award of any Degree/Diploma to any other university.

Place:

Date: Signature:

Name of the candidate: **K. N. B. Kumar**

Roll No.: 701251

Dedicated

to

My beloved parents…

Late **Sri. K. Venkata Raju & Smt. Vijya Bharathi**

My wife…

Madhulatha, for her love and support…

My son…

Bharat, for his innocence, faith and kindness..

ACKNOWLEDGEMENT

I am thankful to **almighty God**, for all his love, care, blessings and making his path in my life to execute his will in my life. I would like to express my sincere thanks to my supervisor **Dr. C. Vanitha,** Associate Professor, Department of Metallurgical and Materials Engineering, National Institute of Technology, Warangal for her valuable guidance throughout the research work.

I am grateful to **Prof. N.V. Ramana Rao**, Director, NIT Warangal who has been constant source of inspiration for me. My heartfelt thanks to **Dr. Asit Kumar Khanra,** Head, Department of Metallurgical and Materials Engineering for his help and continuous encouragement to complete this work. I would like to express my sincere thanks **Prof. GVS Nageshwara Rao, Dr. T. Mahesh kumar,** MMED and **Dr. J. Davidson,** MED, learned members of my Doctoral Scrutiny Committee for being helpful and generous during the entire course of this work. I also thank **Prof. Mantravadi Krishna Mohan,** (Former DSC member) for providing his valuable suggestions in support to my Ph.D. I am also thankful to the teaching and non-teaching faculty members of the Department of Metallurgical and Materials Engineering of NIT, Warangal.

Also, my sincere thanks to **Dr. Y. Raghupathy,** MMED who has guided me to pursue my objectives of my research work.

I wish to thank **Prof. Vivek Pancholi, MMED, IIT Roorkee** for permitting me to carrying out the experimental work and use the testing facilities available at **IIT Roorkee**.

Words are inadequate to express my thanks to all my family members, my father Late **Sri. Venkata Raju**, mother **Smt. Vijya Bharathi,** Sister **Smt. Aruna priya,** especially to my wife **Madhulatha,** son **Bharath Bhushan Raj** deserve special mention of appreciation for exhibiting patience during this long and arduous journey.

Finally, I am extremely thankful to my friends and well-wishers whose list cannot be quoted, for extending their co-operation in successful completion of this work. Without their support, it would have been simply impossible.

I want to express my sincere thanks to all those who directly or indirectly helped me at various stages of this work.

K. NAGABHUSHAN KUMAR

ABSTRACT

Magnesium alloys are mostly used in the automotive industry due to its light weight and applicable for structural applications. Higer fuel economy and pollution control, weight reduction in the transportation sector are the main step to be focused. Since Mg alloys have unique properties, it proved to be the potential source to replace Al alloys in various structural applications. Mg alloys are having low density, high strength to weight ratio and good castability. It is lightest engineering metal having density (1.74g/cm^3) 35% less than aluminum (2.7 g/cm^3) and it is 4 times lighter than steel (7.85 gm/cm^3).

Because of its properties, it is proved as advanced materials for conservation of energy and pollution regulation in environment. The major drawback of Mg based alloy as structural application is its high chemical reactivity leading in many cases to a low welding characteristics and corrosion resistance. However, the welding of Mg alloys is limited which can be crucial for these applications. In order to explore the application of Mg alloys, more efficient welding and joining techniques are needed. Mostly, tungsten inert gas (TIG) and metal inert gas (MIG) methods are main welding techniques for magnesium alloy castings. Mg alloys are highly chemical reactive at moderate temperature which leads to oxidation in welding zone and high inflammability. Because of which conventional fusion welding methods result in Mg alloys. In 1991, friction stir welding (FSW) was introduced which has emerged as a potential tool to join similar and dissimilar metals. FSW completely eliminates the difficulties related to solidification defects (cracks, porosity, evaporative loss, etc.,) which generally appears in fusion welding, because it doesn't melt the base metals. The conventional fusion welding process in which hot cracking is associated can be eliminated completely by FSW. In FSW process, flow pattern of the material and temperature distribution in weld zone is greatly influenced by weld parameters, tool profile and design of the joint; hence affecting the microstructure of the metal.

FSW produces good quality of welds as it doesn't require any filler material which eliminates metallurgical issues.

In the present study microstructure developed during friction stir welding process of Mg cast alloys, and the optimum welding parameter to produce the defect free weld having optimum mechanical properties and the corrosion resistance of friction stir welded weldments has been investigated. As-cast sheets of AZ91 Magnesium alloy to AZ91 Magnesium alloy (Similar welding) as well as AZ31 Magnesium alloy to AZ91 Magnesium alloy (Dissimilar welding) plates of 3mm thickness are joined using Friction stir welding (FSW) technique since there are only limited investigations on FSW of similar and dissimilar Magnesium based alloys. Process parameters were chosen carefully in order to attain defect-free welds. Rotational speed varied from 500 to 1025 rpm and the process parameters like tilt angle, weld speed were varied from 1.5° to 2.5° and 25 to 75mm/min respectively. The microstructure of the AZ91D (gravity die cast) and AZ31 Mg alloy consists of primary α-phase and secondary β ($Mg_{17}Al_{12}$) phase were also been confirmed by X-ray diffraction (XRD) analysis. The initial microstructure present in the alloys completely refined, and was transformed to fine grains in stir zone (SZ) due to dynamic recrystallization. A sharp interface was clearly noticed between SZ and thermo mechanical affected zone in AZ91 Mg alloy side (advancing) of dissimilar weldments. The AZ31 and AZ91 Mg alloys, joined by FSW, exposed that the welding speed had a direct influence on the weld nugget microstructure, where the size of nugget zone increased with reduction in the weld speed and enhancement of deformation is subjected to widening of friction stir zone. In stir zone displayed an ultrafine grain structure of an average grain size ranging from 7-21µm. Microstructural studies, tensile, impact, hardness test, and potentiodynamic studies were carried out to correlate microstructure, mechanical and corrosion properties. Taguchi statistical data analysis technique was used to optimize the rotational speed, traverse speed, and tilt angle to obtain the optimum combinations of process parameters for achieving the good mechanical properties. Analysis of variance (ANOVA) was carried out to find the significance of each process parameter on the quality characteristics. Additionally, regression models have been developed for predicting the mechanical properties. The predicted values are in good compliance with experimental results within the selected range of process parameters. Metallographic studies of each zone revels different features depending on the thermal and mechanical conditions. It was observed that there was a significant increase of hardness in SZ,

because of fine recrystallized grain structure and dissolution of aluminum content. During the tensile test, the strength and ductility of the welded specimen was raised impressively when compared to the base metal with varying welding speed. Fractrographic examination indicates that the welded specimens undergoes brittle fracture. Corrosion studies were carried out in 3.5% NaCl environment. The polarization curves emerged from the weld zones of similar and dissimilar weldments showed an improved corrosion resistance compared with the parent alloys. However, AZ91 Mg alloys showed low corrosion resistance when compared to AZ31 Mg alloy due to larger volume fraction of β-phase present in AZ91 alloy which is low in case of AZ31 Mg alloy. The results show that parent metals (AZ31 Magnesium alloy, AZ91 Magnesium alloy) and weldments underwent localized corrosion and the second phase particles which formed galvanic couples with the matrix are the sources of localized corrosion.

CONTENTS

LIST OF TABLES

Chapter 6 - Corrosion Behavior of Similar AZ91 / AZ91 Mg Alloy Weldments and Dissimilar AZ31 / AZ91 Mg Alloy Weldments

LIST OF FIGURES

Chapter 5 - Friction Stir Welding of AZ91-AZ31 Dissimilar Alloy

Chapter 6 - Corrosion Behavior Of Similar AZ91 / AZ91 Mg Alloy Weldments and Dissimilar AZ31 / AZ91 Mg Alloy Weldments

NOMENCLATURE

SEM	: Scanning electron microscopy
EDX/EDS	: Energy dispersive X-ray spectroscopy
EBSD	: Electron backscattered diffraction
XRD	: X-ray diffraction analysis
FSW	: Friction stir welding
FSP	: Friction stir Processing
SZ	: Stir zone
TMAZ	: Thermo-mechanically affected zone
HAZ	: Heat affected zone
DRX	: Dynamic recrystallization
ANOVA	: Analysis of variance
UTS	: Ultimate tensile strength
%EL	: Percentage of elongation
IS	: Impact strength
DF	: Degree of freedom
ASS	: Adj. Sum of squares
AMS	: Adj. Mean squares
S/N	: Signal to noise ratio
Ecorr	: Free corrosion potential
Icorr	: Corrosion current density
Epit	: Pitting potential

CHAPTER − 1

INTRODUCTION

1. 1 Magnesium and its Alloys

Magnesium and its alloys have been attractive to designers because of its high specific strength in the automotive and aerospace sectors. Its density is only 2/3rd that of aluminium alloys. Magnesium stands in the eighth position in the list of elements which are available abundantly in nature. Literature survey reveals that magnesium occupies 2% of the earth's crust and is 3rd major constitute element present in seawater, with a congregation approximately about 0.13%. Though Magnesium can be obtained in more than 60 minerals, few minerals like Magnetite, carnallite, brucite, olivine and dolomite are of industrial significance. Mg and Mg components are also generated through well water, seawater and bitterns and lake brines [1].

Magnesium being low in the density of 1.74 gm/cc play a vital role as constructional material in an alloyed state, and a majority of Mg alloys have a little greater density than pure Mg. Mg is a flammable element and is habitually obtained in eco-system as oxide phase, silicate or carbonate and in integration with calcium. An enormous quantity of energy is required for extraction of Mg metal, the reactivity of Mg being one of the crucial reasons. Lightweight transforms into higher fuel efficacy, creating components out of Mg is highly interesting to the automobile business. These less-weighed components come by providing the components superior dent and resistance to impact and resistance to fatigue. Mg further manifests superior high-speed machinability and great electrical as well as thermal conductivity [2]. Mg alloys are a combination of Mg with additional metals commonly Zn, Al, Mn, Cu, Si, Zr and rare earth

elements. Mg alloys structure is a hexagonal lattice that influences the basic characteristics of these alloys. Hexagonal lattice's plastic deformation is immensely complex relative to cubic-latticed elements such as Steel, Al and Cu. Hence, Investigations on Mg alloys in wrought form has been studied massively since 2003 and Mg alloys were widely used as-cast alloys. Cast Mg alloys were used in making parts of new generation cars, and Mg engine blocks had been utilized in few superior-performance transporters; die-cast Mg is additionally utilized in bodies of camera and parts in lenses [2].

Pure Mg has immensely weak mechanical properties. Pure Mg should be mixed with various metals that provide enhanced characteristics. Al and Zn are being used individually or in combination to enhance the properties of Mg. These are major frequently mixing metals for ambient temperature employments. Zirconium, Thorium and cerium (absence of Al) are utilized for greater temperatures and create the Mg-Zn-Zr class. Cerium and Thorium are mixed to enhance strength at the temperatures ranging in between 260 – 370OC. Al is the major constituent in enhancing outcomes. As lesser as about 2 – 10 % of Al with very little mixing of Mn and Zn enhances strength and hardness at the expenditure of lesser ductility, without improving weldability and creating the alloy heat-treatable [3].

Alloys of Mg comprising greater than 1.5% Al are liable to influence of stress corrosion and should be relieved from stress in post-weld heat treatment. Ni, Fe and Cu are considered as pollutants because they reduce the resistance of Mg alloys towards corrosion. Zn mixed with Al suppresses dreadful corrosive impacts of Ni and Fe pollutants, which may be available in Mg alloys. The greater Zn present (above 1%), the greater will be hot shortness results weld cracking. Mn enhances yield strength and the resistance to the saltwater of Mg alloys [4].

1. 2 Alloy Designation System

Alloys of Mg are traditionally termed based on method founded through ASTM (American Society of Testing Materials) that comprises both tempering parameters as well as elemental compositions. In preliminary system, that is part 1: shows the two main additional metals and comprises of double code letters presenting both principal, additional metals (or alphabetically if concentrating metals are organized in are same). Part 2: displays the quantity of both the main

metals and comprises of both whole numbers equivalent to the alphabet. Part 3: It comprises of anyone of the succeeding characters: A-preliminary composition, B-secondary composition, C-Ternary composition authenticated through ASTM, D-Superior purity, and E-Superior resistance to corrosion. Part 4: manifests the temper parameters [5].

1. 3 Merits of Magnesium Alloys

Magnesium alloys possess the advantage of opening new intricate, space-efficient design possibilities in many markets. Some of the notable advantages of the Mg alloys are listed below:

i. Majority of the Mg Alloy components are 76% lighter than steel and 34% lighter than aluminum.
ii. Mg alloys have high specific strength and possess superior dimensional stability [4].
iii. Enclosures & housings fabricated using Mg alloys are found to be electrically conductive and provide enhanced EMI shielding without using plating, conductive paints or fillers [2].
iv. All the Magnesium alloy parts & components can be recycled completely.
v. Higher Production rates are possible with Mg alloys. Depending on their configuration & size, Mg components can be cast up to 48% faster than the same components composed of aluminum [6].
vi. Casting of thin walled parts and complex components will be easy in case of Mg alloys as they possess high fluidity.
vii. In Mg alloys, there is an increase in the stiffness, durability and strength. They also exhibit improved impact response [7].
viii. Magnesium alloys have a desirable & low volumetric specific heat compared with alloys of aluminum and zinc, which allows Mg castings to get cooled very quickly, thereby leading to faster cycle times.
ix. Mg alloys have low affinity for iron & their low heat content reduces the effect of die erosion and thermal fatigue. Therefore, Mg alloy dies last for more cycles (two to three times compared with Al dies). [8].

1. 4 Drawbacks of Magnesium Alloys

Magnesium alloys are also found to possess a little amount of drawbacks. Some of the drawbacks of the Mg alloys are listed below:

i. Mg alloys are found to be difficult to deform by a cold working process.
ii. Cost of the Mg alloys is high.
iii. Mg alloys have a low value of elastic modulus.
iv. Mg alloys do not have a preferable value of toughness.
v. Creep resistance at elevated temperatures for Mg alloys is less.
vi. Major issue with Mg alloys is they prone to galvanic corrosion, as they come in contact with other metals and immersed in an electrolyte to make a circuit. [9].

1. 5 Applications of Magnesium Alloys

Mg and Mg alloys are employed in numerous non-structural and structural applications. Structural applications include truck parts, automobile, material-handling, aerospace components and industrial. The automobile applications include brake pedal-assist brackets and clutch, steering column lock housing and manual transmission housings. In manufacturing machinery like printing and clothing machines, Mg alloys are utilized for components that work at enormous speeds. Therefore it must be of lesser weight in order to diminish inertial forces. Components-handling machines include grain shovels, dock boards, and gravity conveyors. Mass scale usage includes luggage, hand-held tackles, ladders, and computer housings. Mg alloys are precious for aerospace implementations due to their lesser weight [1].

1. 6 Weldability of Magnesium Alloys

Magnesium alloys can be welded using the various techniques of resistance and arc welding processes. Mg alloys can also be joined using gas welding technology. Based on the requirement and area of application, Mg alloys are manufactured with various tempers, which depend on the work hardening and heat treatment methods [10]. Mg alloys welded using

conventional welding techniques; the welded portion loses its strength due to the growth of grains in the heat-affected zone and recrystallization [11].

Welding of Mg and its alloys is easy when compared to steels because of their properties. Some of them are listed below.

i. Low melting temperature and high thermal conductivity.
ii. Absence of change in colour when the melting point temperature is reaching.
iii. High coefficient of thermal expansion.

Some alloys of magnesium are subject to corrosion resulting from stress. The weldments subjected to corrosive attack over a period of time normally tend to develop cracks adjacent to the welds [12].

High corrosion, strong cracking susceptibility and large energy consumption are the main properties, are the limiting factors for joining the Mg alloys by Conventional welding processes. Hence the conventional welding processes are suggestible [13]. Since the selection of the welding process for joining magnesium alloys play a vital role in the field of their application in structural components, extra care should be taken while selecting the technique.

1. 7 Organization of the Thesis

The thesis consists of seven chapters. The chapter-wise introduction is given in brief below.

Chapter 1 represents the introduction to magnesium and welding of the magnesium alloys and objective of the present work.

Chapter 2 deals with a comprehensive literature review and scope of present work.

Chapter 3 deals with the experimental details covering a range of aspects namely materials, equipment used, selection of tool pin profiles, sample preparation and experimental work-chart and provide the experimental design and Taguchi method covering the aspects of experimental design, process parameters and pilot experiments.

Chapter 4 represents results, and discussion part provides the influence of process variables, microstructure on similar AZ91 / AZ91 Mg alloy weldments and detail explanation

of outcomes from the experiments carried out.

Chapter 5 represents the influence of process variables, microstructure on dissimilar AZ31 / AZ91 Mg alloy weldments and detail explanation of outcomes from the experiments carried out.

Chapter 6 represents the corrosion behaviour of similar AZ91 / AZ91 Mg alloy weldments and dissimilar AZ31 / AZ91 Mg alloy weldments.

Chapter 7 deals with overall conclusions based on the results of chapters 4, 5 & 6 and this chapter also describe the scope for future work.

CHAPTER − 2

LITERATURE

2. 1 Friction Stir Welding - Principle

Welding is a fabrication technique that joins materials, typically metals or thermoplastics, by causing high heat to weld the pieces together to create the physical bond. Welding can be classified into two types [12]. Primarily as fusion welding that fuses the boundary of an element to the liquid phase, later on, condenses for joining of the materials. Numerous welding processes of fusion welding type are tungsten inert gas arc welding, laser beam welding, shield metal arc welding, electron beam welding, etc. [12]. Secondarily, solid-phase welding that heats the material above the recrystallization temperature or plasticizing phase (not beyond the melting point), later on by implying pressure to combine both the materials by quick diffusion at high temperatures. Fusion processes regularly have eutectic phases and frequently exposed to pores that affect the final characteristics of the joining process. Additionally, the fusion process further dissolves the precipitates in the main matrix and reduces the actual strength by reinforcing materials from precipitation [12].

Friction Stir Welding is one among the solid-state welding processes. It was innovated at TWI (The Welding Institute) and got patented in 1991 by TWI Ltd. of Cambridge, England [14]. It emerged as an extremely popular joining process for welding non-ferrous based metals such as Cu, Al and their alloys. Joining occurs below the solidification temperature of the welded material. FSW results not only a superior quality with high strength but also cost-

effective. During the process, non-generation fumes were additional predominant features of FSW and energy-efficient.

FSW did not require any filler compound like conventional welding methods and relatively easy to do. Processing speeds can be controlled by securing the work sample tightly. In addition, the process eliminates the unwanted intermetallic phase formation, which may have an impact on the properties of the joint or welded portion and efficiency. Also, the FSW process did not allow the formation of any kind of imperfections, such as porosity. It is, therefore, possible to use FSW comfortably to weld copper and its alloys [15].

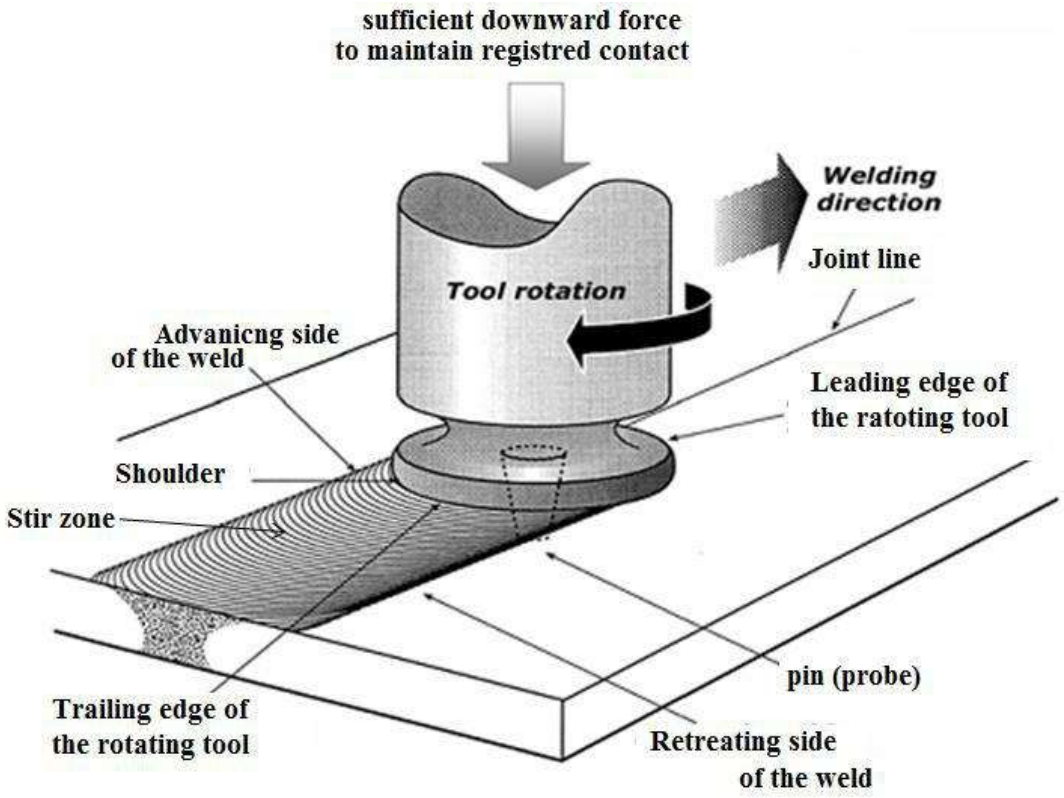

Figure 2.1 Schematic sketch of FSW process [16]

FSW is an imitative method of traditional friction welding techniques. It provides the benefits of solid-state welding for generating lengthy butt as well as lap joints [17]. In this method, a revolving tool pin which is non-consumable having good wear-resistant gets stuck inside the space between the two specimens, which are being joined. The shoulder creates a rigid connection with a top facet of the work specimen in such a way that heat is produced through the tool shoulder due to the friction. The heat generated through the friction softens the

metal surface and push the tool to go forward along the weld center region [18]. The metal gets plasticized and moved across the joining line [19]. FSW was very much preferable for butt welds, as an extent of the pin approximation to the weld specimen thickness. The FSW process schematics is shown in Figure 2.1.

2. 2 Advantages of FSW Process

i. Compared to traditional fusion welding techniques, the FSW method has numerous advantages highlighted below [20 – 22].
ii. FSW methods did not utilize any filler material. Rather, a steel-based machine is needed to weld aluminum alloys. For Aluminum, before swapping it with a new tool, the tool may enter up to 1 kilometer.
iii. During the FSW method, imperfections such as porosity and hot cracking are not seen as melting and phase transformation (i.e. liquid to solid) did not occur in the stir zone.
iv. As it generates very low heat during the welding process, the joint produced by the FSW technique shows superior mechanical characteristics compared to traditional fusion joined materials. In addition, the FSW technique produces fine, equiaxed recrystallized grains.
v. The FSW method was eco-friendly. For instance, neither fumes nor spatters are generated during the process. Usage of shielding gas is also not required as well.
vi. Normally, the welds generated through FSW technique possess a quality appearance. Therefore, capping (extra weld) is not required. Hence, after weld processes such as machining, grinding was not required for the elimination of extra weld metal, sparks, and fluxes.
vii. The FSW process creates a very minute distortion of the part after joining and can be carried out in all welding positions.

2. 3 FSW Parameters

The importance of process parameter is explained below.

2. 3. 1 Rotational Speed (W)

The rotational speed mainly influences the mixing of two alloys by producing sufficient heat to sweep the deformed material from advancing side to retrieving side during the welding process.

2. 3. 2 Welding Speed (V)

Welding speed mainly influences the time the alloy is exposed to high temperature. Low welding speeds provides an increase in the heat input because of the rotating tool being subjected to more contact time with the materials, thereby generating more heat.

Numerous investigations had been taken up to scrutinize the outcome of joining speed and probe rotation upon the weldability of alloys specifically of Mg. These both criteria are crucial to produce superior quality joints because they directly control the energy input and transfer of plastic metal. The energy input per unit extent is given by

$$\text{Heat input} = Q / V$$

Where Q is Energy produced by friction and V is Speed of welding.

The energy produced by friction rises with the probe's rate of rotation, however not in the monotonic path because of the co-efficient of friction at interlock also differs with probe's rate of rotation. Thence, escalating probe's rotation rate or de-escalating joining speed impels a greater temperature, effortless transfer and improves the weldability. This observation was uniform with each and every investigation undertaken previously [23, 24].

Investigations were manifested that, for a uniform joining speed, a reduced probe's rotation rate guides to the generation of internal voids cause the frictional energy was not enough to encourage material transfer. These imperfections can be eliminated with escalating the probe's rotation rate (W). At extremely high probe rotation rates, interior imperfections, a

lacuna of bonding and facet fissures commenced a cause of extra expulsion of the metal produced [25].

Investigations carried out at a uniform probe rotation rate displayed that escalating joining speed caused in interior imperfections and lacuna in bonding resulted in not enough metal transfer. Yan et al. [26] noticed that a lesser joining speed can give regulated dynamic recrystallization encouraging fine grain microstructure.

Gharacheh et al. [27], utilized the weight by volume ratio as operation criteria, noticed that escalating the ratio tends to an advancement in the energy input, an enhanced metal transfer and an extended and deeper joint nugget. The hardness escalated with escalating traverse speed. Increasing traverse speed over a critical value was noticed to decrease the ultimate tensile strength (UTS), whereas the yield strength was kept constant.

Gharachehet. al. noticed that escalating the W/V ratio resulted in a de-escalation of tensile properties. Escalating the probe rate of rotation results in an increase in strength especially tensile strength [28]. Increase in traverse speed over a critical value results in decreasing the ultimate tensile strength (UTS), whereas the yield strength was observed to be unchanged.

For FSW of Mg alloys, modern investigations demonstrated that the weld quality was sensitive to the rate of rotation of the probe and traverse speed. Nakata et al. [29] manifested that the FSW of square butt was carried out flourishingly by utilizing a narrow scale of FSW criteria that was huge probe's rates of rotation and reduced traverse speeds. Larger probe traverse speeds and lesser rates of rotation than that of optimum criteria permitted origination of interior imperfections cause of lacuna in bonding. FSW of Mg alloy has been found better between 800 to 1600 rpm probe rotation rate and 50 to 500 mm/min [30 – 33].

2. 3. 3 Tool Tilt Angle

Tilt angle is the angle at which the tool is positioned against the work surface. The tool is located perpendicular to the work surface at a zero-degree tilt angle. When the tilt angle is small, it affects the welded blank properties by creating a gap between the tool and the blanks that can make it easier to sweep the material away from the tool's shoulder. The tool's forging force

allows the homogenized material flow in the weld region resulting in better weld zone properties. The gap increases as the tool tilt angle increases. The deformed material thus easily escapes from the shoulder of the tool and results defects in the weldment. Therefore, choosing the optimum tilt angle is very important.

A satisfactory angle of tilt for probe must be chosen for optimum productivity of the probe. It predominantly relies on the geometry of the shoulder. It's traditionally set to 3° for plain shoulder , further altered up to 1.5° for a concave shoulder and 0° to 1° for scroll shoulder [34].

2. 3. 4 Welding Pressure

Zhang et al. [35] investigated the impact of the joining pressure at constant tool travel speed and rotation speed. The joining pressure was noticed to influence the heat generated due to friction. Raising the joining pressure rapidly led to the superior welds, whereas, the low pressure resulted in pores [35].

2. 3. 5 Insertion Depth

The depth of insertion has to be regulated, mostly while utilizing the even probe shoulders. If it's very deep, an enormous quantity of flash was generated, tending to a local thinning of the joined plates, because the shoulder perforates through the metal. Whereas the depth of insertion was very less, there was no touch in between the shoulder and the specimen facet that hinders full mixing and creates facet groove origination [36].

2. 3. 6 Preheating or Cooling

The materials with a higher melting point like Ti, Steel, or high thermal conductivity like Cu, should be preheated primarily, as the energy generated by the operation might not be enough. Cooling might be helpful to avoid grain enlargement and dissolution of precipitates while joining materials of lesser melting points like Mg and Al [37].

It has been observed from the literature that of the tool rotational speed, welding speed and tilt angle of the tool is considered to be predominant in improving the properties of weld joints.

2. 4 FSW Microstructure Classification

The preliminary studies in categorizing microstructure were examined and explained by PL Threadgrill [38]. The investigation was built entirely upon data obtained through alloys of aluminum. FSW was invented at TWI, but had been scrutinized among numerous suitable personnel in academia as well as industry, further had also been temporarily undertaken with FSW Licenses Association. Threadgrill had divided weld region into 4 regions based on microstructure that is base metal (BM), heat affected zone (HAZ), thermo-mechanical affected zone (TMAZ), and stir zone (SZ) and is shown in Figure 2.2.

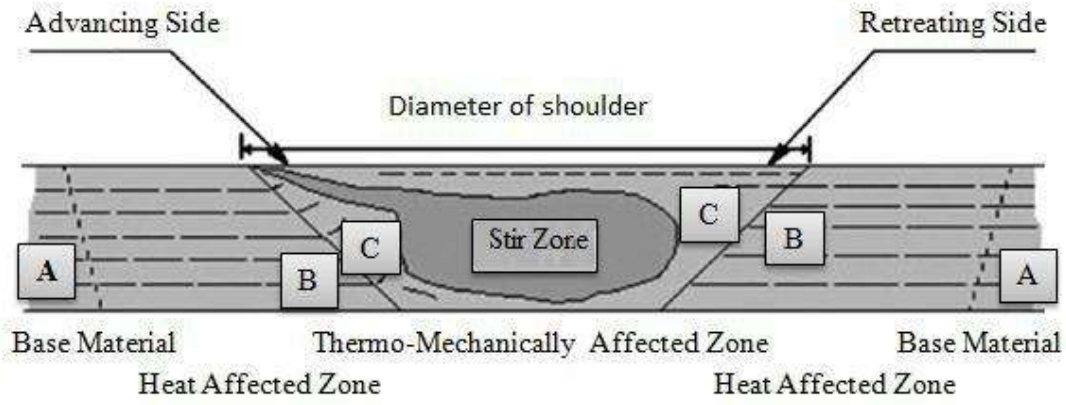

Figure 2.2 Schematic diagram of different zones of friction stir weld, (A-base material, unaffected by the process, B-HAZ, thermally affected but with no visible plastic deformation, C-TMAZ, affected by heat and plastic deformation [16].

2. 4. 1 Stir Zone or Weld Nugget Zone

The nugget zone is nothing but the region of TMAZ which had undergone deformation due to thermal cycling generated through the friction between the material and the tool. It was a TMAZ component, located at a core below the device. The nugget was distinguished with a minute, and equiaxed microstructure attained through the impact of dynamic recrystallization occurs in this region. Nugget was also defined by forming circular circles, commonly referred to like the design of the onion ring. Numerous studies have shown the root of onion rings, especially

variation in the secondary phase, grain dimensions, and dissimilarities in texture, etc. The nugget region hardness was typically greater when compared with HAZ [39 – 40].

The joint nugget region of FSWed of Mg alloys resembles like elliptical or basin shape, which can be distinguished through shear recrystallized grains. Although, Lee et al. [41] scrutinized that the joint nugget could be classified into double zones. The Zone (I), situated on the higher side of joint nugget displayed, which was not completely recrystallized region by deformation surfaces across the grains. The Zone (II) displayed as complete recrystallization with absence of deformation films like twins, etc. Predominantly, FSW emerged in production of tiny recrystallized grains in nugget joint of alloys especially in magnesium [42, 43, and 44]. The coarse β-$Mg_{17}Al_{12}$ and α-Mg phase, second phase in cast Mg alloys are eliminated after FSW [42, 43]. Lee et al. [43] and Park et al. [44] manifested that the grain dimensions in the joint nugget, the device rotation rate increased and the traverse speed decreased, resulting in an increase in energy input encouraging the expansion of recrystallized grains.

2. 4. 2 Thermomechanically Affected Zone (TMAZ)

TMAZ was situated on both sides of the nugget which was advanced and retreat side of the nugget zone. The structure was remarkably deformed and revolved cause of probe shearing. On advancing side, TMAZ was distinguished with the existence of metal flow on the higher facet of the joint. The arm comprises of metal, which was dragged through the shoulder via the retreating direction of the joint around the back end of the probe and dumped on the advancing side [38].

2. 4. 3 Heat Affected Zone (HAZ)

HAZ was a familiar weld region, which was observed in plenty of welding techniques. It was distinctly observed in the fusion joints as compared to friction joints cause of the enormous quantity of energy discharged in fusion welding than that of FSW methods. The HAZ in FSW was not exposed to mechanical transformation while welding, but it encounters thermal cycling. The temperature gradient in HAZ was lesser than TMAZ. Normally, in alloys, which are heat treatable, the HAZ displays low hardness [45,46].

2. 4. 4 Parent Metal or Unaffected Zone

This is the zone which didn't get affected by heat, didn't undergo any deformation even though it experienced a thermal cycle and no traceable changes in microstructure or properties [38].

2. 5 Material Flow in FSW Process

The metal transfer not only relies upon the probe geometry during FSW but also stays complicated. Traverse speed, probe rate of rotation, spindle angle, plunge depth and type of material are the important criteria which decide the final quality of the weldment. Figures 2.3 (a) and (b) indicates the various region, namely, deformation region, forging region and extrusion region, through which the metal transfer modules are actually generated. The metal transfer in the FSW method was investigated through numerous strategies tracers, or through FSW of dissimilar alloys to follow the pattern of metal transfer. Colligan et al. [47, 48] described that the metal flow in FSW was attributed to either via chaotic mixing or simple extrusion process. FSW of AA7075 plates and both being in T6 condition resulted in tiny spheres across the weld joint displayed that along the metal mixed by the probe, majority of the metal travelled plainly via extrusion throughout the retreating side.

Li. Et al. [49,50] investigated the structures of dissimilar FSW of AA6061 and AA2024 Al alloys and reported that dynamic chaotic stirring provides metal transfer within the joint. Siedel and Reynolds [51] investigated the flow of metal in numerous friction stir joints utilizing a marker insertion method and noticed that there was no chaotic stirring at the weld facet. Schmidt et al. [52] reported that a portion of the shear sheet revolves with the pin while the process takes place in FSW.

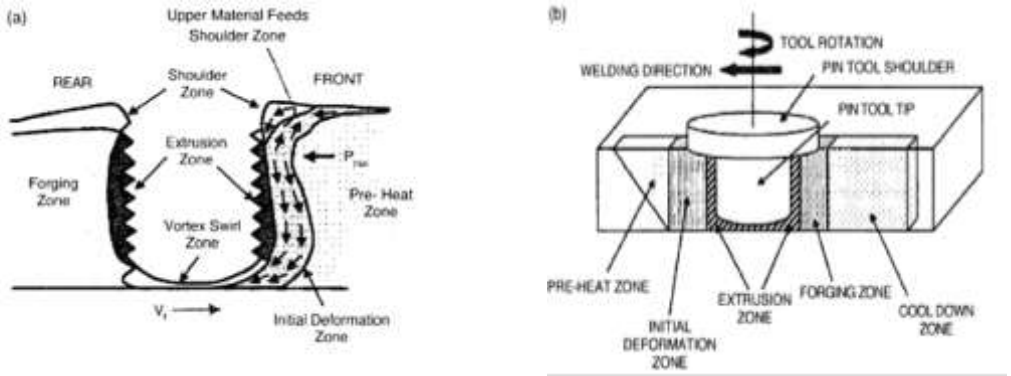

Figure 2.3. (a) Metal flow patterns and (b) metallurgical processing zones developed during friction stir welding [53].

2. 6 Defects in FSW

Wayne et al. categorized the 3 types of defects or flaws that arise in FSW, namely lack of penetration, joint line remnants, and voids. Imperfections are furthermore categorized as maintained by codes into tolerable and intolerable imperfections. Imperfections inside the joint can be produced if inappropriate welding criteria were applied. The usage of the spoiled tooltip, a tiny tool, a low or high rate of rotation, insufficient traversing speed and lesser pressure can tend for the unacceptable quality of the weldment [54-57]. W. Abreast reviewed the possible imperfections/defects caused due to the improper regulation of the FSW criteria is displayed in Figure 2.4. The welding parameters such as rotation rate (W) vs friction stir welding speed (V), manifests the operative method in attaining a suitable weld in case of Al alloys. Minor alteration in the speed of welding or rotation speed may generate imperfections which include, lack of penetration, wormhole flaw, nugget collapse, lack of fusion, root flaw imperfection, scalloping etc. Conventionally, observed in the metallographic investigations of the FSW microstructures [55].

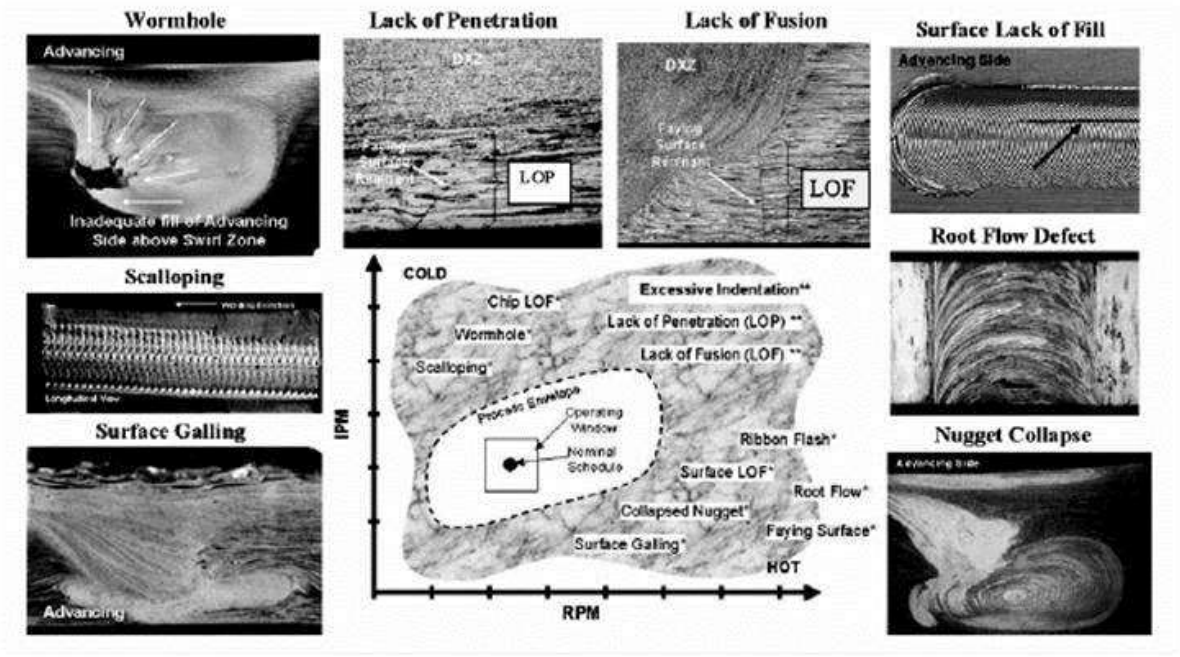

Figure 2.4 Characteristic defect types occur with different FSW parameters [54].

2. 6. 1 Voids

This class of imperfections are produced within the weld while there is a huge traverse speed, very low rotation speed [58,59], inappropriate pressure [60], as well as improper joint gap [60,61]. Applying a lesser shoulder may also tend to lack of metal transfer. Normally, void originated is seen in the advancing side [43]. If the correct welding pressure is not used, the forging behaviour will be quite different from the probe shoulder in attaining complete joining [60]. Combination of huge traversing speeds and very less probe rotation rates during FSW, the metal requires less work per unit of joint length, i.e. less probe rotations per mm. Beneath such parameters, the plastically deformed metal may not approach a suitably huge temperature [59]. Usually, voids have variable size and are oriented in any angle and don't have any specific morphology

2. 6. 2 Joint Line Remnants

FSW joints may comprise non-continuous regions that form as an outcome of inappropriate plastic deformation of the metal because of the non-existence of the pressure essential to damage the metal. The outcome of inappropriate dispersion of the oxides, which can be attributed to weak facet cleansing, preheat treatment that tends to inappropriate bonding [62]. This non-continuity was traditionally created either at the root of the joint and/or at the interface. Joint line remnants are also termed as lazy S, a zigzag line, kissing bond, and it should be diagnosed with a lot of care during the metallographic analysis, destructive inspection utilizing bend inspection and/or in worse parameters, can be noticed in the joint root by visual inspection [63].

It may also oxide which gets accumulated within the joint line. Metallographic studies can reveal oxide particles scattered across the actual joint-line semi-continuously. The morphology of the oxide particles decides the extremity of this flaw and the efficacy on the structure coherence [60, 63, and 64]. Employing huge traverse speed and a shoulder with large dia, as well as inappropriate probe arrangement with the weld line, may tend for creation of such imperfections. Suitable regulation of the welding criteria and elimination of the oxides through the facet by machining, preliminarily to joining can diminish such imperfections [63].

2. 6. 3 Root Flaw/Lack of Penetration

The utilizing of poorly designed or a destructed tool is an unsuitable depth of plunge, weak joint arrangement or an alteration in the thickness of the work specimens may tend for creation of the weld line characteristics is called root imperfections or lack of penetration. In the most significant weld line imperfections are habitually situated at the joint root. The suitable penetration depth of the probe is required to guarantee that stirring takes place above the complete plate thickness. A lacuna in precision in whichever of the over considered conditions tends to root imperfection formation, designating lack of binding [65].

2. 6. 4 Other Flaw Types

The characteristics of the flash type were found on the top facet, usually because of the enormous depth of plunges. In addition, more flash features were sometimes added to ensure adequate penetration, especially in the joint where the fit is poor. Local melting, though FSW has been a topic of recurrent discussion. In addition, the FSW of 7050-T7451, produced at TWI [66], displayed the TMAZ area below the sample, providing the appropriate liquidation confirmation. In addition, the scarcity of phenomenon occurring in FSW somewhat in the scrutiny of Al arc welded joints, as per the various cases examined regarding liquation fissuring. Johnson and. Al [67] manifested liquidation occurring in the TMAZ section during the FSW alloy of ZK60 Mg, which can be eliminated by optimizing FSW Liquation had been investigated by Sato et al., too. [68]. During the non-similar AA 1050 to Mg alloy FSW, the cause of intermetallic melting ($Mg_{17}Al_{12}$) process, the temperature passes through the secondary melting point in the Mg alloy during the FSW method. Table 2.1 lists the welding parameters used to weld different grades of the Mg based alloys with other alloys [68].

2. 6. 5 Corrosion

Corrosion is a destruction process of metal/materials due to their reaction with the surrounding environment. There are several methods to determine the corrosion mechanism and behaviour of the material with which one can choose the material for the environment. Electrochemical techniques are versatile and employed at a large scale to study the process of corrosion as a function of electrochemical reactions.

An electronic instrument, potentiostat, is used to carry out electrochemical studies. In general, potentiostat/galvanostat controls the potential difference/current between a working electrode (WE) and a reference electrode (RE) by inducing a current through a counter or auxiliary electrode. Open circuit potential (OCP), also known as Corrosion potential ($E_{corr)}$ is equilibrium condition where the rate of oxidation and rate of reduction is equal. E_{corr} is defined as potential between WE and RE in an open electrochemical cell condition when no current or potential is applied to the cell. The obtained spectrum is also known as a potentiodynamic scan. Potentiodynamic polarization scan offers a significant amount of information related to

corrosion processes, such as rate of corrosion, relative anodic and cathodic behaviour of electrodes and passivity. Another technique, Electrochemical Impedance Spectroscopy (EIS) is also utilized to provide a detailed investigation of the corrosion process, including passive layer investigation. EIS uses a scan test frequency to analyse resistive and capacitive characteristics of a corrosion cell [69].

2. 7 Corrosion Behavior of Magnesium and its Alloys

2. 7. 1 Corrosion Mechanism of Pure Magnesium

Magnesium (Mg) usage has been limited due to its highly anodic nature (poor corrosion performance) which leads to immediate oxidation of Mg alloys, especially in the presence of metallic impurities or presence of an aggressive electrolyte (such Cl^- ions). However, instantly formed oxide/passive layer on Mg offers considerable protection to the surface of the metal exposed to the atmosphere such as industrial and marine environments. The surface passive oxide film formed on the surface of, of magnesium alloys showed better atmospheric corrosion resistance than that of mild steel. Hence the corrosion rate of Mg alloys stands between aluminum and mild steel. In a few cases, Mg may even have better corrosion resistance than some aluminum alloys [69].

The corrosion reaction for Mg in the presence of water can be expressed as follows [70]:

$$Mg + 2H_2O \longrightarrow Mg(OH)_2 + H_2 \quad (1)$$

This simplified equation can be written into the cathodic and anodic partial reactions:

$$Mg \longrightarrow Mg^{2+} + 2e^- \text{ (reaction at anode)} \quad (2)$$

$$2H_2O + 2e^- \longrightarrow H_2 + 2OH^- \text{ (reaction at cathode)} \quad (3)$$

Hydrogen molecules plays a vital role in corrosion process of Mg The reduction reaction as follows:

$$2Mg^+ + 2H_2O \longrightarrow 2Mg^+ + 2OH^- + 2H^+ \quad (4)$$

The reaction yields magnesium hydroxide as a corrosion product. However, different atmosphere conditions and solutions will yield other types of products [71].

$$Mg_2+ + 2\ OH- \longrightarrow Mg(OH)_2 \qquad (5)$$

The main conclusions that can be made from the previous reactions are (i) the dissolved oxygen in the corrosive media has no role to play in corrosion of Mg [67, 70], (ii) A significant alkalization of the solution is attained when the volume of the electrolyte is small.

Though magnesium being an active metal with a standard potential of -2.37 V (SHE) [70, 71]. Its standard potential is much lower, and the metal shows stability in 3% NaCl solutions with -1.63 V (SCE), or -1.38 V (SHE) [69]. This proves that the hydroxide layer (passive film) formed separates the electrolyte and metallic surface, which is responsible for the better potential [69].

The localized corrosion is observed in pure magnesium is generally associated with the surface film, which is metastable and partially protective, which subsequently leads to a pitting potential (Epit). Furthermore, it was observed that the value of pitting potential was more negative than the value of free corrosion potential (E_{corr}). The corrosion process starts with the formation of irregular and shallow pits on the surface. The formed pits display an unusual penetration pattern when compared with the pits formed in other metal/electrolyte systems. The corrosion penetration was lateral in case of magnesium which covers the whole surface whereas penetration was vertical in-depth in other systems (Aluminium and stainless steels). Therefore, the deep pits are rarely observed during pitting corrosion for Mg and Mg alloy systems [70].

The alkalization of the solution caused by the cathodic reaction leads to such unusual corrosion on Mg. Consequently, the increase in the pH value leads to stabilization of the surface film by forming the layer of $Mg(OH)_2$ film, and the same reduce the corrosion rate inside the pit. The edges of the pits with low pH value will open the gate for anodic dissolution, which leads to lateral pitting corrosion and this kind of the second phase undermining was very common in magnesium alloys [70].

Table 2.1 Summary of processing parameters, parent alloys and significant remarks from the literature review.

Author	Year	Parameters	Material	Remark
Gaohui Li et al. [72]	2020	600 rpm, 300, 350,400 mm/min	ZK 60 Mg alloy	In the Stir zone, significant softening occurs because the strengthening occurring from the grain refining does not compensate for the strength losses incurred by the dissolution of the precipitates.
Fet weng et al. [73]	2020	700 rpm, 4 mm/sec	Mg–Y–Nd magnesium alloy Mg alloy	The mechanical properties and microstructural characteristics of the double-side FSW of thick Mg alloy (20 mm thick) were investigated, and it was confirmed that the overlap zone shows relative hardness and equal texture distribution with the parent alloy. Fine equiaxial grains are mostly occupied by the nugget region of the weld.
Yang Zheng et al. [74]	2019	800 rpm,100 mm/min	6061 Al/AZ31 Mg	Zr interlayer was used to join 6061 Al and AZ31 Mg. The results revealed that the Zr interlayer was smashed at the central part and dissolved in the stir zone. It also prevented the formation of Al–Mg intermetallic compounds. The corrosion rate of representative regions increased in the order of Al alloy, Mg alloy, heat-affected zone, stir zone. Corrosion resistance for the Al/Zr/Mg joint was better compared with the Al/Mg joint

Kulwant Singh et al. [75]	2018	1400 rpm, 25 mm/min.	AZ61 Mg alloy	Investigated the mechanical properties as well as microstructural characteristics of FSW sample of AZ61-Mg alloy joint and reported that the nugget region consists of ultra-fine and uniform grains settling to dynamic recrystallization. Grains were coarser in advancing region than grains of a retreating region of TMAZ. Mode of failure was ductile
Yael Templeman et al. [76]	2017	2500 rpm, 0.1 mm/min	AZ50 & AZ31 Mg alloy	Studied the effect of microstructural development and corrosion behavior during dissimilar alloys AZ50 and AZ31 Mg alloy by FSW. Al-enrichment due to β phase dissolution in the ά-Mg granules in nugget region
Shude Ji et. al. [77]	2017	1200 rpm, 40mm/min.	Al 6061-T6& AZ31 Mg alloy	Investigated on origination of intermetallic complexes throughout FSW process and its influence on the mechanical properties of Al 6061-T6& AZ31 Mg alloy. Nugget zone revealed the Al_3Mg_2 and $Al_{12}Mg_{17}$ intermetallics.
Vedat Veli ÇAY et. al. [78]	2017	1500 to 2300 rpm, 100 to 190 mm/min.	AZ31B Mg alloy	Reported that the fracture occurred was between the junction of the TMAZ and the HAZ. A similar scenario was observed in all the cases attempted.

S. Mironov et. al. [79]	2017	2000 rpm, 200 mm/min.	AZ31 Mg alloy	Studied about the tensile performance of FSW specimen of AZ31 Mg mixture and reported that failure fissure propagated across stir region which was impacted by onion ring shape structure originated through FSW.
C.Luo et. al. [80]	2016	1000 rpm 80 to 240 mm/min	AZ91D & ZG61 Mg alloy	Investigated FSW of dissimilar wrought Mg alloys AZ91D/ZG61plates.The micro hardness of ZG61 / AZ91D specimens was better than that of AZ91D/ ZG61 specimens.
Nikul Patela et. al. [81]	2016	710 to 1400 rpm,28 to 56 mm/min.	AZ91 Mg alloy	Studied the impact of tool geometry as well as process parameters on the durability of AZ91Mg. They found that the tool having threaded straight cylindrical spike description of a diameter of 18 mm and process parameters of 710 rpm and 28 mm/min is appropriate to produce a quality weld.
Weideng wang1 et. al. [82]	2016	800 to 1600 rpm, 120 m/min.	AZ31 Mg alloy	Investigated the role of tool rotation speed on temperature description as well as mechanical properties of FSW specimen of AZ31 magnesium alloy and mentioned that optimum joint efficiency of 90.2% had been attained at an optimum tool revolving condition of 1200 rpm.

S. Ugender et. al. [83]	2015	900 to 1400 rpm, 25 to 75 mm/min.	AZ31 Mg alloy	Studied the impact of tool composition and rotational velocity on mechanical characteristics of FSW specimen of AZ31B. They developed regression models to predict the properties and correlate the process parameters such as tool tilt angles, rotational speeds and feed rates co-relation. Modeling results were confirmed with the experimentation.
S. Rouhi et. al. [84]	2015	800 to 1600 rpm, 40 mm/min.	AZ91C Mg alloy	Investigated the influence of welding atmosphere upon mechanical as well as microstructural characteristics of FSWed AZ91C Mg compound specimens and reported that underwater environment of the ultimate toughness of weld is slightly better than the air environment.
M. Tabasi et. al. [85]	2015	450 to 1100 rpm, 11.2 to 45 mm/min.	Al 7075 & AZ31 Mg alloy	FSW of dissimilar Al 7075 & AZ31 Mg alloy was investigated using silicon carbide nanoparticles of size 30-40 nm for the formation of metal matrix composites and noticed that dynamic recrystallization occurring during the process.
B. Ratna Sunil et. al. [86]	2015	1400 to 1800 rpm, 25 to 100 mm/min.	AZ91 & AZ31 Mg alloy	The investigation made on the FSW of dissimilar AZ91 & AZ31 Mg alloy. The volume fraction of β intermetallic in AZ31 Mg is lesser than in

				AZ91 alloy. The dissolution of the intermetallic was narrowed to the retreating region. Improved solidity in nugget area could be featured to particle purification and availability of $Mg_{17}Al_{12}$ grains coupled by solid mixture strengthening
AlirezaMasaudian et. al. [87]	2014	600 to 1400 rpm, 20 to 60 mm/min	AZ31-O Mg & 6061-T6 Al alloy	Dissimilar FSW amongst AZ31-O Mg as well as 6061-T6 Al materials were researched. The embedded microstructure was originated in few areas in the stir region, and this complicated flow structure might be accountable for irregular microhardness scattering in stir region.
Sevvel P et. al. [88]	2014	45 to 1500 rpm, 0.25 to 500 mm/min.	AZ31B Mg alloy	Studied the characterization of mechanical characteristics and microstructural evaluation of FSWed AZ31B Mg material after choosing thoroughly optimized operating criterions. It was observed high rotational speed and low traverse speed led to good quality weld due to adequate heat origination producing in swift solidification of particles.
S. Ugender et. al. [89]	2014	900 to 1800 rpm, 40 mm/min.	AZ31B Mg alloy	Scrutinized the characteristics of AZ31B Mg alloy by FSW. Reported that joining tool metal and speed of rotation were distinguished as the predominant process criterions that significantly influence the

				SZ mechanical properties as well as microstructure of weldment.
Inderjeet Singha et. al. [90]	2014	1200 & 1950 rpm, 40 & 60 mm/min.	AZ31-O Mg alloy	Examined the impact of joining criterions on similar FSW specimens of AZ31B-O Mg material and noticed rupture nature in majority of the samples between SZ and TMAZ near advancing zone due to diminishing point in this area. In addition, reports revealed that the specimens were fractured at an angle of 45^0 in common of all the joints.
Sevvel P et. al. [91]	2014	1800 rpm, 50 mm/min.	AZ31B Mg alloy	Studied the influence of axial load for improving the tensile characteristics of FSW AZ31B Mg material. The joints were welded by varying axial forces (3, 4, 5 kN), keeping other FSW parameter constant and they found that the joint fabricated at 5 kN was exhibiting highest strength compared to other weldments.
B.S Naik et. al. [92]	2013	1000 rpm and 1500 rpm, 10 mm/sec, 20 mm/sec.	AZ31B-H24 Mg alloy	Studied the fatigue and microstructural characteristics of a friction stir lap joined AZ31B-H24 Mg metal. The fractographic investigation confirmed that ruptured facet showed the numerous fissure commencement sites beginning from the extremity of the hooking imperfection situated in the top specimen.

Pourahmad et. al [93]	2013	800 to 2000 rpm, 35 to 75 mm/min.	Al 6063 Mg and AZ31 Mg alloy	Examined the materials flow and phase transformation in friction stir welding of Al 6013/Mg alloys. samples were acquired imperfections free at 1600 rpm and 35mm/min at a tilt angle of 3º. An islanding, interlocking and zigzag interface was evidenced in few regions. They explored the specimen region and observed extrusion patterns of Mg into Al and vice versa were observed.
Venkateswaran et. al. [94]	2012	900 to 2700 rpm, 1.69-6.4 mm/min.	AA6063 & AZ31 Mg alloy	Studied about the various factors that can affect FSW of Al/Mg dissimilar metals (AA6063 & AZ31 Mg alloy). The microhardness scattering of weld specimens is predominantly determined by the formation of intermetallic such as Al_3Mg_2 and $Al_{12}Mg_{17}$ in all conditions. Mechanical interlocking through production of complex weld interfaces provided the high strength.
Yuan-Ching Lin et. al. [95]	2011	1250 & 2500 rpm, 1 to 2 mm/sec.	AZ61 Mg alloy	Studied the influences of operating criterions on robustness of Mg metal AZ61 FS spot joints and reported that heat input plays a vital role in controlling grain growth in the TMAZ. Due to the heat input grain grows faster in TMAZ. It was also reported that the SZ consists of a fine-grained structure and

				is responsible for the high strength of the SZ.
X. Cao et. al. [96]	2010	500 to 2000 rpm, 20 mm/s	AZ61A Mg alloy	Studied the influence of tool spinning velocity and probe distance on lap welded standard of an FSWed Mg alloy and reported that the ultimate shear stress preliminarily advances with enhancement in tool spinning velocity but reduces later. Shear strength may be increased by enhancing probe distance and piercing extent into extremity of the sheet.
A. Razal Rose1 et. al. [97]	2010	1200 rpm, 90 mm/min.	AZ61A Mg alloy	Studied the influence of axial load on ultimate and microstructural criterions of FSWed AZ61A Mg material and reported that the ultimate strength in the weld region was 83% of the base metal for the given processing parameter
X. Cao et. al. [98]	2008	2000 rpm, 5 to 30 mm/min.	AZ31 Mg alloy	Studied the impact of joining velocity on lap welded standard of FSWed AZ31 Mg material for the scrutiny. It was reported that the joining velocity has a remarkable influence upon the formation of hooking defects and it decreases with the welding speed.
X. Cao et. al. [99]	2008	2000 rpm, 5 to 30 mm/min.	AZ31B-H24 Mg alloy	Studied the impact of joining velocity on the standard of FSW butt welds of AZ31B-H24 Mg alloy. It was reported

				that the joining velocity has a noteworthy effect on both yield and ultimate strength. Yield strength enhances with escalating joining velocity whereas, ultimate strength enhances with escalating joining velocity up to 15 mm/s and stays changeless in range of 15 to 30 mm/sec.
L. Commin et. al. [100]	2008	600 to 1300 rpm, 200 to 2000 mm/min.	AZ31B Mg alloy	Studied about the FSW of AZ31 Mg material rolled sheets. Impact of operating criterions and reported that temperature distribution is unsymmetrical across retreating and advancing side, whereas it is uniform along the weld line, cause of the heat energy supplied through plastic deformation.
G.Padmanaban et. al. [101]	2008	1600 rpm, 0.67 mm/min.	AZ31B Mg alloy	Investigated the choosing of FSW tool pin description, shoulder dimension sand used AZ31B Mg alloy for the study. It was reported that the high rigidity and mechanical characteristics of specimens may be attributed to the equiaxed and subgrains and mainly the absence of defects in the nugget zone.

2. 8 Research Gaps in the Literature

From the detailed literature survey on friction stir welding of magnesium based alloys, the following research gaps are identified as

i. From available literature, it can be summarized that there is limited understanding of the influence of input process parameters with their response affecting the FSW performance.
ii. From the available literature, no/limited research work has been found on the polarization studies of dissimilar FSWed Mg based alloys.
iii. Although several studies have reported the corrosion resistance of FS Welded Mg–Al–Zn alloys they are not concentrated on the surface corrosion resistance.
iv. It is evident from the reviewed literature that less amount of work has been done so far on FSW of Mg based alloys though it is a highly essential aspect in the competitive world to satisfy customer requirements.

2. 9 Objectives of Research Work

Based on the gaps identified from the literature, following objectives were formulated to determine the optimum welding parameter and correlate the development of microstructure during similar and dissimilar friction stir welding of Mg based alloys with the mechanical properties. The main objectives of the thesis are

i. To correlate the microstructure and mechanical properties of friction stir similar welded alloy (AZ91D-AZ91D alloy)
ii. To correlate the microstructure and mechanical properties of friction stir dissimilar welded alloy (AZ91D-AZ31C alloy)
iii. To study the effect of microstructure on the corrosion properties of weldments
iv. To compare the properties of the similar and dissimilar weldment

CHAPTER − 3

EXPERIMENTAL AND METHODOLOGY

3. 1 Materials

3. 1. 1 Work Material

Gravity die cast AZ91D Mg alloy (commercial grade) and AZ31C Mg alloy (commercial grade) in the form of casted blocks were supplied by Exclusive Magnesium Pvt. Ltd, Hyderabad, and were used in the present studies. Cast blocks were cut using wire electric discharge machine into 130 mm long, 45 mm wide, and 3 mm thickness. The chemical compositions of the base metals (AZ91D Mg alloy and AZ31C Mg alloy) in as received condition are given in Table 3.1

Table 3.1. Chemical Composition of AZ91D Mg alloy and AZ31 Mg alloy (% Wt).

Base Metal	**Al**	**Zn**	**Si**	**Cu**	**Ni**	**Mn**	**Mg**
AZ91D Mg alloy	8.84	0.59	0.218	0.05	0.008	0.21	Balance
AZ31C Mg alloy	2.45	0.41	0.312	0.05	0.008	0.21	Balance

3. 1. 2 Tool Material

Most of the time tool temperature reaches the solidus temperature of the base metal in case of FSW. Proper tool material selection is vital in achieving the optimum combination of the microstructure and mechanical properties for a particular application. In the present investigation, AISI- H13 tool steel has been used as a tool material believed to possess good

elevated temperatures such as high strength and adequate toughness. It also has good stability and wear resistance. They are readily available and inexpensive too [102]. The typical chemical composition and physical properties of H13 tool steel are presented in Table 3.2.

Table 3.2 Chemical composition of AISI-H13 tool steel (wt%.).

Element	**C**	**Mn**	**Si**	**Cr**	**V**	**Mo**	**P**	**S**	**Fe**
Amount (wt.%)	0.42	0.28	1.00	5.20	1.05	1.45	0.015	0.003	Balance

3. 2 Experimental Design

3. 2. 1 Design of Experiments

Experimentation is an essential component in research and investigations, whether it may be engineering, agriculture, medicine or any. An experiment can be described as a test or series of tests where significant modifications are made to a system's input variables so that the system's output performance can be observed and the reasons for changing responses can be analyzed. In particular, experiments are conducted to investigate the performance of processes or a system of processes. The variables which are predominant for the study have both controllable and uncontrollable parameters. The main motive of experimentation is to examine the effect of the process parameter on various responses.

3. 2. 2 Taguchi Design

Taguchi method is a mathematical technique invented by Genichi Taguchi to advance the efficiency of the manufactured products, which was later extended for many engineering applications. Based on orthogonal arrays Taguchi developed a robust design to reduce variations in the experiment with optimum settings of controllable parameters. Taguchi designs are a special subset of fractional factorial designs. The traditional fractional factorial designs are not promised for consistency among the designs and also are complex to execute. To overcome these problems, Taguchi comes up with an exclusive set of Orthogonal Arrays (OA) in the position of fractional factorial experiments. A systematic investigation of a process has

been incorporated through the experimental design to investigate the effects of process variables on responses [103].

In Taguchi method signal to noise (S / N) ratio, a loss function is used to determine the difference between the experimental/observed and the expected response value. The loss function also converts to a utility function. The utility function is also named as Signal-to-Noise (S/N) ratio. According to the expected response, S/N ratios are

i. Lower the better (Lower response is desirable)
ii. Nominal the best (Average response is desirable)
iii. Higher the better (Higher response is desirable)

The S/N ratio for the i^{th} performance characteristic in the j^{th} experiment can be determined as:

Lower the better (for making the system response as low as possible):

$$(S/\mathrm{N})_{IJ} = -10 * Log_{10}\left(\frac{1}{n}\sum_{k=1}^{n} y_{ijk}^{2}\right) \quad (3.1)$$

Higher the better (for making the system response as high as possible):

$$(S/N)_{IJ} = -10 * Log_{10}\left(\frac{1}{n}\sum_{k=1}^{n} \frac{1}{y_{ijk}^{2}}\right) \quad (3.2)$$

Where n = number of tests; y_{ijk} = experimental value of i^{th} performance characteristic in the j^{th} experiment at the k^{th} test [103].

3. 3 Selection of Tool Pin Profiles

Trial experiments were carried out with tools having the pin profiles such as cylindrical (profile 1), taper cylindrical (profile 2 and 3). Profile 2 was found to produce good quality of weld joints in comparison to profile 1 and 3. Hence profile 2 has been used to weld the similar and dissimilar metals, as it has the advantage with tool shoulder shape, namely concave shape and allows the easy material flow. Tool pin is to generate the frictional heat and stir the metal being welded. The shoulder supplies the additional frictional heat to prevent the plasticized material being escaped from the stir zone [104]. The tool pin specification is given in Table 3.3.

Table 3.3 Dimension of the different tool pin.

Profile	**Shoulder Diameter**	**Pin Diameter (Shoulder end)**	**Pin Diameter (Tip end)**	**Aspect Ratio**
Profile 1 (Cylindrical)	18	7	7	2.57
Profile 2 (Taper cylindrical)	18	7	2	2.57
Profile 3 (Taper cylindrical)	18	7	3	2.57
Other details: Length of the pin is 2.6 mm; Profile 2 and 3 has left hand thread of 0.5 mm pitch.				

3. 4 FSW of AZ91 Mg Alloy and AZ31 Mg Plates

Prior to welding, the plates were cleaned with a stainless steel brush to remove oxide on the surface and then cleaned with acetone in order to remove any surface pollutant. The butt joint welds of 3mm thick were produced using a commercially available automated vertical milling machine (Make: Universal) as shown in Figure 3.1. After extensive trials, the process parameters were chosen as per Taguchi L9 matrix aiming at good quality, defect-free and full-penetration weld joints.

3. 5 Characterization

3. 5. 1 Metallography

Metallography of the friction stir welded (transverse direction) specimens were prepared by standard metallographic procedure. The cut samples were polished by using different grades of emery papers and finally with disc polisher by using alumina suspension as grinding media. The polished specimens were etched with acetic glycol for 10-15 Seconds. The composition of the Acetic glycol etchant was a mixture of 1ml nitric acid, 20ml acetic acid, 20ml distilled water and 60ml ethylene glycol.The microstructural aspects were studied under the Optical Microscope model no: QMM-500coupled withImage Analysis Software (Quasmo-Iview 3.7).

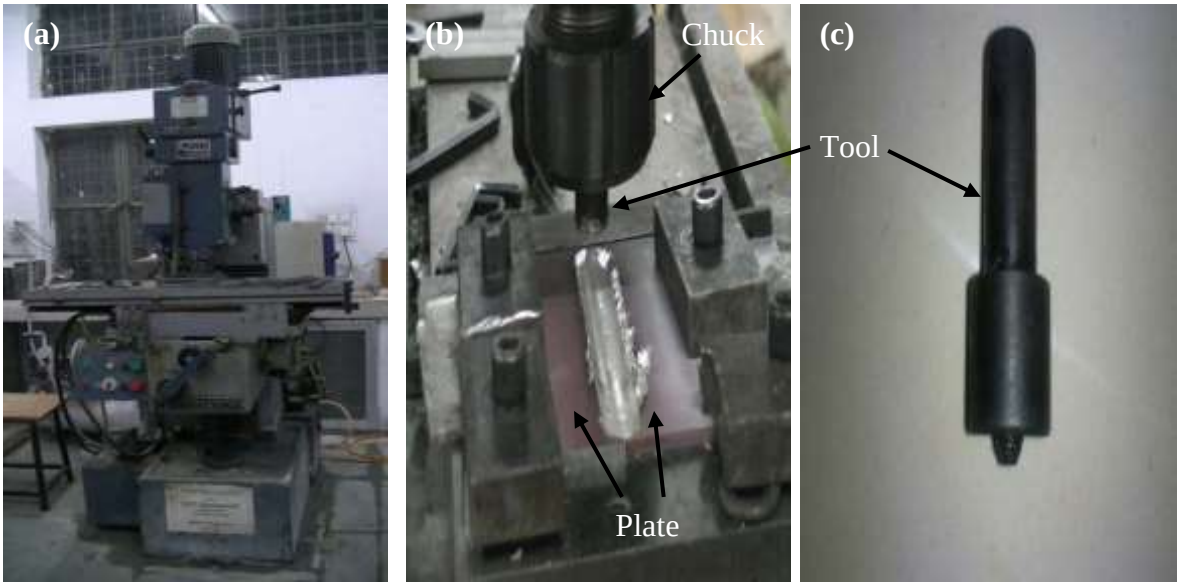

Figure 3.1. Photograph showing (a) Milling machine (Vertical) used for FSW (b) FSWed plates, (c) Tool used for FSW.

Table 3.4. Process parameters and their level used for joining of Similar (AZ91Mg and AZ91 Mg alloy) and dissimilar (AZ91 Mg and AZ31 Mg alloy) plates.

Nomenclature	**Process parameters**			
Tool details	H13 tool steel (tapered cylindrical pin with 0.5 mm pitch left-hand thread) Diameter of the pin: 7 mm of shoulder end and 2 mm tip end Length of the pin: 2.6 mm Shoulder diameter: 18 mm Plunge depth is 0.2 mm excess of pin length Axial load: 10KN			
Taguchi L_9 matrix[#]		**Welding speed(rpm)**	**Tool rotational speed (mm/minute)**	**Tilt angle (°)**
	Level-1	25	500	1.5
	Level-2	50	720	2
	Level-3	75	1025	2.5

[#]Process parameters are chosen as per Taguchi L_9 matrix for both Similar (AZ91D Mg alloy to AZ91D Mg alloy) and Dissimilar welding (AZ31C Mg alloy to AZ91D Mg alloy)

Scanning electron microscope (SEM) attached with energy dispersive spectroscopy (EDS) facility of model: VEGA 3 TESCAN has been used to carry out the fractography and to study the microstructural and its chemical features at different zones of weldments and tested

tensile samples. The images were processed and analysed using ImageJ software to achive quantitative information about grain size, porosity and interconnectivity of the surface.

3. 5. 2 Radiography

FSW joints surface and the weld zone were inspected by X-ray radiography (Model no. XXGH/XXGHA2505) as per ASME Sec IX to observe the weld defects. Single wall, single image (SWSI) technique was adopted for studies. The X-rays were exposed for 1 minute to the weld length up to 130 mm. The source to film distance was maintained at1000 mm, and the image was captured on Agfn-D4 film with 2% sensitivity and with the density of 2 to 2.5.

3. 5. 3 X-ray Diffraction (XRD) Analysis

The nature of phases formed in the weldments were analysed by using powder X-ray diffractometer (X'Pert Powder, PANalytical, The Netherlands). CuKα radiation (λ= 0.15406 nm) with 45 kV, 30 mA are used for the during the analysis. Phases identification was analyzed using X'pert High Score Plus software with diffraction database. The X-ray diffraction pattern was recorded for 2θ range from 30º to 80º at scanning steps of 0.01º.

3. 5. 4 Tensile Test

In order to determine the joint strength of the welds, the transverse tensile tests were performed using computer controlled universal testing machine (UTM) (Model no. S500, Make: Instron) testing machine. Wire electric discharge machine was used to prepare test specimens following the standards ASTM E8/E8M-11. The tensile specimen used for the testing is shown in Figure 3.2 (schematic). Tensile tests were conducted at room temperature. Cross head speed of 2 mm/min was use for the same.

3. 5. 5 Impact Test

Impact test (charpy 'V' notch) was carried as per the ASTM E-370 standards using pendulum type charpy impact tester . Tests were conducted at room temperature. Transverse section of

the weld zone was used and the notch was made in the transverse direction and is given in the schematic Figure 3.3.

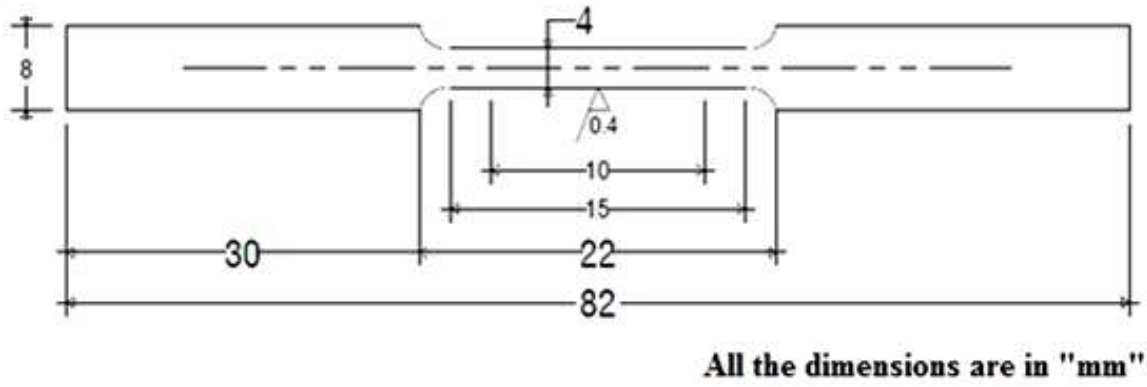

Figure 3.2 Schematic sketch of tensile test specimen

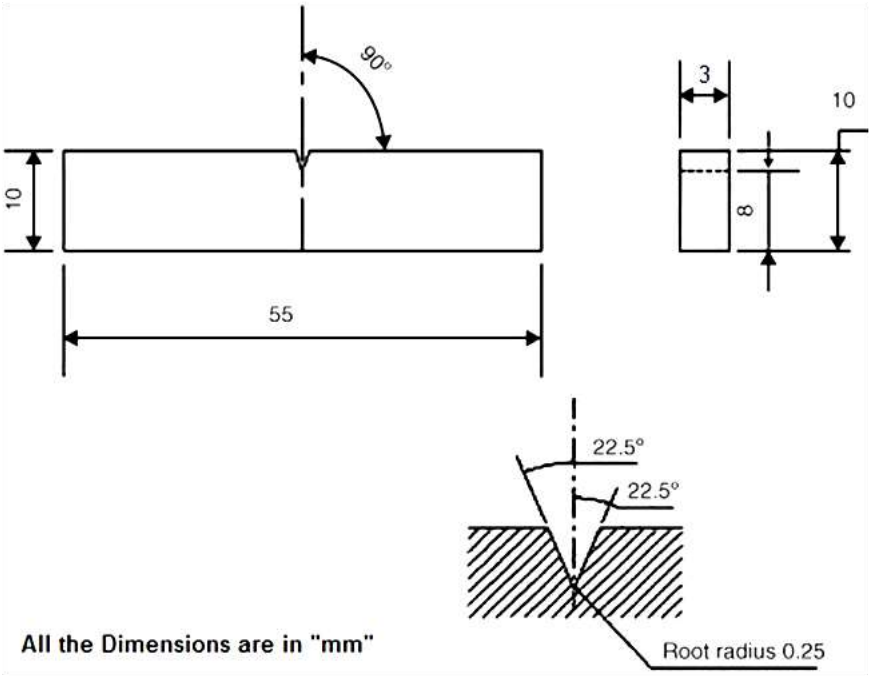

Figure 3.3. Schematic sketch of charpy V-notch impact specimen

3. 5. 6 Micro Hardness Test

A digital Vickers microhardness tester of Model: Autograph and Shiatzu make) has been used to measure the hardness. For the same 200 gm load was applied for a dwell period of 15 seconds. Transverse section of the weld direction or the cross section was used and the reading were taken at an interval of 1 mm across all the zones and the schematic diagram of microhardness examination is shown in Figure 3.4.

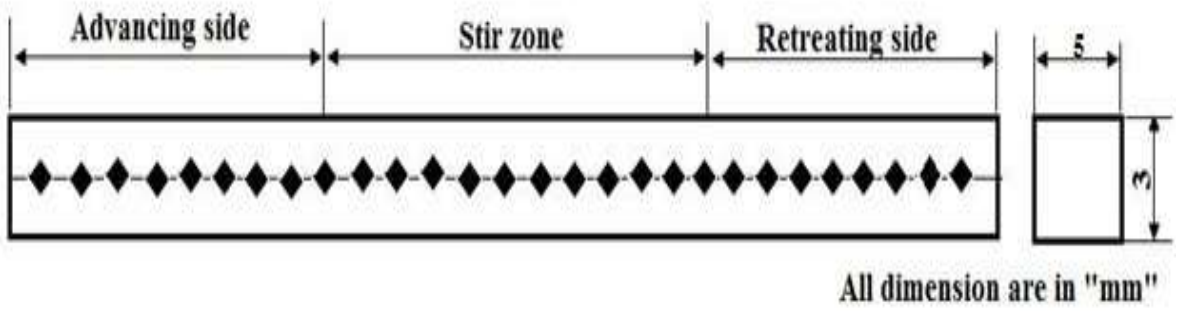

Figure 3.4 Schematic sketch of microhardness survey

3. 5. 7 Electrochemical Measurements

Electrochemical measurements of both similar and dissimilar weldments were performed in 3.5 NaCl solution. The 3.5g of NaCl is dissolved in 100 milliliter of water with ultra purity and having the resistivity of 18.2 Ωcm. Samples were polished using 2000 grit paper and then cleaned using ultrapure water and then dried. Three-electrode system with stagnant circumstances was used for electrochemical studies. The test specimens were surrounded in a teflon holder. In this electrochemical study test specimen took the role of working electrode, saturated calomel electrode took the role of reference electrode. Graphite rod has been used as counter electrode. Measurements were performed using a potentiostat / galvanostat (PARSTAT 4000) built with Versa Studio software. Three samples from each welded plate were used for the test. The surface corrosion resistance of the weldment was measured by taking the surface specimens (18 mm x 20 mm) as shown in Figure 3.5. The potential scanned from − 0.5 to 0.5 mV versus open current potential with a scan rate of 5 mV/s.

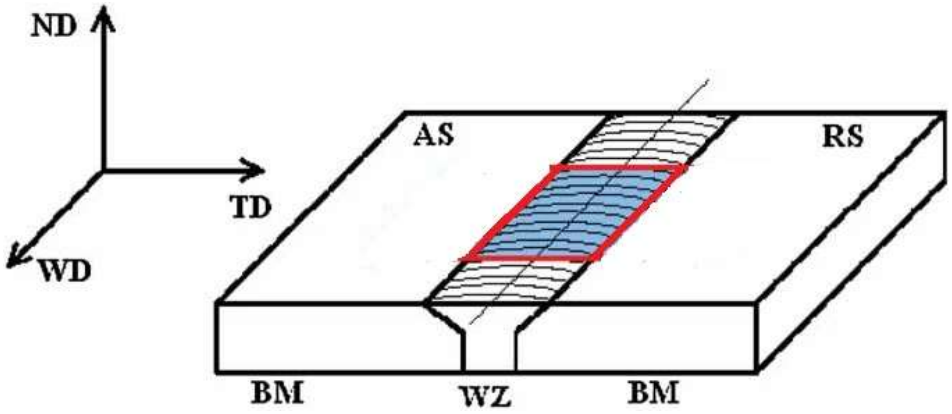

Figure 3.5 Schematic illustration of the measurement surface used in the present study

3. 6 Optimization Techniques

3. 6. 1 ANOVA Analysis

Analysis of Variance (ANOVA) is a statistical method which determines the experimental outcomes. ANOVA is used to measure the variance that each variable contributes. In ANOVA, the degree of freedom (DF) gives detailed information about the process parameters for analysis, and the total number of experiments is defined by total DF. Adjusted Square Sum (ASS) quantifies the amount of variation in the response data described in the model by each term Adjusted Mean Squares (AMS) measures the amount of factor variation, irrespective of the order it has entered. F- Test is a statistical test to correlate the fitted data of the samples investigated from population. High F- value used to assess the factor's statistical significance and its correlation with the response. P is a probability that further tests the significance of the term. If P <= 0.05, the factor is considered statistically significant. It has been found from the present observations that all the parameters have less than 0.05, indicating that there are highly significant at a confidence level of 95 % [105].

3. 6. 2 Regression Analysis

Study of regression is a statistical method used to identify correlations between variables to

predict intermediate values within the level range. The usage of a single independent variable is known as simple regression analysis, whereas more than one independent variable is referred as multiple regression analysis. Nonlinear regression models were established in this study to predict the tensile as well as impact properties based on the results of the experiment. The best fit for experimental values can be achieved using second-order polynomial curve [103].

The commonly used regression model [105] is expressed, is given as follows.

Y= f (speed of rotation, traverse speed, tilt angle)

Y= f (A, B, C)

The general model of regression for the three factors is given by the following equation

$$Y= b0+ b_1A + b_2B + b_3C+ \varepsilon \quad (3.3)$$

Where,Y: Characteristics of output parameters A, B and C; b0 - free term, the quadratic terms are the coefficients b_1, b_2 and b_3; ε - Experimental error

Applying the experimental design to analyze process characteristics in FSW has been the most appropriate method, as it allows the best parameters to be selected to fulfil the multi-objective response parameters. Several researchers applied the Taguchi methodology, gray relation analysis, and surface methodology and ANOVA analysis on magnesium-based alloys by choosing various process parameters. Most of the FSW experiments were carried out by using these methods, to reduce the number of experiments since FSW process involves many parameters.

In present work, taguchi based experimental design has been used for conducting the experiments. ANOVA was used to observe the role of welding parameter on the mechanical properties of similar and dissimilar weld joints. The Flow chart showing the experimental design and analysis process is shown in Figure 3.6

3. 7 Taguchi Orthogonal Array for Experimentation

It has been decided to decided to vary the three parameters at three levels, L9 (34) Orthogonal Array (OA) has been used for experimental design so as to explore the experimental region systematically explored. The layout of the standard L9 (34) OA is given in Table 3.5 [105].

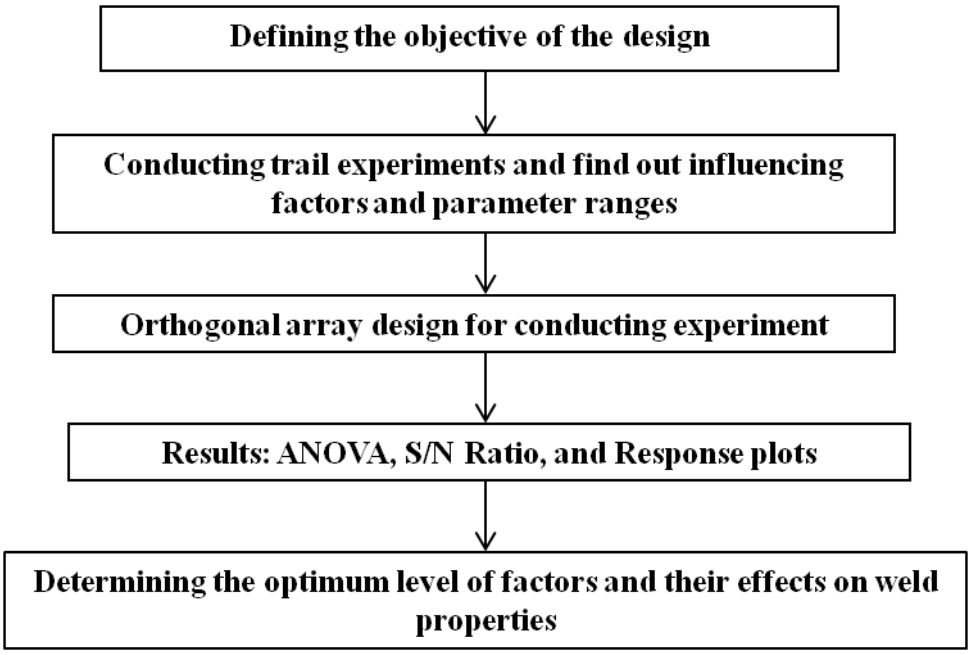

Figure 3.6 Flow chart showing the experimental design and analysis process

Table 3.5 Layout of L9 Orthogonal Array.

Row	Column 1	Column 2	Column 3	Rotational speed(rpm)	Welding speed(mm/min)	Tool Tilt Angle(Degree)
1	1	1	1	500	25	1.5
2	1	2	2	500	50	2
3	1	3	3	500	75	2.5
4	2	1	2	720	25	2
5	2	2	3	720	50	2.5
6	2	3	1	720	75	1.5
7	3	1	3	1025	25	2.5
8	3	2	1	1025	50	1.5
9	3	3	2	1025	75	2

As shown, the L9 OA consists of a three level columns with nine rows combination. The factors are assigned (columns as well as rows) to show the factors' levels combination of each experiment. As the present study involves three factors, they are assigned to the first three columns of the array.

3. 8 Overall Research Plan

The present investigation is aimed for improved mechanical and corrosion properties of similar and dissimilar Mg based alloys. The overall work plan is given in Figure 3.7.

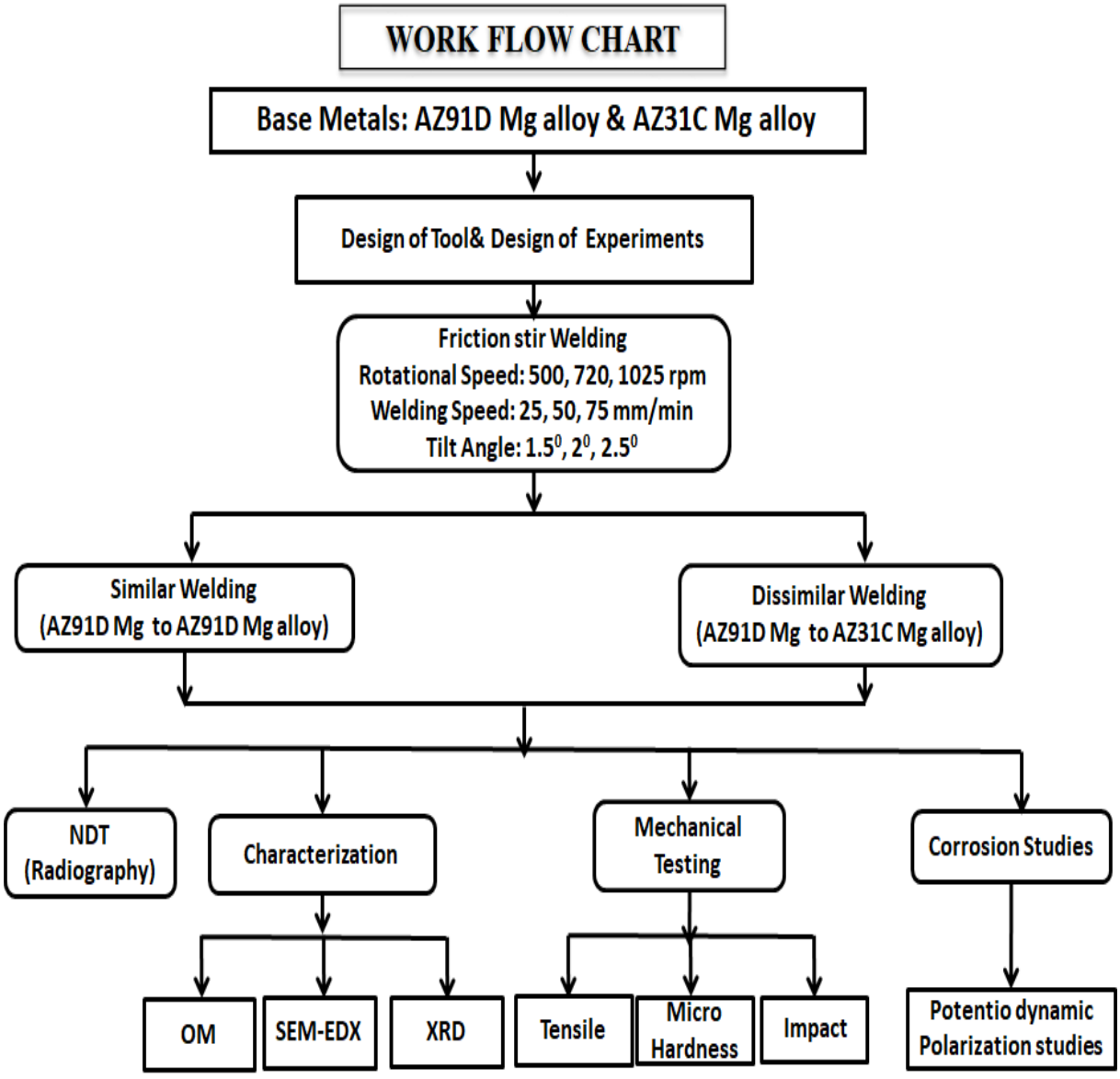

Figure 3.7 Flow chart showing the processing and characterization methods.

CHAPTER − 4

FRICTION STIR WELDING OF AZ91-AZ91 SIMILAR ALLOY

4. 1 Introduction

The objective of the present work is to study the influence of welding parameters and correlate the same with the microstructure, mechanical properties and corrosion properties of FSWed magnesium based AZ91 Mg alloy. Similar AZ91 to AZ91 Mg alloy plates of 130 mm long, 45 mm wide and 3 mm thickness butt joints were processed using a commercially available automated milling machine of vertical type as shown in Figure 3.2 (Chapter 3).The plates were firmly fixed on the working table of the vertical milling machine using clamps as shown in Figure 3.2 (b) and non-consumable tool was inserted between butt joint (Chapter 3). Plunge depth was given in such a manner that no consumable tool shoulder should completely come in contact with the surface of plates to be welded, then the tool forwards along the traverse direction. Joining parameters are chosen as per Taguchi L9 matrix for both similar (AZ91 Mg alloy to AZ91 Mg alloy) and optimized process parameters were obtained after the welding process.

The friction stir welding process parameters exert major effect on the temperature generation and material flow pattern during the welding, thereby influencing the microstructural evolution of the weldment. This microstructural modification of the alloy leads to enhancement of properties. The observations on mechanical properties are illustrated in this chapter. Taguchi method was used to obtain the optimum combinations of processing.

Regression models were developed to predict the mechanical properties. The obtained results were correlated with the microstructure and fracture features of weldments. The details about parent alloys, experimental layout and testing procedures adopted are already discussed in Chapter 3. The selection of process variables and their ranges and detailed results are presented in the following sections.

4. 2 Trail Experiments

The combinations of various parameters used for the pilot experiments along with the observations made are given in Table 4.1. The butt welding joints produced at 1525 rpm rotational speed are shown in Figure 4.1 The butt welding joints were produced with varying rotational speeds of 500, 720 and 1025 rpm, varying raveling speeds (25, 50, 75 mm/min) and tilt angles (1.5^0, 2^0 and 2.5^0) of similar and dissimilar weldments are shown in Figure 4.6 and Figure 5.1 of chapter 5. The joints produced were good in quality and defect-free with respect to processing parameters. As shown in Figure 4.2 (SEM image) flaws were observed for the samples welded at the condition of 1525 rpm rotational speed irrespective of the welding speed.

The tunnel form of the defect (Figure 4.2) was found in the weld for the tool rotational speed crosses 1025 rpm. Figure 4.2 shows the welding defects in stir zone at a fixed tool rotation speed, 1525 rpm and various traverse speed. There are small flaws that are generated in the advancing side of the stir zone called the tunnel defect. This might be due to low heat, reduced intensity of the residual stresses and inadequate plunge force.

Tunnel-hole defects are found more in the case of dissimilar FSWed alloys. Defect free weld quality samples were obtained using the process parameter of tilt angle of the tool between 1.5˚ and 2˚. In general, it was observed that the generated heat is not sufficient at low tool rotational speed and developed defective welded joints similar to those associated with the built-up edge formation in machine tool operations. At high tool rotational speed, the amount of heat generated increased which resulted in melting of the samples. The ranges for three process parameters were selected based on the trail experiments with the tool tilt angle of 1.5˚ to 2.5˚, rotational speed of 500 to 1025 rpm and welding speed of 25 to 75 mm/min and. Decision was made to use the process parameters at three levels to study any non-linear behavior. The process parameters considered during the experimentation are given in Table 4.2.

Table 4.1 Results of pilot experiments

Experimental Trial No.	Rotational speed (rpm)	Welding speed (mm/min)	Tilt angle (degree)	Observation
1	500	25	1.5	Defect free
2	500	50	2	Defect free
3	500	75	2.5	Defect free
4	720	25	2	Defect free
5	720	50	2.5	Defect free
6	720	75	1.5	Defect free
7	1025	25	2.5	Defect free
8	1025	50	1.5	Defect free
9	1025	75	2	Defect free
10	1525	25	1.5	Defective
11	1525	50	2	Defective
12	1525	75	2.5	Defective

Table 4.2 Working range of the chosen process variables

Process Parameter	**Rotational Speed (rpm)**	**Welding Speed (mm/min)**	**Tool Tilt Angle (degree)**
Level 1	500	25	1.5
Level 2	720	50	2
Level 3	1025	75	2.5

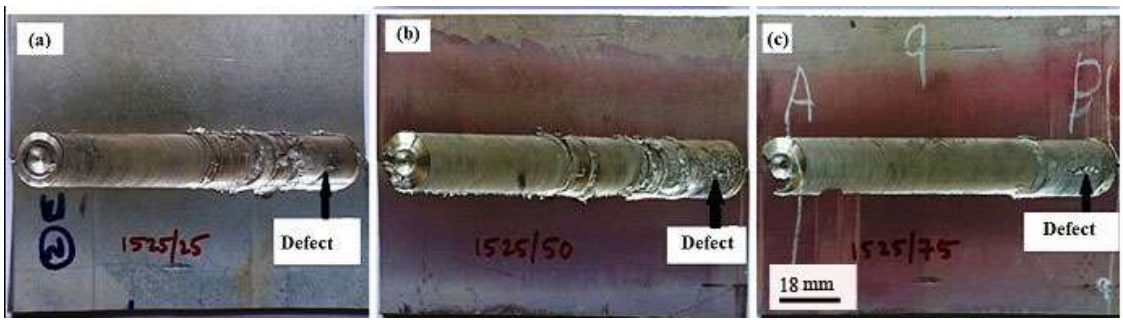

Figure 4.1 Surface appearances of AZ91 Mg alloy weldments at various welding conditions, 1525 rpm at (a) 25 mm/min, (b) 50 mm/min, and (c) 75 mm/min.

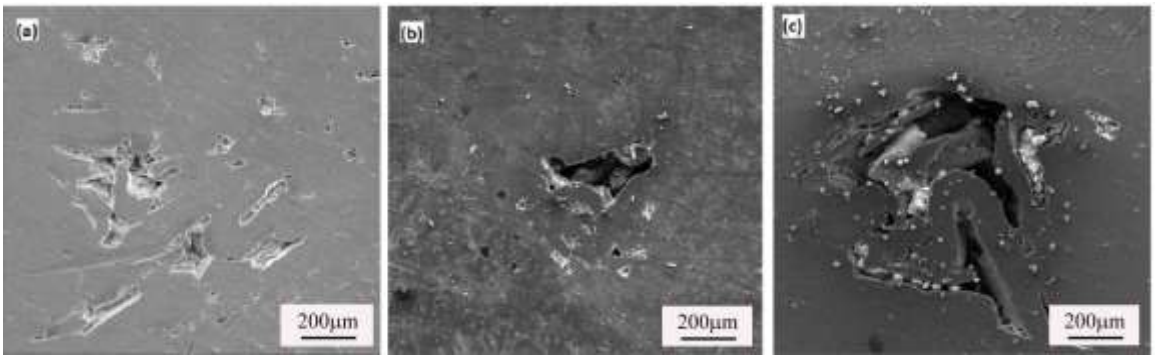

Figure 4.2 SEM images of the AZ91 Mg alloy weldment FSWed at the condition 1525 rpm (a) 25mm/min, (b) 50 mm/min, (c) 75mm/min.

4. 3 Microstructural Developments

4. 3. 1 Microstructure of the Parent Alloy

Figure 4.3 shows the SEM microstructure of AZ91 and AZ31 Magnesium alloy (parental alloys) which reveals mixture of primary α-phase and β-intermetallic compounds (eutectic β ($Al_{12}Mg_{17}$)). However, the volume fraction of β phase in AZ31C was found to be lower than AZ91D.

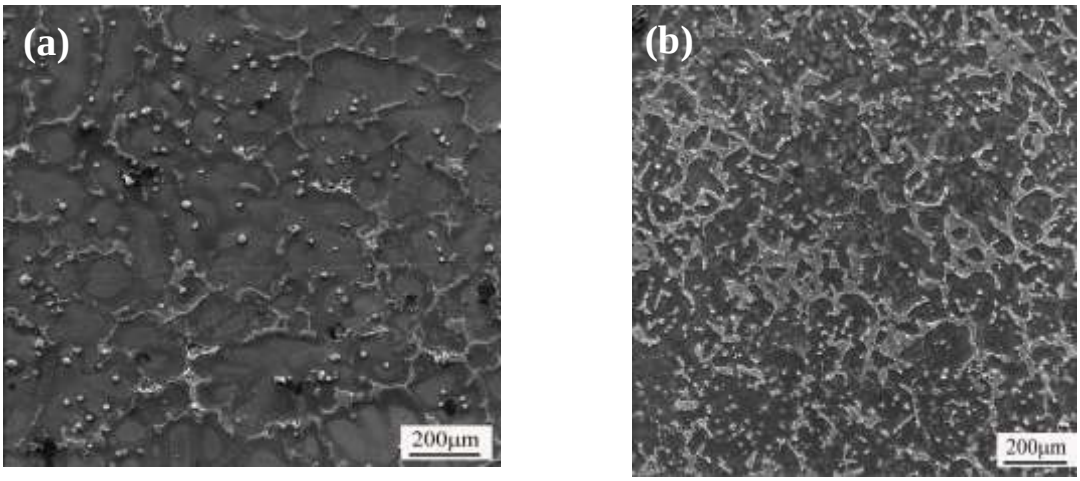

Figure 4.3 SEM micrograph of (a) AZ91D Mg alloy (b) AZ31C Mg alloy in the received condition.

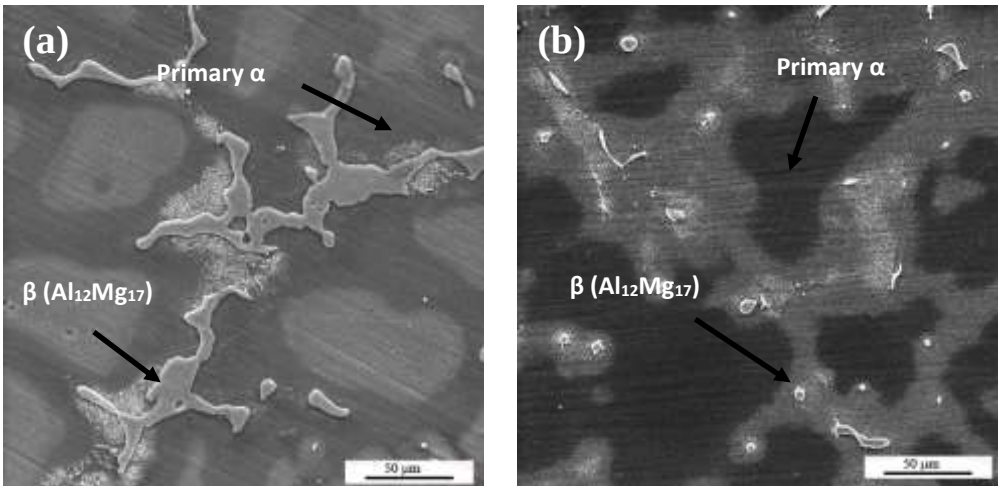

Figure 4.4 SEM micrograph of (a) AZ91D Mg alloy (b) AZ31C Mg alloy in the received condition & (c) & (d) corresponding images at higher magnification (500X).

From Figure 4.5 and Table 4.3 the EDS analysis the following observation has been made

i. Both AZ91D alloy and AZ31C alloy revealed that primary α phase was rich in Mg.

ii. Eutectic α phase in AZ91D alloy had more aluminum and less zinc as compared to AZ31C alloy.

iii. Both AZ91D alloy and AZ31C alloy revealed Mg, Al and Zn in the β secondary phase particles. It indicates that the secondary phase is an intermetallic.

iv. β secondary phase in AZ91D alloy showed higher Al and lower Zn content and AZ31C alloy showed lower Al and higher Zn content.

v. The above said points have been supported by the SEM images of the AZ91D Mg alloy and AZ31C alloy ie the volume fraction of the β precipitate was found to be more in AZ91D Mg alloy than in AZ31C alloy.

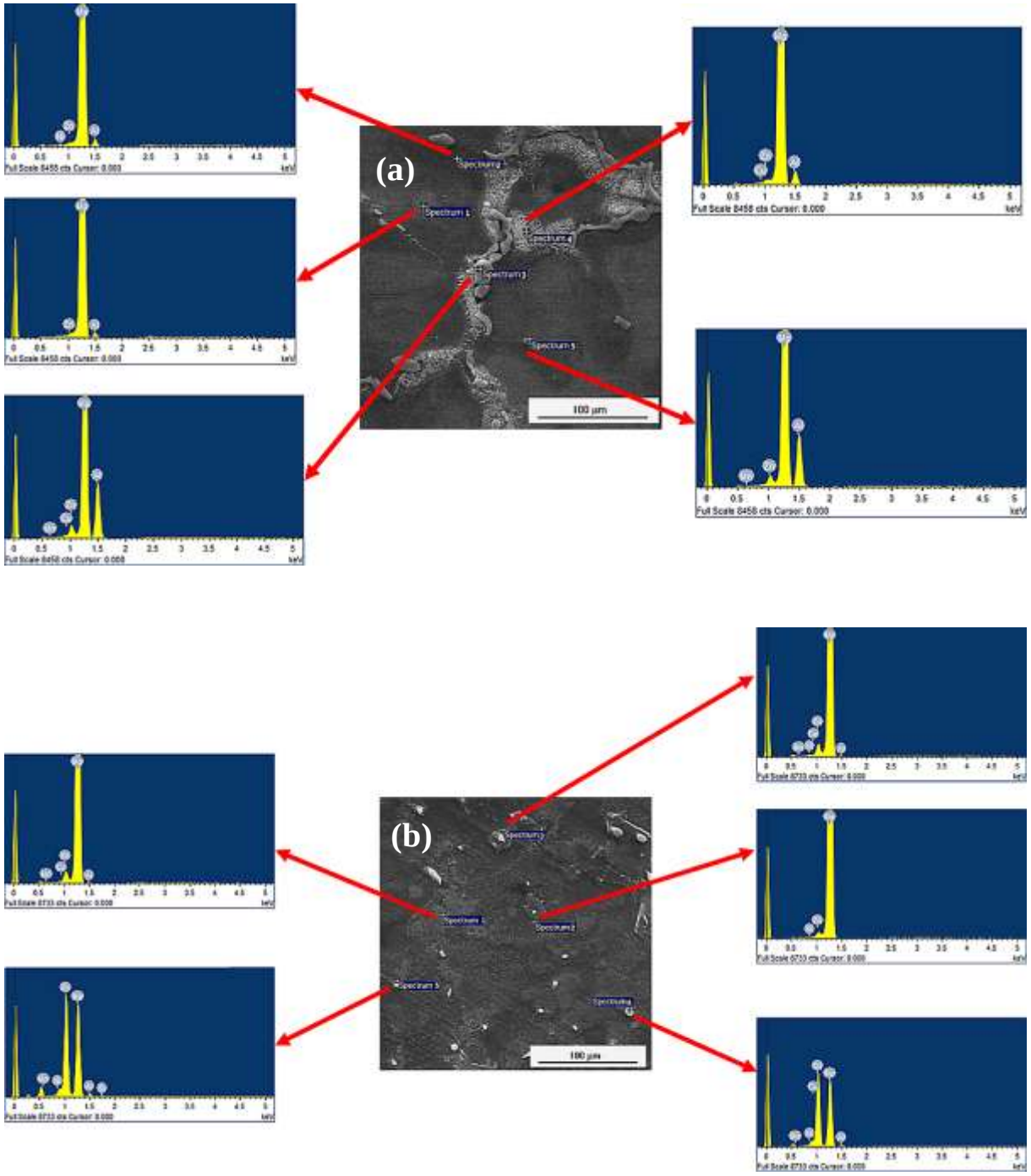

Figure 4.5 SEM micrographs showing locations for EDS analysis for (a) as received AZ91D Mg alloy and (b) as received AZ31Mg alloy.

Table 4.3. EDS elemental analysis of as received AZ91D Mg alloy and AZ31Mg alloy (Mass %).

S No.	Element	AZ91D Mg alloy Spectrum					AZ31C Mg alloy Spectrum				
		1 Eutectic α	2 Primary α	3 β	4 Eutectic mixture	5 β	1 Eutectic α	2 Primary α	3 Primary α	4 β	5 β
1	Mg	94.9	92.2	60.1	87.4	66.0	94.8	97.6	95.0	57.8	59.58
2	Al	4.7	7.17	36.5	11.6	31.7	0.84	0.23	0.57	1.9	2.75
3	Si	---	0.02	0.04	0.07	0.05	0.04	0.11	0.07	0.09	0.56
4	Mn	---	---	0.03	---	0.04	0.08	---	0.06	0.02	0.06
5	Ni	---	0.03	---	---	---	---	0.07	0.06	0.06	0.06
6	Cu	---	---	0.01	0.02	---	0.01	---	0.13	0.05	---
7	Zn	0.30	0.50	3.2	0.80	2.19	4.17	1.90	4.04	39.9	36.99
	Total	100	100	100	100	100	100	100	100	100	100

4. 3. 2 Macrostructure of the Similar FSWed AZ91 Mg Alloy to AZ91 Mg Alloy

The butt welding joints were produced with varying rotational speeds of 500 to 1025 rpm, varying traverse speeds (25 to 75 mm/min), and tilt angles (1.5^0, 2^0 and 2.5^0) are shown in Figure 4.6.The joints produced were good in quality and defect-free with respect to processing parameters. This has been confirmed through X-ray radiography and visual inspections performed on the FSW joints for determining defects generated during welding. Figure 4.7 shows the transverse cross sectional macrostructures of the similar joints welded at different processing parameters. The weld zone is wider at the top surface than at the bottom surface, because the top surface has experienced frictional heat and extreme deformation by contacting taper cylindrical tool shoulder with surface of the joint to be welded. The shape of the stir zone

is mostly like pin profile. The shape of nugget zone is influenced by pin profile, materials to be welded, and the rate of their thermal conductivity.

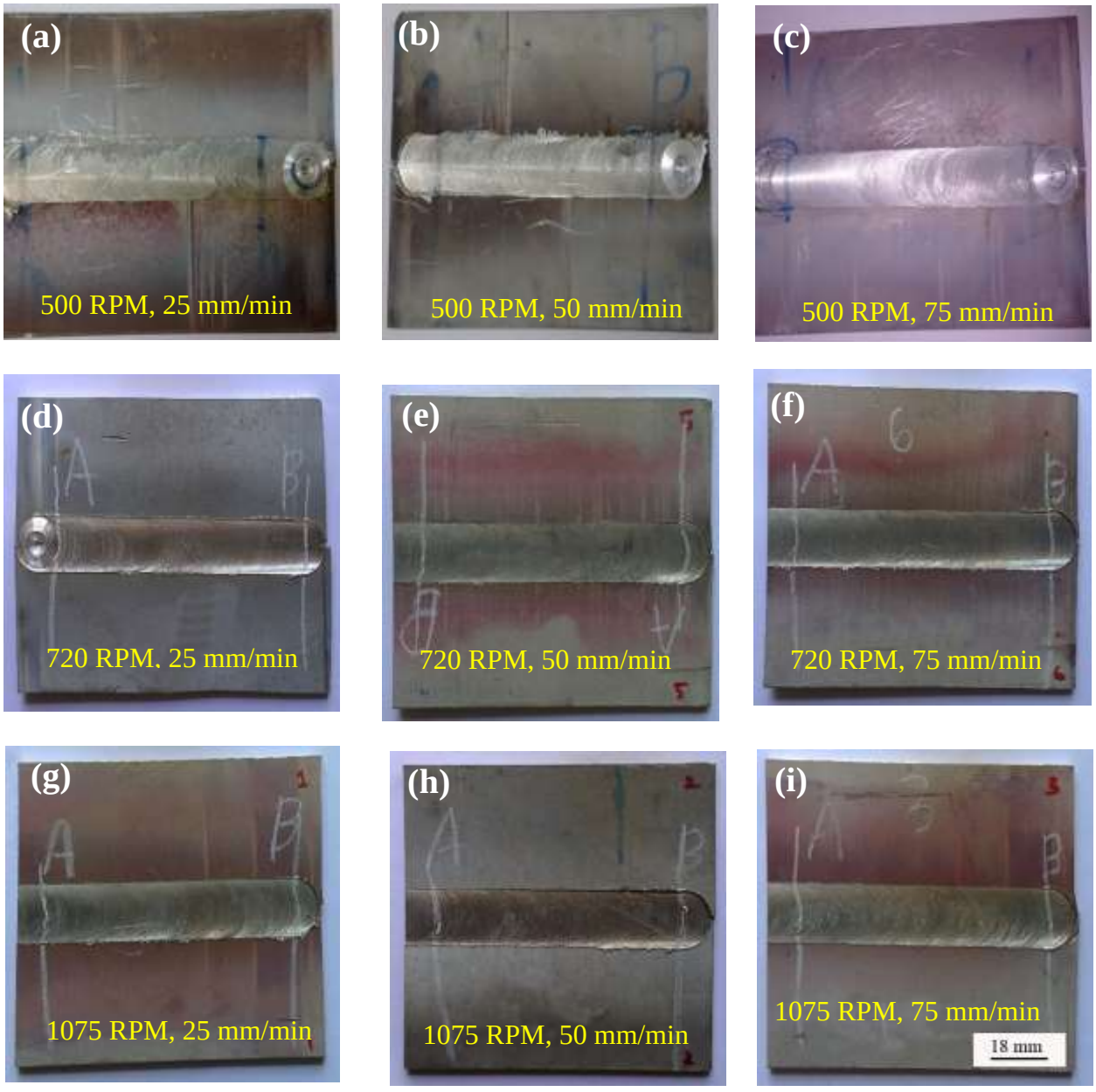

Figure 4.6 Surface appearances of similar welded AZ91 Mg alloy weldments at different welding conditions.

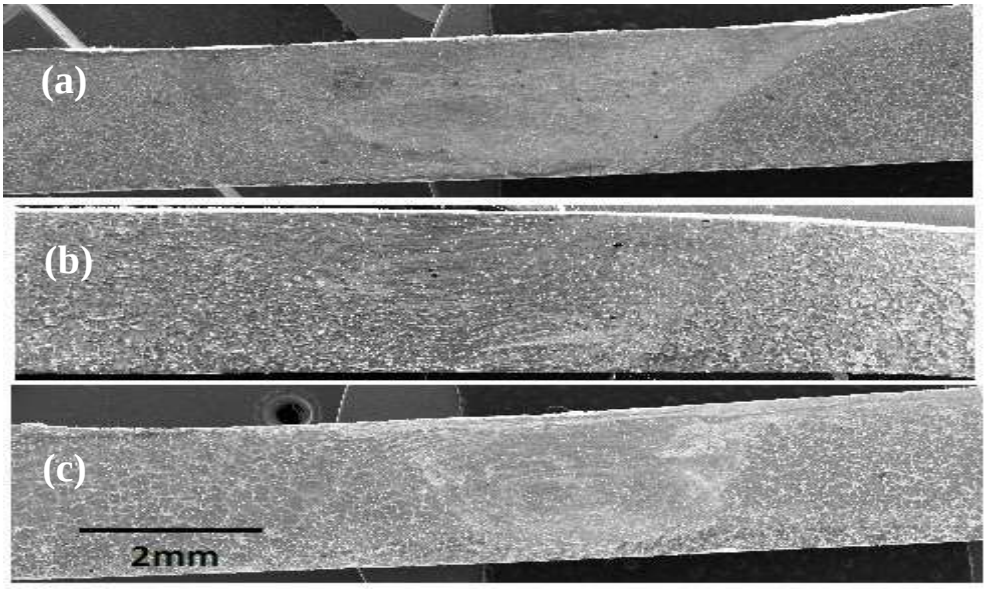

Figure 4.7. Macrostructures of similar welded AZ91 Mg alloy of cross section of the joints welded at 1025 rpm at (a) 25 mm/min, (b) 50 mm/min, and (c) 75 mm/min.

4. 3. 3 Development of Microstructure in the Different Weld Zones of Similar Weldments

SEM microstructures of the various zones of the weldments prepared with different tool rotational speed, weld speeds and tool tilt angle are shown in Figure 4.8 to 4.16.

The welds consist of three regions with different structural morphology namely heat affected zone (HAZ), Thermo-mechanically affected zone (TMAZ), and (c) stir zone (SZ).

Each zone exhibits unique features of microstructure, based on different thermal and mechanical conditions experienced by each zone. Since HAZ experiences heating and cooling cycles, with a maximum temperature below the melting point, grains are coarse in size and shows the secondary phase β intermetallics in primary α magnesium solid solution matrix. β phases is surrounded by the eutectic mixture. Volume fraction of β decreases on increasing the traverse speed at any constant rotation speed.

Since in TMAZ, the grains not only undergoes the thermal effect but also the plastic deformation. The zone composed of partially recrystallization grains and β intermetallics and the morphology of eutectic β was entirely different from the TMAZ. The eutectic morphology got disappeared due to dissolution of eutectic mixture and β intermetallics coarse network also got broken into small particles. Both near spherical and elongated particles were observed and

were located around the tool rotation direction in TMAZ. In case of SZ, the dendrite structure of base material has completely disappeared in the stir zone and fine equiaxed grain structure was observed due to the fragmentation of the β and simultaneous plastic deformation and dynamic recrystallization.

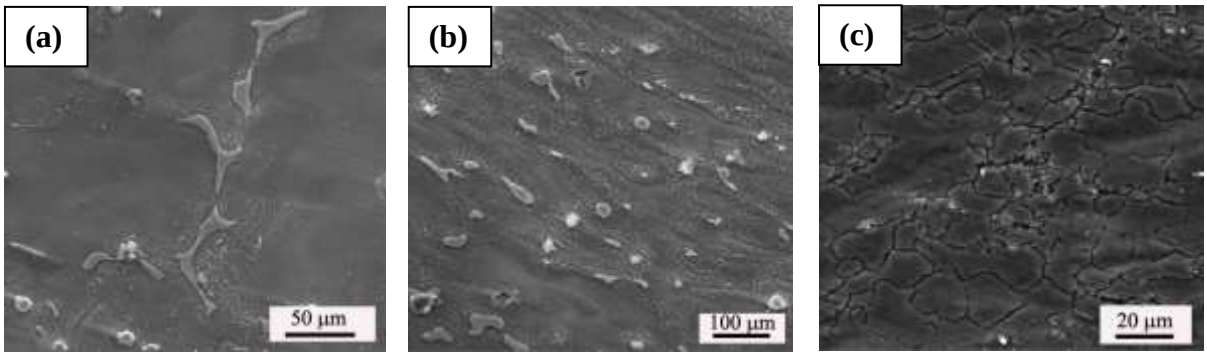

Figure 4.8 SEM micrographs of AZ91D Mg alloy weldment of condition 500 rpm, 25 mm/min at (a) HAZ, (b) TMAZ, (c) SZ.

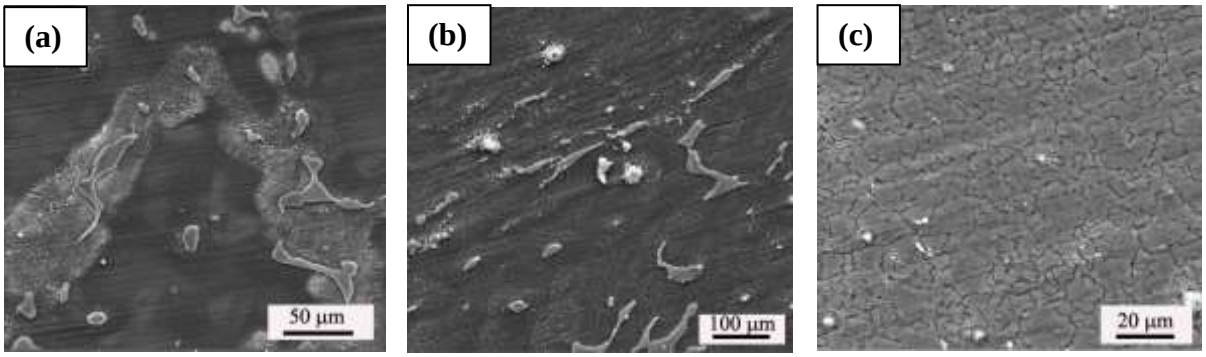

Figure 4.9 SEM micrographs of AZ91D Mg alloy weldment of condition 500 rpm, 50 mm/min at (a) HAZ, (b) TMAZ, (c) SZ.

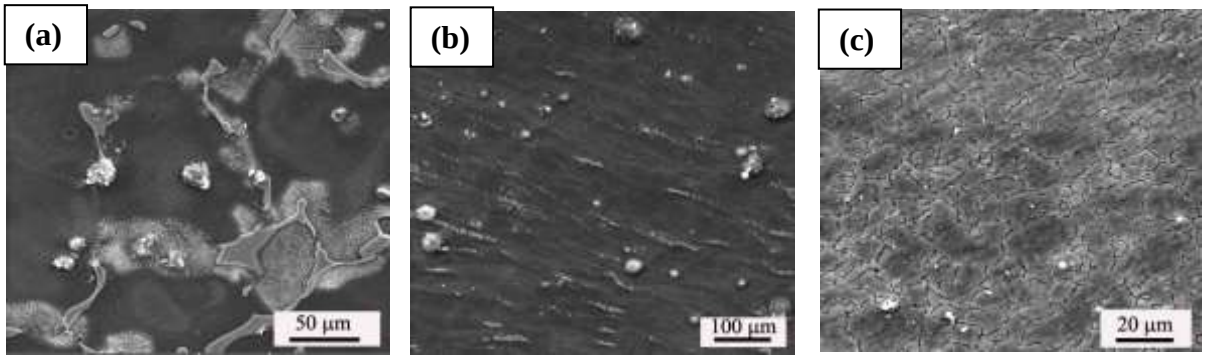

Figure 4.10 SEM micrographs of AZ91D Mg alloy weldment of condition 500 rpm, 75 mm/min at (a) HAZ, (b) TMAZ, (c) SZ.

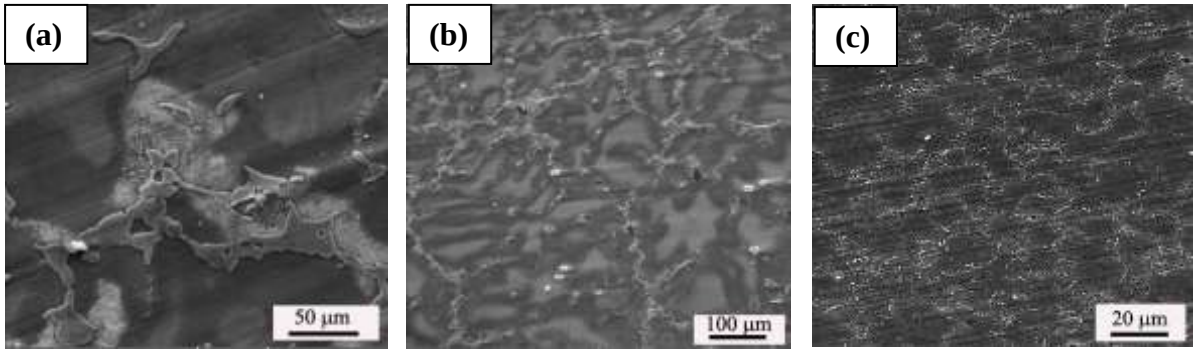

Figure 4.11 SEM micrographs of AZ91D Mg alloy weldment of condition 720 rpm, 25 mm/min at (a) HAZ, (b) TMAZ, (c) SZ

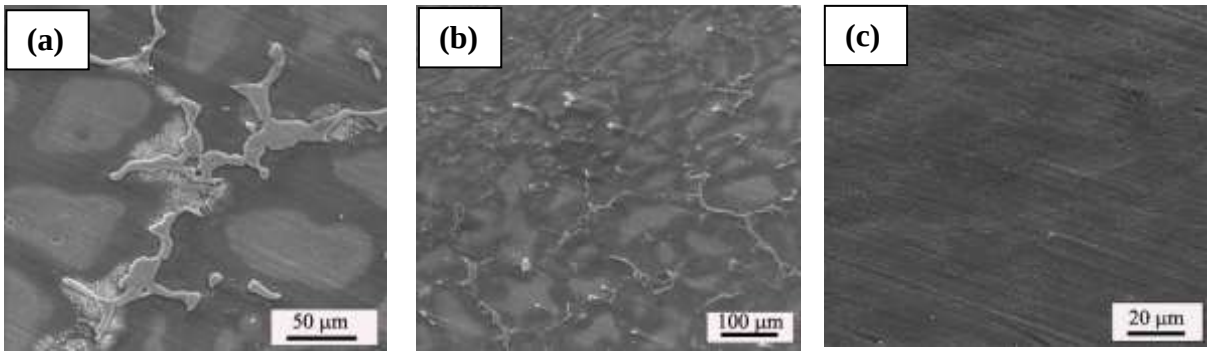

Figure 4.12 SEM micrographs of AZ91D Mg alloy weldment of condition 720 rpm, 50 mm/min at (a) HAZ, (b) TMAZ, (c) SZ.

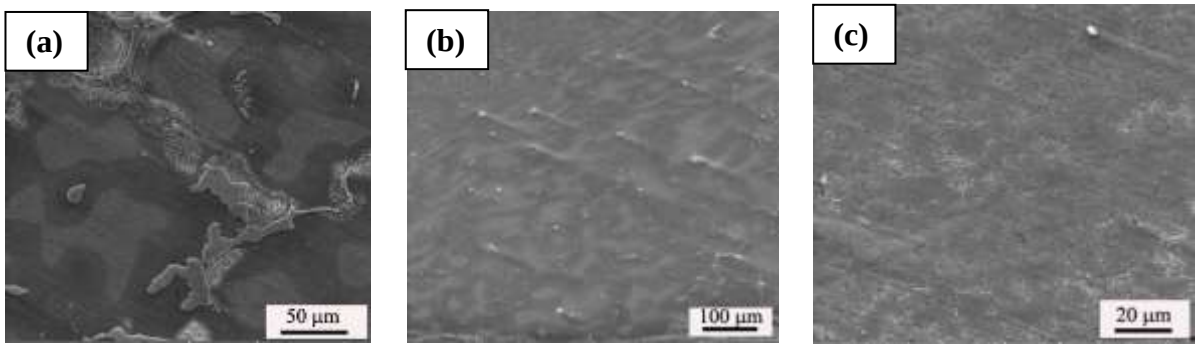

Figure 4.13 SEM micrographs of AZ91D Mg alloy weldment of condition 720 rpm, 75 mm/min at (a) HAZ, (b) TMAZ, (c) SZ.

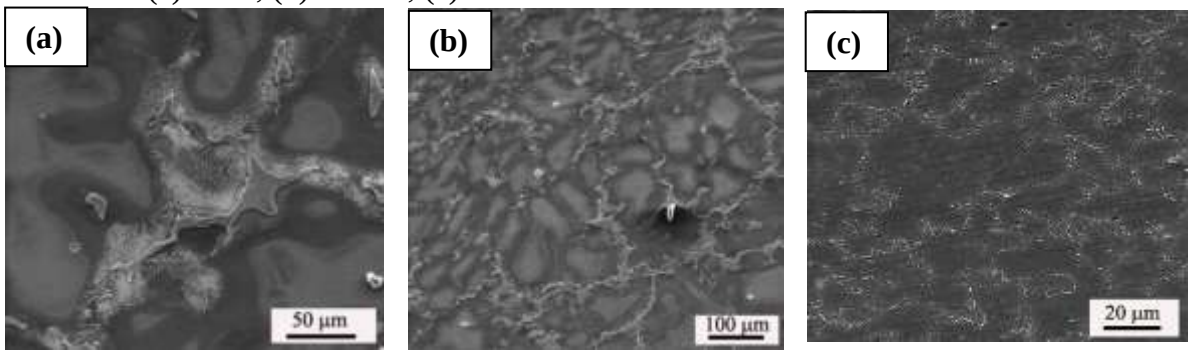

Figure 4.14 SEM micrographs of AZ91D Mg alloy weldment of condition 1025 rpm, 25 mm/min at (a) HAZ, (b) TMAZ, (c) SZ

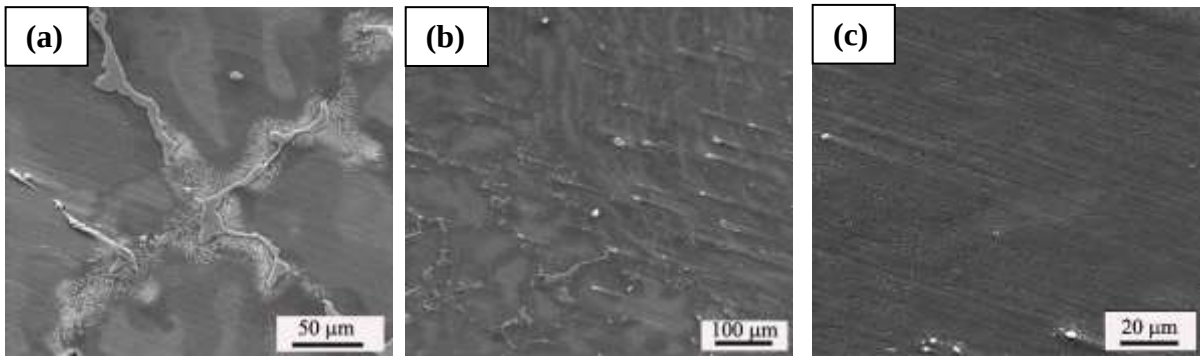

Figure 4.15 SEM micrographs of AZ91D Mg alloy weldment of condition 1025 rpm, 50 mm/min at (a) HAZ, (b) TMAZ, (c) SZ

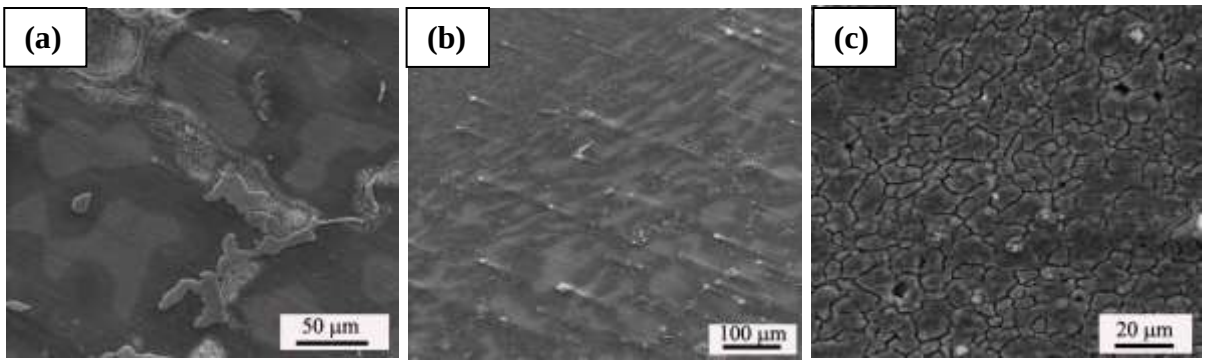

Figure 4.16 SEM micrographs of AZ91D Mg alloy weldment of condition 1025 rpm, 75 mm/min at (a) HAZ, (b) TMAZ, (c) SZ

Moreover, each stir zone had shown different grain size with an increase in welding speed. Figure 4.17 shows the variation of grain size with varying welding speeds and tool rotational speeds. This trend can be expressed in the form of equation Q/V, i.e. heat input per unit length, where Q is heat generated due to friction between tool and material to be welded and V is the welding or traverse speed. The heat generation "Q" increases as tool rotational speed increases [106].

As a consequence, at lower welding speeds the heat input increases. The grain size is coarser at lower welding speeds due to the enhancement of heat input, which promotes the growth of recrystallization of the grains. Figure 4.18 illustrates the XRD patterns of base material and FSW specimens, and the presence of α-phase and β ($Mg_{17}Al_{12}$) phases are confirmed. Process parameters of the friction stir welding are responsible for the different phases formed in the microstructure of the welded plates. Welding speed increases the particle distribution and occupies major role in the phase formation of the welded plate.

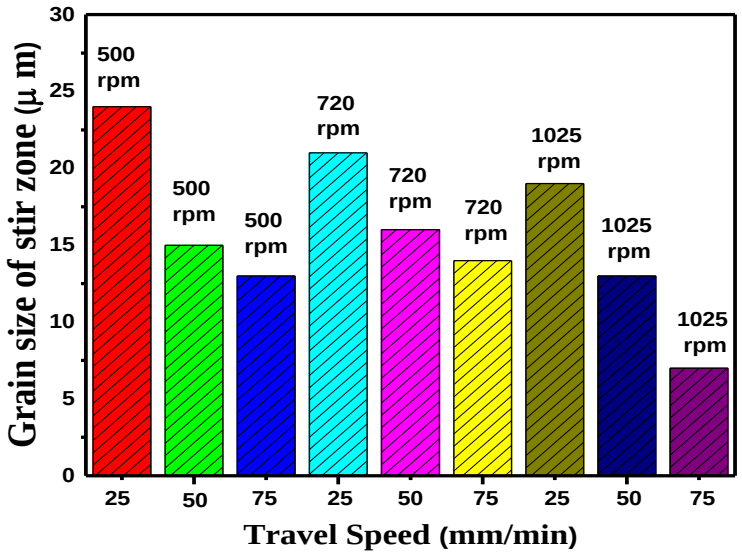

Figure 4.17 Grain size variations with varying welding speeds.

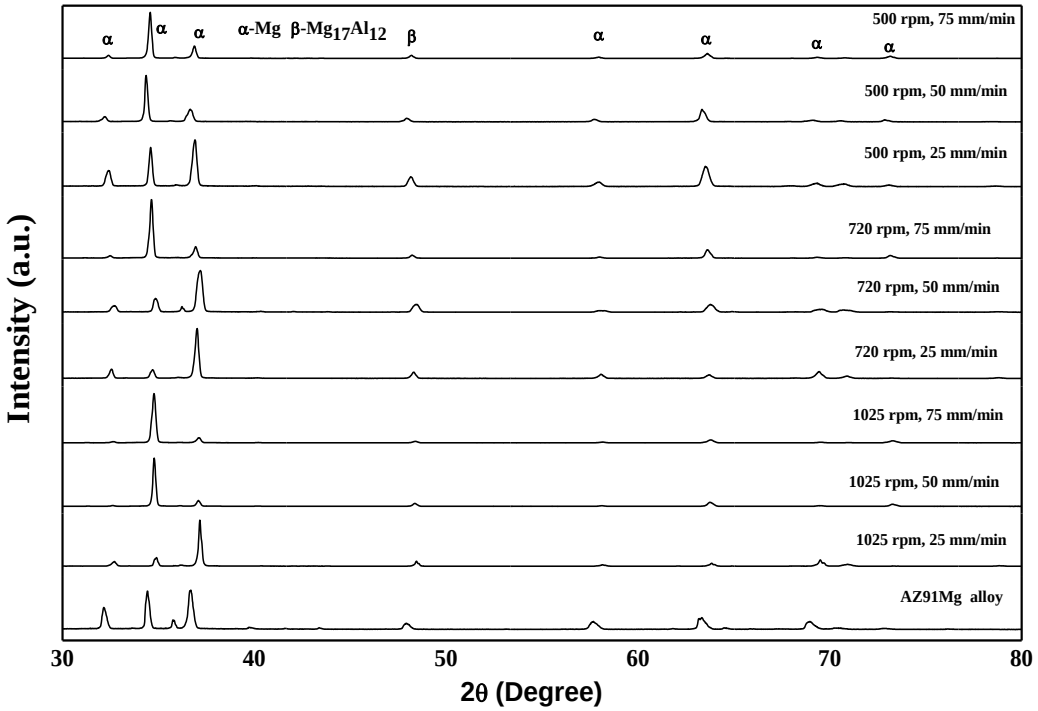

Figure 4.18 XRD patterns of parent alloy (AZ91 Mg alloy) and weldments.

4. 4 Microhardness Measurements of Similar Weldments

Figure 4.19 shows micro hardness profile of similar welded specimens (AZ91D- AZ91D Mg alloy) of transverse section of the sample at different welding conditions of 25, 50, and 75 mm/min traverse speed 500 to 1025 rpm tool rotation speed respectively.

The hardness of parental material (AZ91Mg alloy) is about 68 HV. Irrespective of the weld parameter the weld center or the stir zone revealed the maximum hardness and then got decreased on increasing distance from the weld center and turned minimum in the heat affected zone. Overall the weldment showed higher hardness than the base alloy.

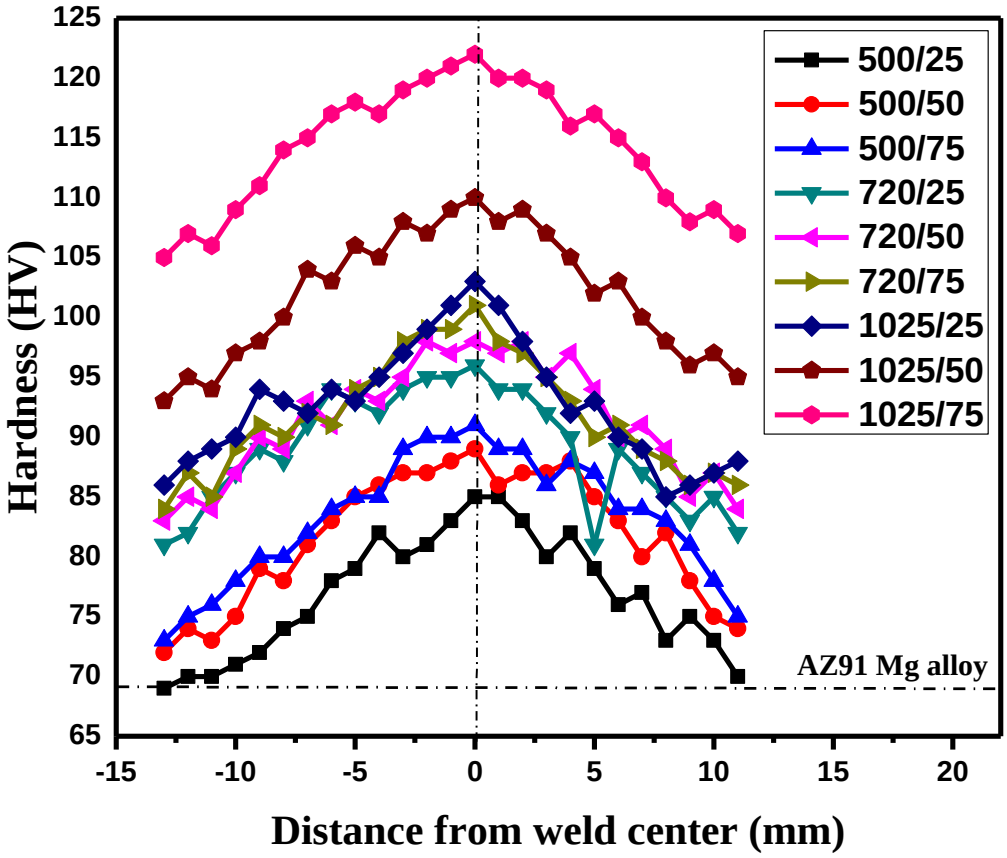

Figure 4.19. Hardness profiles of the similar weldments (AZ91Mg alloy to AZ91Mg alloy) at various processing parameters.

Among all the weld conditions, sample welded at 1025 rpm, 75 mm/min showed the maximum hardness of 122 HV and the sample welded at 500 rpm, 25 mm/min showed the maximum hardness of 85 at the center or in the stir zone.

Due to the stirring action β intermetallic compound dissolves in α-matrix which is softer than the β phase and leads to the solid solution strengthening. In addition to the solid solution effect heat produced due to the friction action of the tool pin especially on high rotation speed provides the dynamically recrystallized, fine and eqiaxed grains which leads to the maximum hardness at the at the center or in the stir zone. TMAZ shows the lower hardness compared to the stir zone due to the coarse grains. HAZ revealed the coarse grain due to low cooling rate and still its hardness is better than base alloy.

At constant rotation speed, on increasing the traverse speed the hardness is high due to the high cooling rate which leads to fine grain size. At constant traverse speed increasing the rotational speed, heat generated is sufficient the cause plastic flow easily and fragment the grains into finer size. Parent alloy shows the poor hardness compared with the welded samples due to the coarse grain nature of the α grains and the β network intermetallics or on the other hand the hardness range was wide cause of the different phases present in base material (Mg solid solution (eutectic α phase) and β intermetallic compounds (eutectic β ($Al_{12}Mg_{17}$)).

4. 5 Tensile Properties of Similar Weldments

Figure 4.20 and 4.21 shows the effect of welding speed on tensile strength and ductility of welded specimens. The base metal in as-cast conditions exhibited lower tensile strength (109 MPa) and elongation (EL) of 3 % as compared to weldments [107]. The friction stir welded plate which was processed at the welding speed of 50 mm/min, 1025 rpm showed maximum ultimate tensile strength of 178 MPa and higher elongation of 11 % , which is about 63 % and 262 % greater than the tensile strength and elongation of parent alloy. The tensile strength and ductility of friction stir welded plates processed at welding speed of 25 mm/min,720 rpm is 120 MPa, and 7 % respectively. However, there was a significant improvement in tensile strength as a function of welding speed. The elongation noticeably changed as a function of the welding speed, although a maximum elongation of about 11 % was obtained at the welding speed of 50 mm/min. The friction stir welded plate processed at the welding speed of 50 mm/min, 1025 rpm showed higher tensile strength is attributed to the particle distribution and grain refinement. The welding speed of the process is responsible for the particle distribution and the grain refinement [108-110]. The other hand friction stir welded plate processed at the

welding speed of 25 mm/min , 720 rpm showed lower tensile strength due to the formation of brittle β ($Mg_{17}Al_{12}$) phase formation in the microstructure. Increasing the rotation speed the grains gets refined and increased the tensile strength. Increasing the weld speed resulted in the less heat input which led to the inhibition of the grain growth and improved the tensile strength. Fine disbursement of secondary phase particle and its distribution also added strength to the above said mechanism. In addition to the increase in tensile strength the ductility also increased due to the breakage of the coarse β intermetallics into fine particles as shown in Figure 4.21.

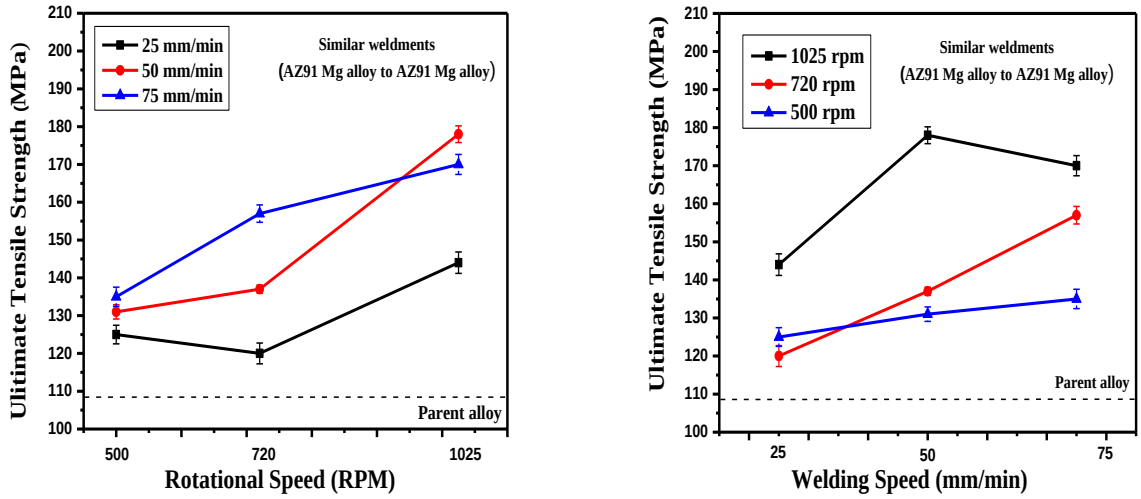

Figure 4.20. Effect of the rotation speed and welding speed on the tensile strength of similar weldments.

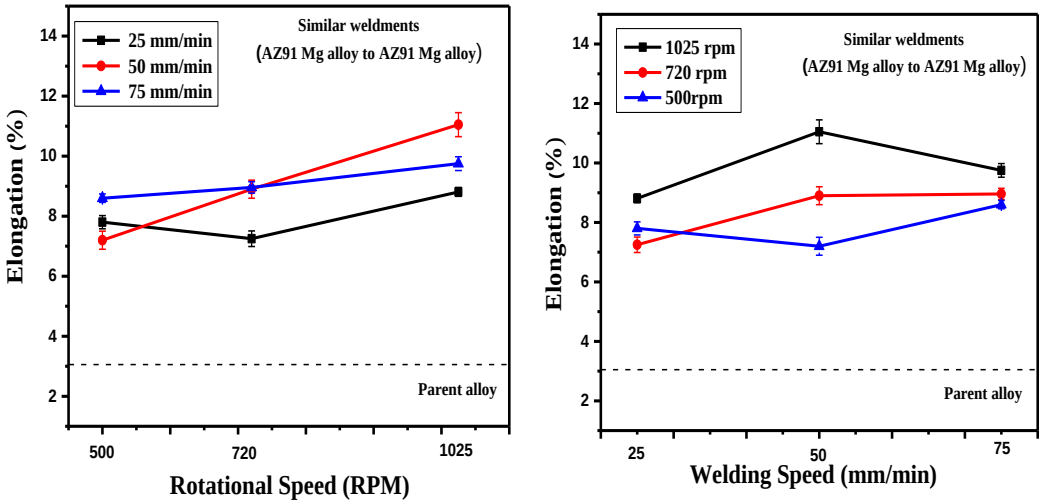

Figure 4.21. Effect of the rotation speed and welding speed on elongation of similar weldments.

Table 4.4 Mechanical properties of parent alloy and similar (AZ91D to AZ91 D Mg alloy) weldments.

S No.	**Welding Condition**	**UTS* (MPa)**	**% El***	**Impact* strength (J/mm^2)**
1	AZ91DMg alloy (As received)	109	3.0483	0.580
2	500 rpm, 25 mm/min,1.5°	125	7.8	0.661
3	500 rpm, 50 mm/min, 2°	131	7.2	0.670
4	500 rpm, 75 mm/min,1.5°	135	8.6	0.728
5	720 rpm, 25 mm/min, 2°	120	7.25	0.642
6	720 rpm, 50 mm/min, 2.5°	137	8.9	0.662
7	720 rpm, 75 mm/min,1.5°	157	8.964	0.643
8	1025 rpm, 25 mm/min, 2.5°	144	8.815	0.605
9	1025 rpm, 50 mm/min,1.5°	178	11.05	0.588
10	1025 rpm, 75 mm/min, 2°	170	9.752	0.589

* Averge of three values

Figure 4.22 (a)-(j) show the SEM fractographic image of the surface of tensile fractured parent as well as weldment at different conditions. It indicated that fracture occurred at the interface of the weldment. Fractography of the SEM image revealed the river pattern and confirmed that that the mode of fracture is brittle in nature. The uneven distribution of eutectic β ($Al_{12}Mg_{17}$) and shrinkage defects present in the unaffected base material are responsible for preferential crack initiation. The some of the region showed presence of quasi-cleavage fractured surfaces and was also observed that crack initiated at β intermetallics and propagated along the grain boundary.

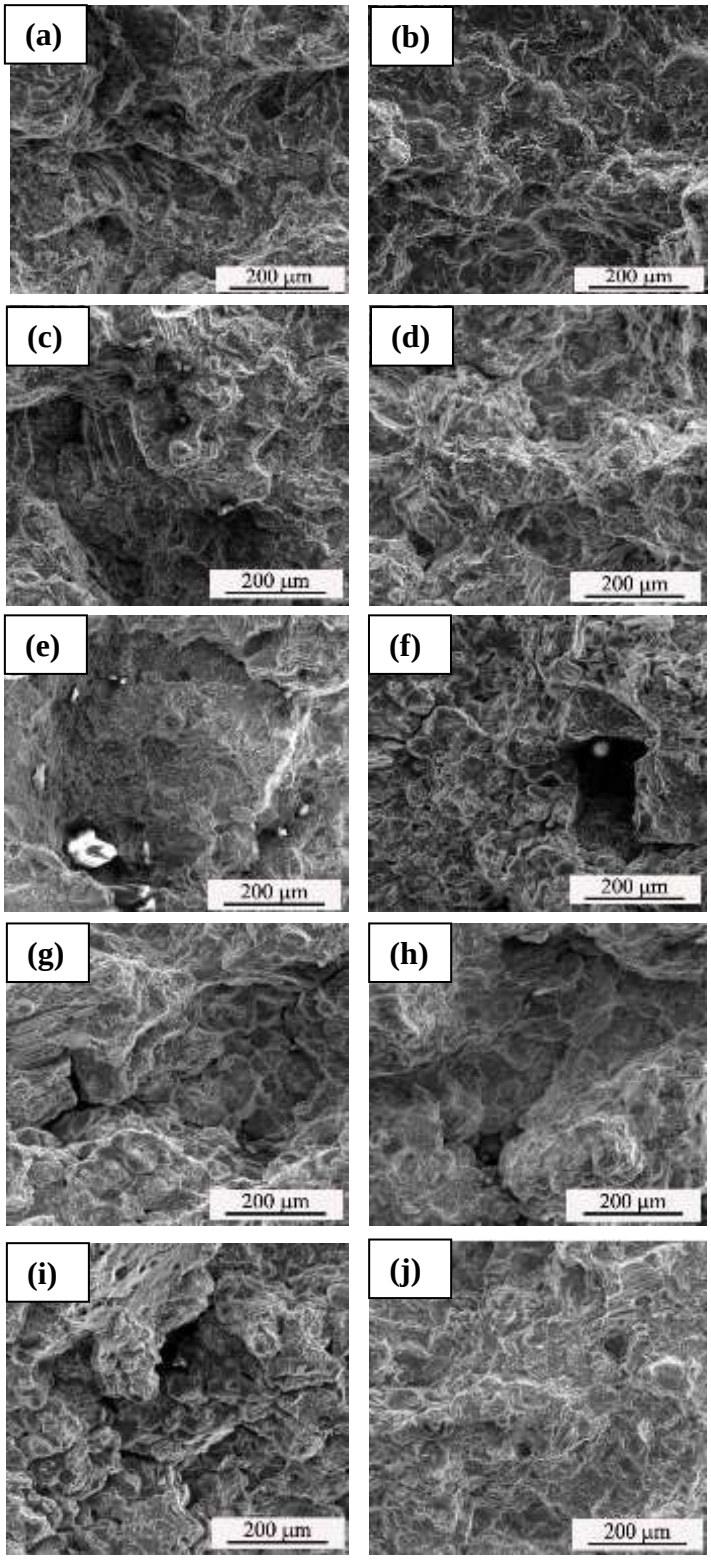

Figure 4.22 SEM images of fractured surface of tensile specimens (a) AZ91D Mg alloy (b) 1025 rpm, 25 mm/min, (c) 1025 rpm, 50 mm/min, (d) 1025 rpm, 75 mm/min (e) 720 rpm, 25 mm/min, (f) 720 rpm, 50 mm/min (g) 720 rpm, 75 mm/min (h) 500 rpm, 25 mm/min (i) 500 rpm, 50 mm/min (j) 500 rpm, 75 mm/min showing brittle mode of fracture.

4. 6 Impact Properties of Similar Weldments

The effect of welding speed and rotational speed on impact strength has been given in Figure 4.23 and Figure 4.24. Samples welded at low rotational speed and low traverse speed showed the high imact strength as compared to the high rotational and traverse speed. It's a expected fact that higher the strength lower will be the impact energy. However the increment in the absorbed energy before the fracture is very low and hence it can be recorded that both rotational and traverse speed has not affected the impact strength much and remain almost same values.

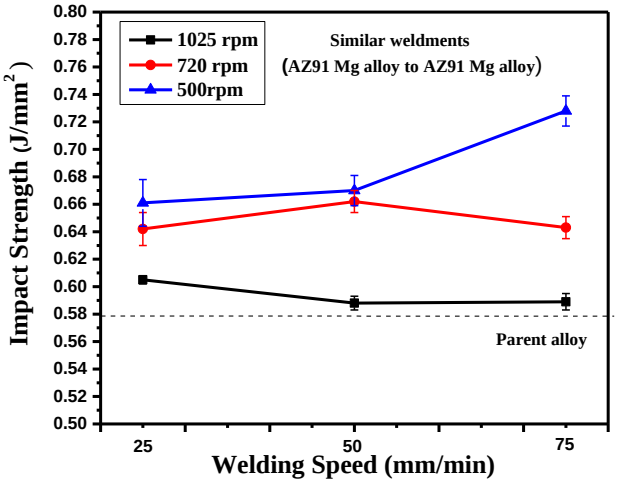

Figure 4.23 Influence of welding speed on the impact strength of similar weldments.

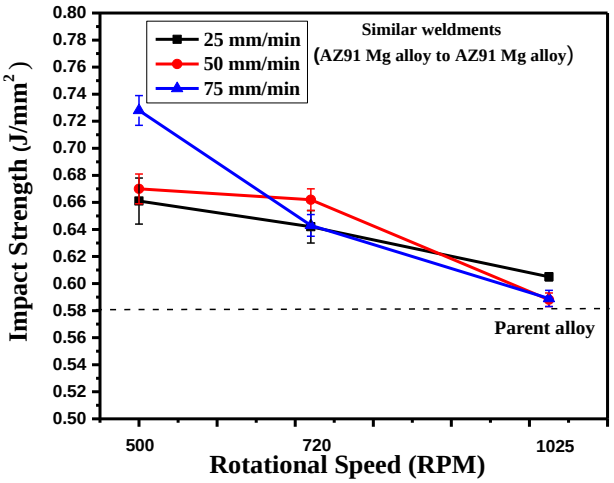

Figure 4.24 Influence of rotational speed on the impact strength of similar weldments.

4. 7 Optimization of Process Parameter Using Taguchi Method

A most popular software MINITAB- 17 was used to design and analysis the experiments. In this analysis, the Taguchi array selection, ANOVA and regression replicas were developed. The optimization of FSW welding exercise parameters by this software to know the effect of each welding exercise parameters on the output mechanical properties. From the ANOVA analysis, the contributions of each process parameter and its significance on the mechanical properties have been studied.

4. 7. 1 The Signal-to-Noise (S/N) Ratio Analysis for Responses

For the analysis of the results, Taguchi suggested a logarithmic conversion of mean square deviation, known a signal-to-noise (S/N) ratio. In this present study, the S/N ratio was selected to maximize the mechanical properties, for this the "Larger-the better" criterion has been selected and the formula is given in Eq. 5.1

$$N = -10\text{Log}\left(\left(\frac{1}{n}\right)\sum\frac{1}{(yi.)^2}\right) \qquad (5.1)$$

Where '$\mathbf{y_i}$' -The experimental value of the i^{th} experiment, and 'n' - denotes the number of experiments. In this present study, the influence of each FSW process parameters on the properties such as tensile strength, percent elongation, impact strength, and microhardness were analyzed.

4. 7. 2 Effect on Mechanical Properties of Similar Weldments by Process Parameters

The ultimate tensile strength (UTS), ductility in terms of % of elongation (% EL) and impact strength (IS) of the parent metal and welded joints of similar weldments were estimated and depicted in Table 4.4.

It was noted from results that the IS of the FSW joints is not greatly improved. The joint made at processing condition 500 rpm, 50 mm/min, 1.5º resulted in higher impact strength compared to all other condition of joints. The tensile strength and percentage of elongation of the weldments significantly compared to parent AZ91 Mg alloy. The joint made at processing

condition at processing condition 1025 rpm, 50 mm/min, 1.5º exhibit significance tensile strength and percentage elongation compared to other joints welded at different process parameters condition. The better ductility was noticed at weld zone when compared to other welded joints due to fine grains.

4. 7. 2. 1. Ultimate Tensile Strength

To study the effect of rotational speed (RS), welding speed, traverse speed, and tool tilt angle (TTA), the UTS of similar welds is examined. The primer effects for mean and S/N ratio are mapped as shown in Figure 4.25 and Figure 4.26 respectively.

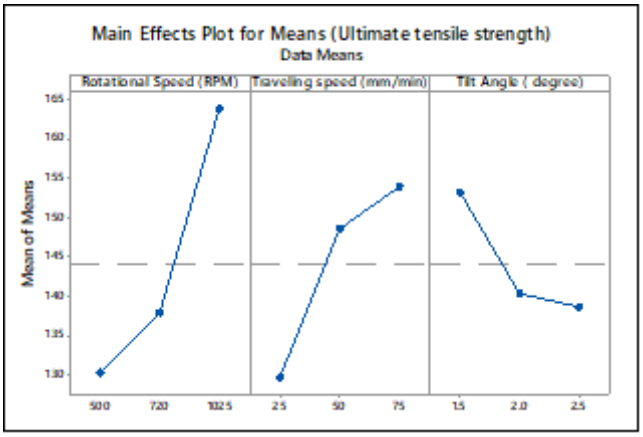

Figure 4.25 Effects plot for means of similar weldments (UTS)

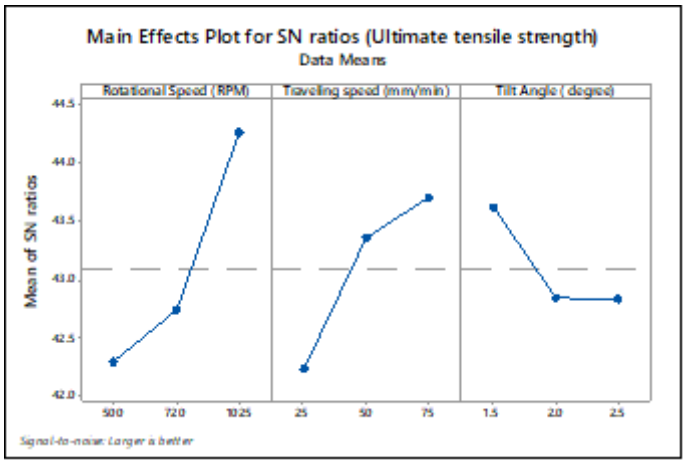

Figure 4.26 Effects plot for S/N ratio of similar weldments (UTS)

It is noticed the greater S/N ratio expressed that to improved characteristics of quality. Hence the optimum level of processing parameters is the highest value of the S/N ratio. The mean and S/N ratio results indicated that the UTS is at the higher at level 1 for rotational speed, level 2 for traverse speed, and level 3 for tool tilt angle. This means that the rotational speed is 1025 rpm, the traverse speed is 75 mm/min and the tilt angle of the tool is 1.5º.

4. 7. 2. 2. Percentage Elongation

To study the effect of RS, TS, and TTA, the percentage of elongation of similar welds is examined. The effects are plotted for mean and S/N ratio in Figure 4.27 and Figure 4.28 correspondingly.

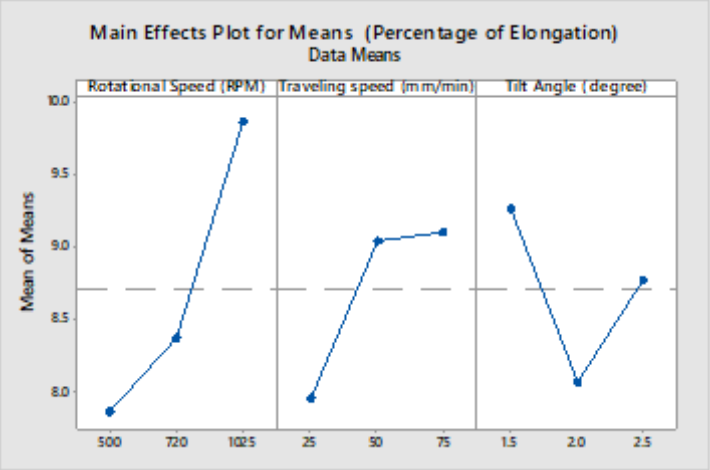

Figure 4.27 Effects plot for means of similar weldments (%EL)

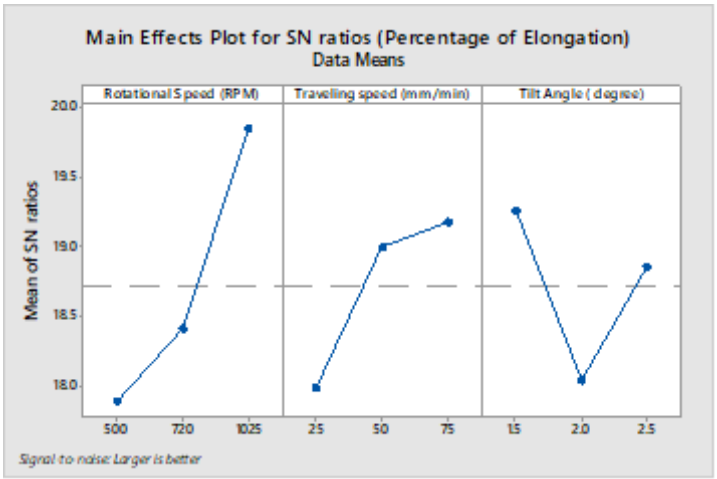

Figure 4.28 Effects plot for S/N ratio of similar weldments (%EL)

Both mean and S/N ratio values stated that the % of EL is at highest for RS at level 1, TS at level 3 and TTA at level 2. This means that the rotational speed is 1025 rpm, the travel speed is 75 mm / min and the tilt angle of the tool is 1.5°.

4. 7. 2. 3. Impact Strength

The effect of rotational speed, welding speed, tool tilt angle, and the impact strength of similar welds was examined. The effects are mapped in Figure 4.29 and Figure 4.30 for mean and S/N ratio respectively.

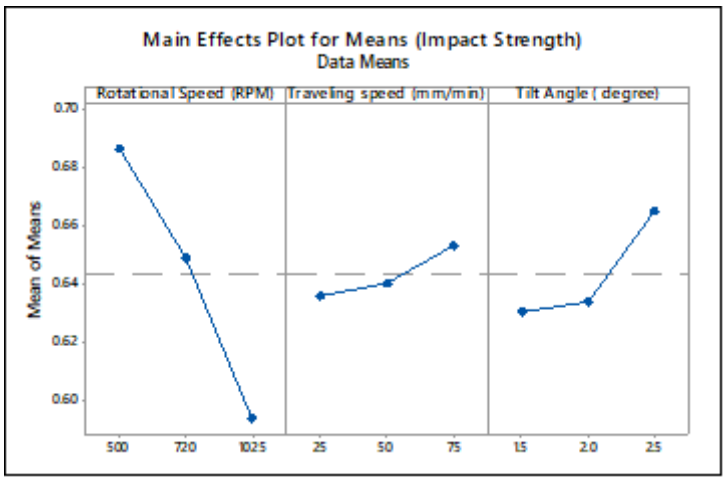

Figure 4.29 Effects plot for Mean of similar weldments (IS)

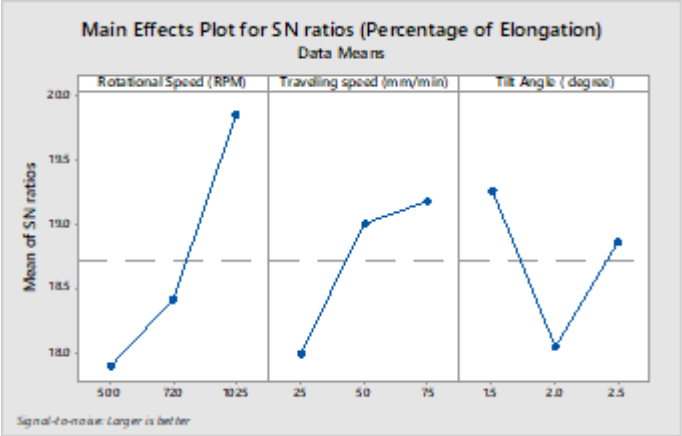

Figure 4.30 Effects plot for S/N ratio of similar weldments (IS)

Both mean and S/N ratio values showed that the IS is at highest for RS at level 1, TS at level 3 and TTA at level 2. This means that the RS is 500rpm, the TS is 75mm/min and the TTA of the tool is 2.5º. The optimizationof test parameters by the help of a Taguchi method makes it possible to assess the effects of individual elements on notifythe quality characteristics independently of other elements. By identifying the S/N ratio for every factorat corresponding level the effect of each RS, welding speed, and TTA can be determined. 4.24 to 4.28 showed the main effect plots (mean and S/N ratios) of various responses, such as TS,%EL and IS. The combination of optimum parameters express the better mechanical properties, obtained from the analysis of main effect plots and are shown in Table 4.10.

Figures 4.25 to 4.28 show the main effect plot for UTS, and % EL. At a higher RS of 1025 rpm and a moderate TS of 75mm/min, the increase in UTS and % EL of the similar weld was found. The increased UTS of the similar weldments over the parent alloy is due to the grain refinement in the weld zone. Due to this reason, elongation of the friction stir welded specimens at elevated temperature has been improved as compared to parent alloy.

Figure 4.29 shows variation of the values of impact strength at various rotational speeds. It was noticed that at lower rotational speeds, the weldments showed higher impact strength compared to higher rotational speeds. This may be related to the frictional heat that causes matrix softening. The welding speed provides frictional heat to the work piece surface. The heat input rises with lower welding speeds. The size of grain is coarser at lower welding speeds due to increased heat input, which promotes the growth of grain recrystallization [106].

The is an essential test parameter to affects the material flow around the tool pin and the flow under the tool shoulder by helping the material behind the tool to consolidate [111]. The tool inclination angle helps to forge the material behind the tool shoulder [112]. At TTA (i.e., 1.5º and 2.5º), generally it was observed the UTS, %EL and Impact strength improved. This can be attributed to the presence of enough surface flash at the TTA and produces adequate metal in the stir zone [113]. The properties are enhanced at the moderate TTA, where the welding force on the pin is improved, allowing material flow to move across the pin and the shoulder of the tool properly [114].

4. 8 Analysis of Variance (ANOVA) of Tensile and Impact Properties of Similar Weldments

ANOVA is performed to determine the effect of factors on different quality characteristics of similar welds, and the results were depicted in Table 4.5. ANOVA results showed that RS and TS have a significant effect on tensile strength, percenta-ge of elongation, while traverse speed has a lower percentage of contribution on impact strength in comparison to RS and TTA. It is observed that lower values are considered to be the R^2 (Coefficient of correlation) values of all the built models. The calculated R^2 values for UTS, elongation and impact strength are 92.58, 94.35, and 94.69% respectively for the developed models. Therefore, the models built are found to be adequate. The models are therefore statistically significant at a confidence level of 95 %. To predict the UTS, % of EL and IS, within the factorial space used the regression equation used. The correlation coefficients were shown in Table 4.6.

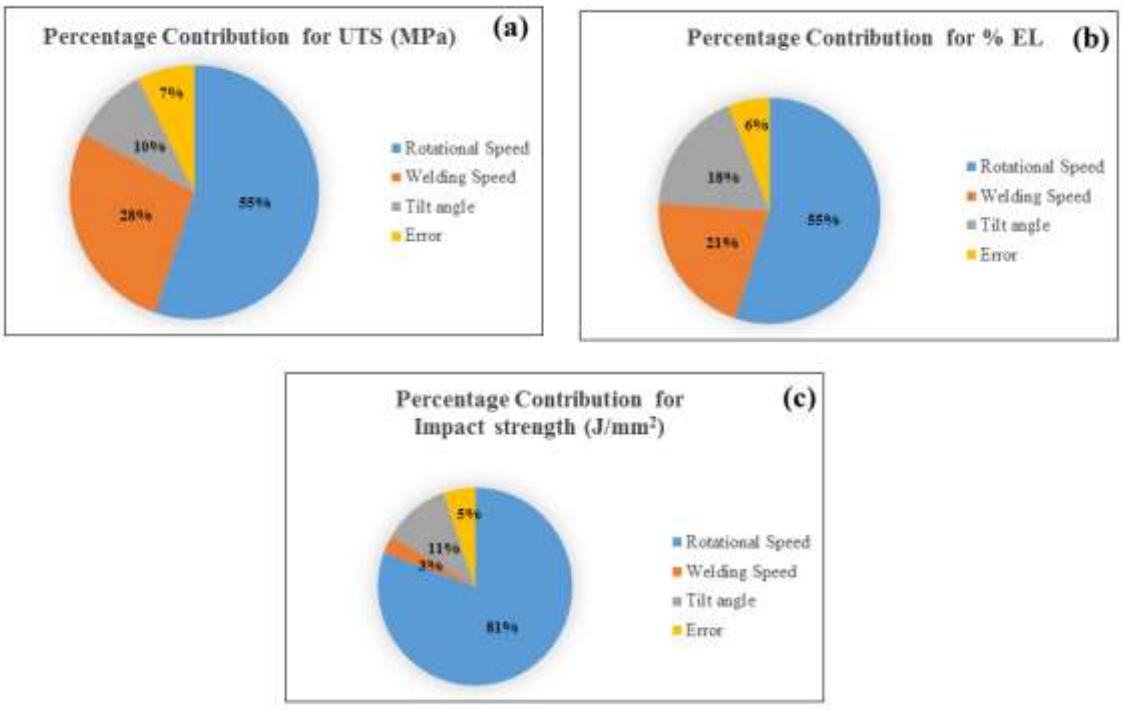

Figure 4.31.Percentage of contribution of selected parameter for (a) ultimate tensile strength (b) percentage of elongation (c) impact strength.

Table 4.5. ANOVA results for various responses of the similar weldments.

Process Parameter	Degree of freedom (DF)	Adj. Sum of squares (ASS)	Adj. Mean squares (AMS)	F-Value	P-Value	% contribution
Ultimate tensile strength						
RS	1	1786	1785.96	37.19	0.002	55.17625
TS	1	888.2	888.17	18.5	0.008	27.43983
TTA	1	322.7	322.67	6.72	0.049	9.969415
Error	5	240.1	48.02			7.417591
Total	8	3236.9				100
Percentage of Elongation						
RS	2	6.5304	3.2652	9.7	0.093	54.76456
TS	2	2.5254	1.2627	3.75	0.211	21.17825
TTA	2	2.1954	1.0977	3.26	0.235	18.41083
Error	2	0.6734				5.647197
Total	8	11.9245				100
Impact Strength						
RS	1	0.012934	0.012934	75.88	0	80.65602
TS	1	0.00045	0.00045	2.64	0.165	2.806186
TTA	1	0.0018	0.0018	10.56	0.023	11.22474
Error	5	0.000852	0.00017			5.313046
Total	8	0.016036				100

Table 4.6 Regression equations for the mechanical properties of the similar weldments.

Sl. No.	**Response**	**Regression equation**	**R-sq (%)**
1.	UTS (MPa)	UTS = 100.1 0.0654 RS (RPM) + 0.487 TS (mm/ minute) - 14.67 TTA (degree)	92.58
2.	%EL	% EL = 5.64 + 0.00389 RS (RPM) + 0.0230 TS (mm/ minute) - 0.500 TTA (degree)	94.35
3.	IS (J/mm^2)	Impact Strength (J/mm2) = 0.6883 - 0.000176 RS (RPM) + 0.000346 TS (mm/ minute) + 0.0346 TTA (degree)	94.69

4. 9 Optimization and Validation of Interactions on Quality Characteristics of Similar Weldments

A validation test is the final step in the design process for the experiment. For the justification of the optimum results obtained the conformation tests are conducted and results are shown in Table 4.7 and Table 4.8 respectively. The obtained confirmation test results for tensile strength, traverse speed, and impact strength from regression equation were closer with least error ($\pm$6%). Thus, the resulting equations obtained are able to predict the mechanical properties to the acceptable level of precision.

Table 4.7 Optimum conditions of the performance characteristics of similar weldments.

Sl.N	**Performance characteristics**	**Optimum condition**	**Optimum value**
1	UTS (MPa)	RS at 1025 rpm, TS at 75 mm/ minute, Tilt angle at 1.5˚	181.655
2	%EL	RS at 1025 rpm, TS at 75 mm/ minute, TTA at 1.5˚	10.60225
3	IS (J/mm^2)	RS at 500 rpm, TS at 75 mm/ minute, TA at 2.5˚	0.71275

Table 4.8 Confirmation test results for validation of optimum values of similar weldments.

Sl. No.	Performance characteristics	Optimum condition	Optimum value	Conformation test results*
1.	UTS (MPa)	RS at 1025 rpm, TS at 75 mm/ minute, Tilt angle at 1.5 ˚	181.655	192.5543
2.	%EL	RS at 1025 rpm, TS at 75 mm/ minute, TTA at 1.5 ˚	10.60225	11.23839
3.	IS (J/mm^2)	RS at 500 rpm, TS at 75 mm/minute, TTA at 2.5 ˚	0.71275	0.70323

4. 10 Chapter Summary

In this chapter, the effect of FSW process parameters on the microstructure and mechanical properties of AZ91D /AZ91similar FSWed weldments are summarized as follows.

i. The initial microstructure of the AZ91D Mg alloy consists of primary α-phase, eutectic α and intermetallics β ($Mg_{17}Al_{12}$) phase in as-received condition which were confirmed by X-ray diffraction (XRD) analysis.

ii. There were small flaws that were generated at a fixed tool rotation speed, 1525 rpm, in the advancing side of the SZ of similar weldments called the tunnel defects. However defect-free welds were produced with varying tool rotational speeds of 500, 720, 1025 rpm respectively for the welding conditions of 25, 50, and 75mm / minute.

iii. The parent AZ91 Mg alloy's original grain structure (dendritic) disappeared entirely in the stir region and was substituted with fine grains. Due to frictional heat input provided by the tool, the intermetallic phase β was dissolved. In the SZ grain refinement occurred due to dynamic recrystallisation (DRX). The recrystallized grain structure in the SZ is formed due to severe plastic deformation taking place with development of frictional heat during welding.

iv. Hardness improved significantly at high rotational speeds and high traverse speeds due to more dynamic crystallization in the stir field. Fine disbursement of secondary phase particle and its distribution also added strength to the above said mechanism Compared

to parent AZ91 Mg alloy, the average grain size of the SZ is substantially smaller regardless of the varying process parameters.

v. Increasing the rotation speed, grains got refined and increased the tensile strength. Increasing the weld speed resulted in the less heat input which led to the inhibition of the grain growth and improved the tensile strength. Fine disbursement of secondary phase particle and its distribution also added strength to the above said mechanism. In addition to the increase in tensile strength the ductility also increased due to the breakage of the coarse β intermetallics into fine particles.

vi. The mode of fracture was observed to be the brittle in nature.

vii. Processing parameter didn't much affect the impact strength.

viii. The FSW process parameters have significant effect on micro-structural, mechanical and corrosion properties of the similar welds. The optimum condition obtained for ultimate tensile strength and percentage of elongation at rotational speed of 1025 RPM, transverse speed 75 mm/min, and tilt angle of 1.5º. The optimum condition obtained for impact strength is at rotational speed of 500 rpm, transverse speed of 75 mm/min, and tilt angle of 2.5º. The results obtained agree well with the established theory.

ix. ANOVA findings showed that rotational speed and welding speed have a major effect on tensile strength, percentage of elongation, while welding speed has less percentage of contribution on impact strength in comparison to rotational speed and tilt angle. It is observed that lower values are considered to be the R^2 values of all the built models. The calculated R^2 values for UTS, elongation and impact strength are 92.58, 94.35, and 94.69 % respectively for the developed models. The models built are therefore very adequate and are statistically valid at a 95 % confidence level.

CHAPTER − 5

FRICTION STIR WELDING OF AZ91-AZ31 DISSIMILAR ALLOY

5.1 Introduction

The dissimilar butt welded joints were produced with different rotational speeds of 500, 720, and 1025 rpm, traverse speeds of 25, 50, and 75 mm/min, and tilt angle from 1.5°, 2°, and 2.5° are shown in Figure 5.1. During welding, the AZ91Mg alloy plate was kept on the advancing side, and AZ31Mg alloy plate was kept on the retrieving side with respect to tool rotational direction. The fabricated weldments were good in quality and defect-free irrespective of weld parameters, as mentioned in Table 3.4(Chapter3). The same was confirmed by visual inspection and X-ray radiography as well. Since the AZ91 has more aluminium contentment than AZ31, the amount of β phase is more in AZ911 Mg Alloy compared to AZ91 Mg Alloy. The AZ31 Mg alloy displays lower brittleness as compared to AZ91 Mg alloy, the ease of plastic deformation in AZ31 Mg Alloy is superior to AZ91 Mg alloy, and hence the metal flow is more complex in nature during dissimilar welding of AZ31 and AZ91 Mg alloys. Thermal stresses heat generated during fabrication of AZ91 Mg Alloy and AZ31 Mg Alloy due to the dissimilarity in the Co-efficient of thermal conductivity. Misbalancing of these thermal stresses leads to hot cracking. The chance of hot cracks initiation is more during the welding of dissimilar metals when compared to similar metals due to dissimilarity in the heat transmission of the parent metals during welding. So the

process parameters are to be chosen carefully to avoid hot cracking, as shown in Table 3.4(Chapter3). In the present case the time allowed for rising temperature and material plastic flow between the joint is sufficient for developing efficient metallurgical joints.

5.2 Results and Discussions

5.2.1 Macrostructure of the Dissimilar FSWed AZ91 Mg Alloy to AZ31 Mg Alloy

During welding, the AZ91Mg alloy plate was kept on the advancing side, and the AZ31Mg alloy plate was kept on the retrieving side with respect to tool rotational direction and the resultant weldments were good in quality and defect-free irrespective of weld parameters as mentioned in Table 3.4 (Chapter 3).

The surface appearances of dissimilar welded specimens at different welding conditions is shown in Figure 5.1 shows. There was no defect found on the macroscopic scale. Figure 5.2 shows the macrostructure of cross-section (transverse section) of the AZ31 Mg alloy/AZ91 Mg alloy joint produced after FSW at different processing parameters. The top surface of the weld zone is wider than the bottom surface due to contacting tapered cylindrical tool shoulder with the top surface has experienced functional heat and extreme deformation with the surface of the specimen to be welded. The pin profile's morphology is duplicated in Stir Zone. The content of AZ31 Mg alloy appeared to be more in the stir zone when compared to AZ91 Mg alloy, as shown in Figure 5.2 (b),(c). In contrast, for the welding condition 500 rpm, 25 mm/minute (Figure 5.2(a)), the AZ91 Mg alloy region is high and well diffused in the AZ31 Mg alloy matrix. The region, as marked by the black arrow in Figure 5.2(b) and (c) represents fine AZ31 Mg alloy surrounded by AZ91 Mg alloy.

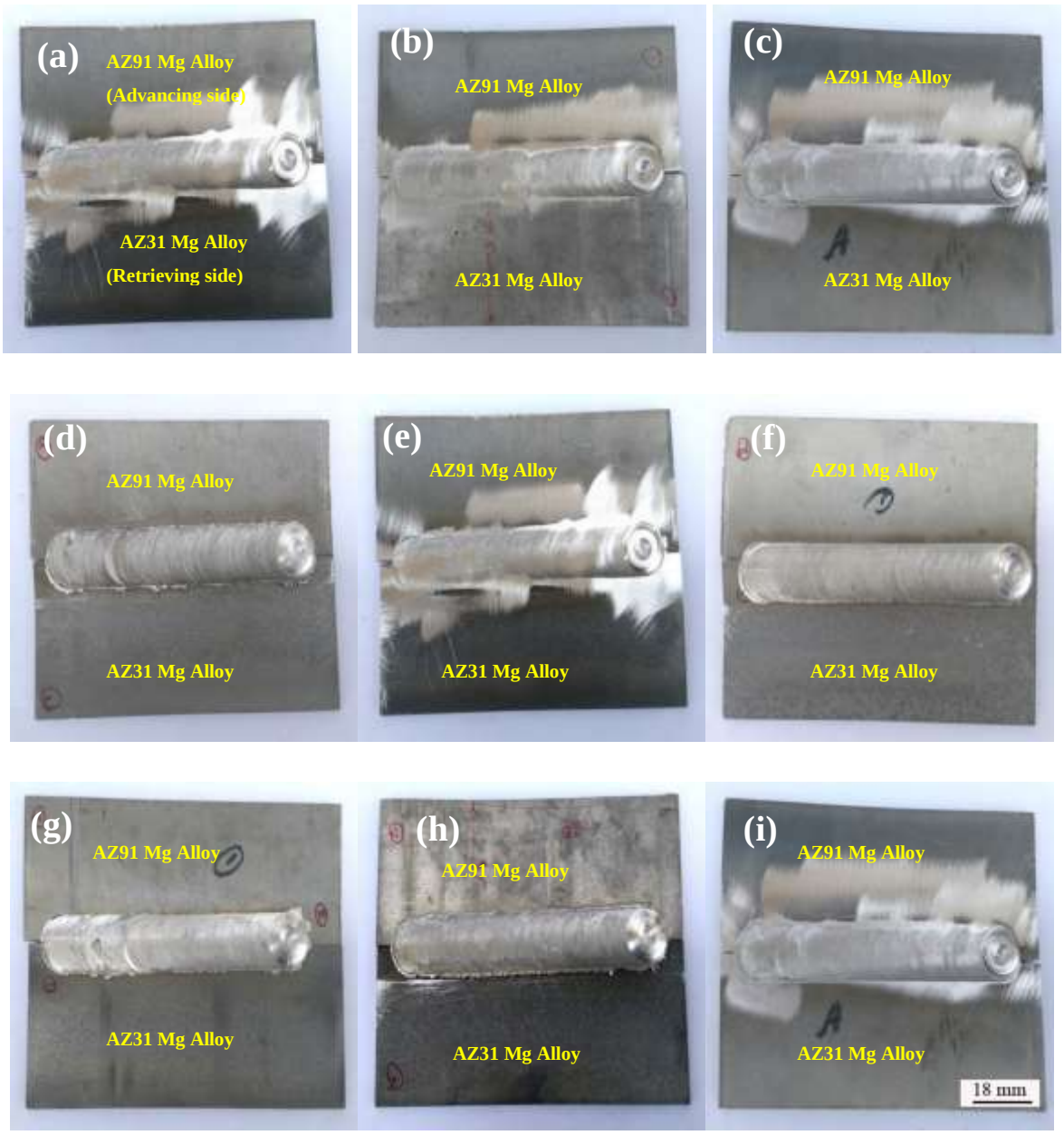

Figure 5.1 Surface appearances of dissimilar welded weldments (AZ31 Mg alloy to AZ91 Mg alloy) at different welding conditions, (a) 500 rpm, 25 mm/min (b) 500 rpm, 50 mm/min (c) 500 rpm, 75 mm/min (d) 720 rpm, 25 mm/min (e) 720 rpm, 50 mm/min (f) 720 rpm, 75 mm/min (g) 1025 rpm, 25 mm/min (h)1025 rpm, 50 mm/min and (i) 1025 rpm, 75 mm/min

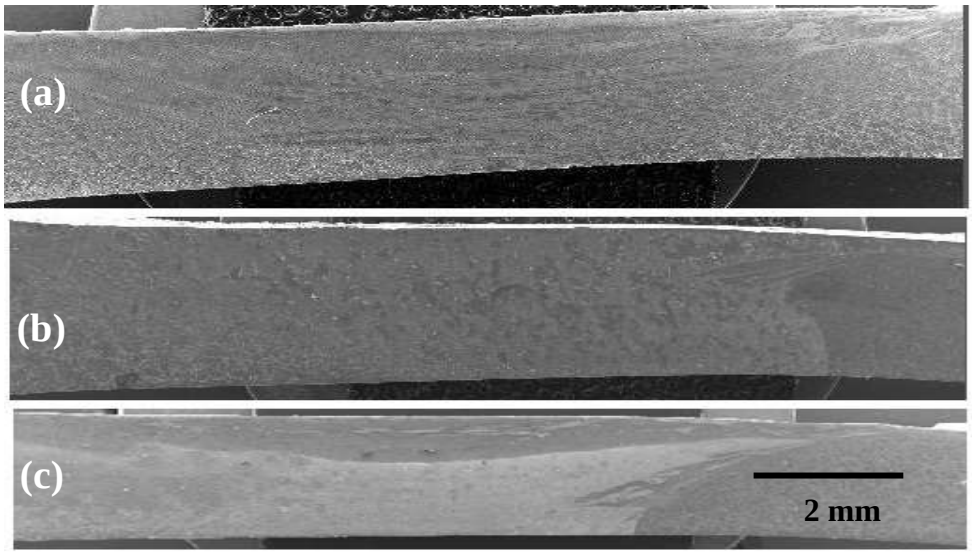

Figure 5.2 Macro structures of FS Welded AZ31/AZ91 Mg alloy cross sectional joint at various welding conditions, a) 500 rpm, at 25 mm/min, (b) 720 rpm, at 50 mm/m, and (c) 1025 rpm, at 75 mm/min.

Therefore, it confirms the presence of mixed region of dissimilar metals (AZ31Mg alloy and AZ91 Mg alloy). The profile of weld pool is influenced by tool pin profile, materials to be fabricated and their rate of thermal conductivity. From the inspection of stir zone it was noticed that for varying tool rotational speed of 500rpm to 1025rpm and welding speed of 25 mm/min to 75 mm/min has no defects in the weld zone, as shown in Figure 5.2. Each weld zone for various welding conditions exhibits unique microstructure.

5.2.2 Development of Microstructure in the Different Weld Zones of Dissimilar Weldments

SEM microstructure of the respective AZ91D Mg alloy/AZ31C dissimilar weldments in different zones is shown in Figure 5.3 to 5.11. The weld consists of three regions named as heat affected zone (HAZ)(a), thermomechanical affected zone (TMAZ)(b), and stir zone (SZ)(c) respectively. Each zone exhibits unique features of microstructure based up on the thermal and mechanical conditions. A sharp interface was clearly noticed between HAZ, SZ and TMAZ at AZ91 Mg

alloy side (advancing). In the HAZ, due to thermal effect produced by tool, the volume fraction of β intermetallic compound undergone dissolution and reduced to smaller fraction. In case of TMAZ, the combined effects of thermal and plastic deformation was seen. The region was composed of partially observed recrystallized grains and β intermetallic compounds. The β intermetallic compounds were seen around the direction of tool rotation in TAMZ. The grains in TMAZ were elongated and equiaxed. In the SZ, The β intermetallic compound disappeared due to transformation of β phase into α phase by diffusion and also the dendrite grain structure of base metal transformed to fine grains.

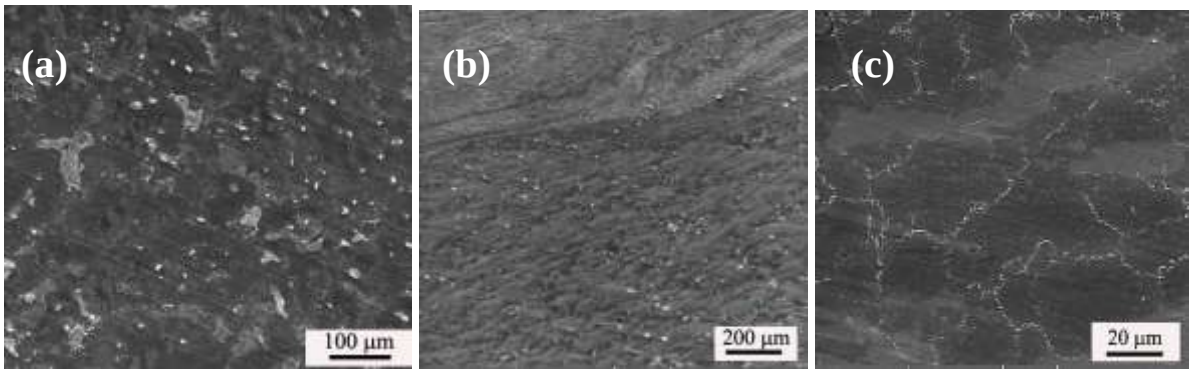

Figure 5.3 SEM micrographs of AZ91D Mg alloy/AZ31C Mg alloy weldment of condition 500 rpm,25 mm/min near the welds (a) HAZ, (b) TMAZ, (c) SZ.

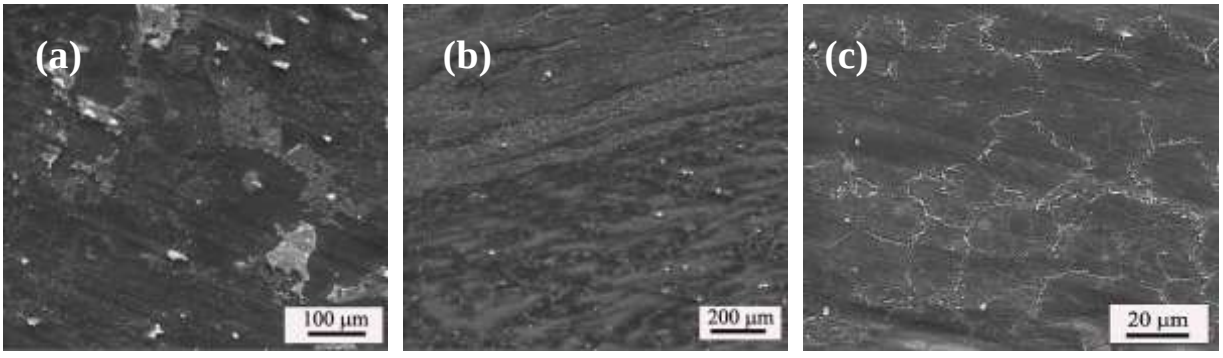

Figure 5.4 SEM micrographs of AZ91D Mg alloy/AZ31C Mg alloy weldment of condition 500 rpm, 50 mm/min near the welds (a) HAZ, (b) TMAZ, (c) SZ.

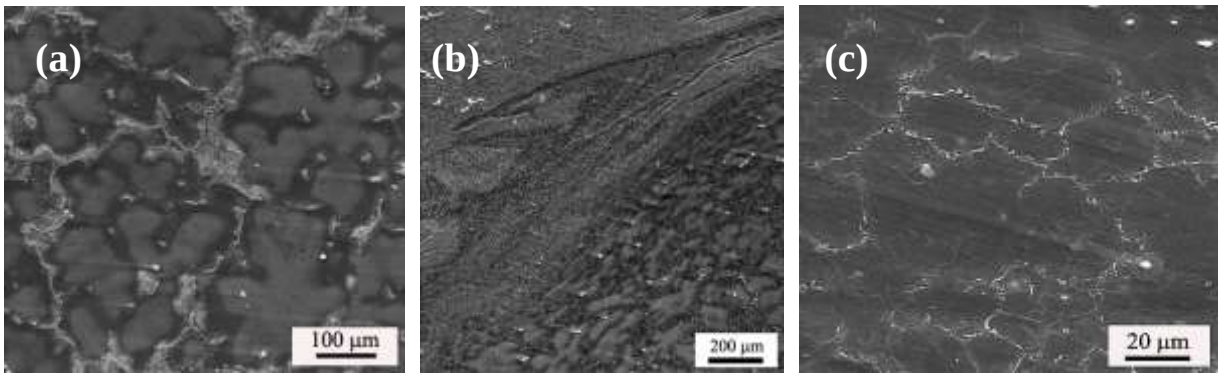

Figure 5.5 SEM micrographs of AZ91D Mg alloy/AZ31C Mg alloy weldment of condition 500 rpm, 75 mm/min near the welds (a) HAZ, (b) TMAZ (c) SZ.

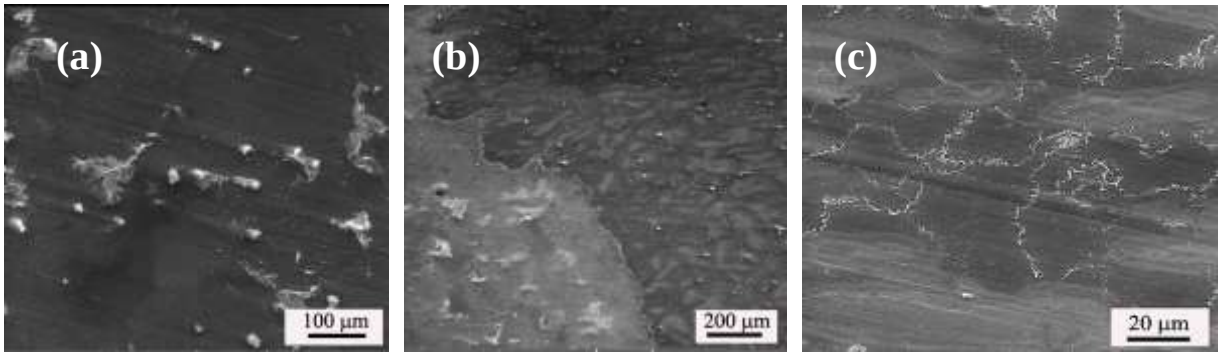

Figure 5.6 SEM micrographs of AZ91D Mg alloy/AZ31C Mg alloy weldment of condition 720 rpm,25 mm/min near the welds (a) HAZ, (b) TMAZ, (c) SZ.

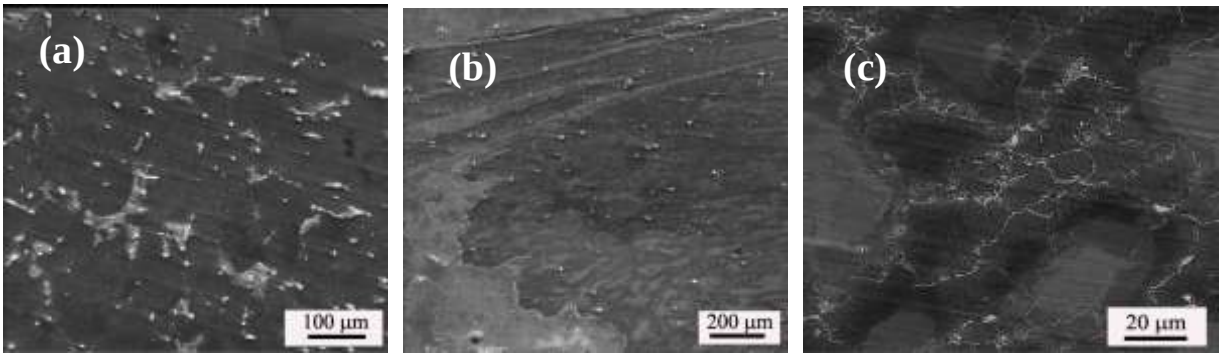

Figure 5.7 SEM micrographs of AZ91D Mg alloy /AZ31C Mg weldment of condition 720 rpm, 50 mm/min near the welds (a) HAZ, (b) TMAZ, (c) SZ.

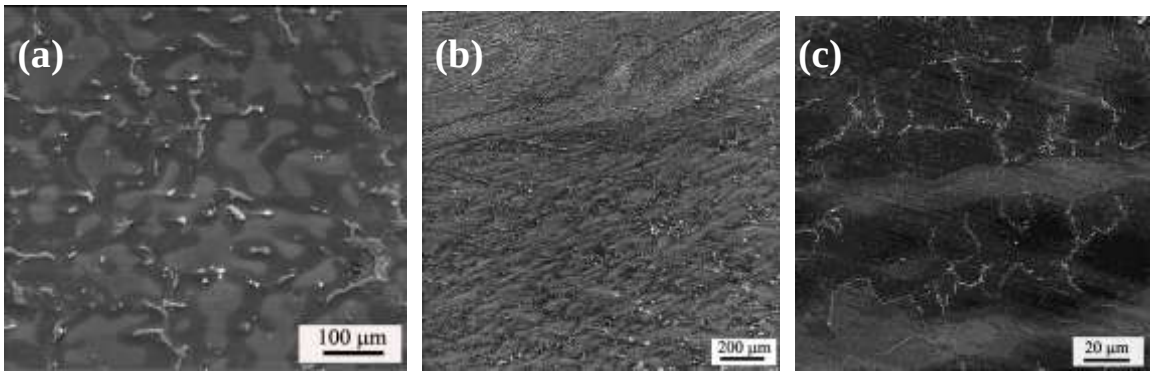

Figure 5.8 SEM micrographs of AZ91D Mg alloy/AZ31C Mg alloy weldment of condition 720 rpm, 75 mm/min near the welds (a) HAZ, (b) TMAZ, (c) SZ.

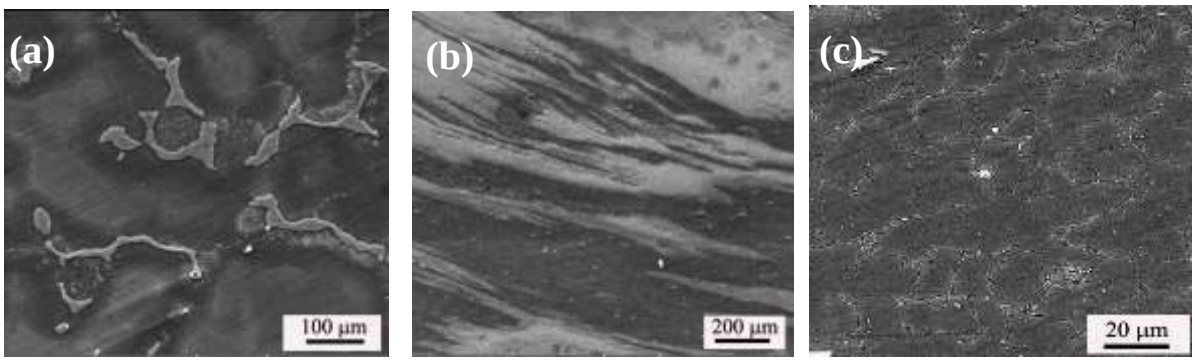

Figure 5.9 SEM micrographs of AZ91D Mg alloy/AZ31C Mg alloy weldment of condition1025 rpm, 25 mm/min near the welds (a) HAZ, (b) TMAZ, (c) SZ

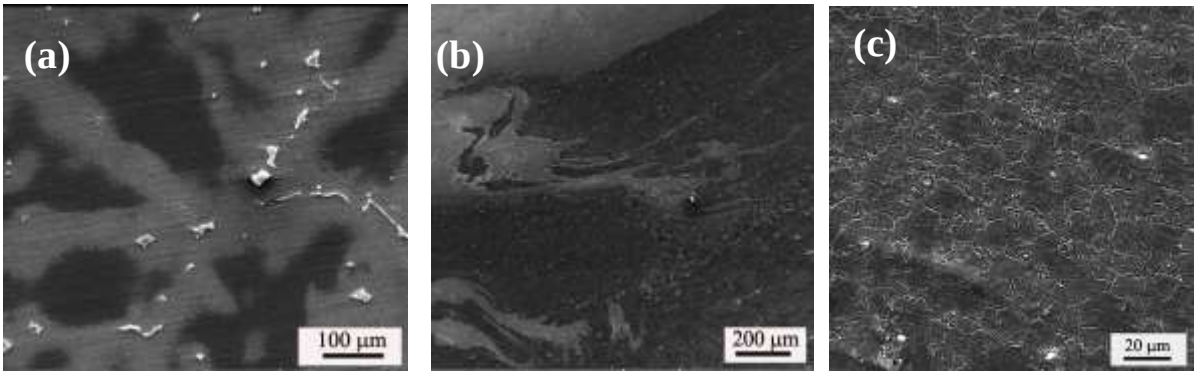

Figure 5.10 SEM micrographs of AZ91D Mg alloy/AZ31C Mg alloy weldment of condition 1025 rpm, 50 mm/min near the welds (a) HAZ, (b) TMAZ, (c) SZ.

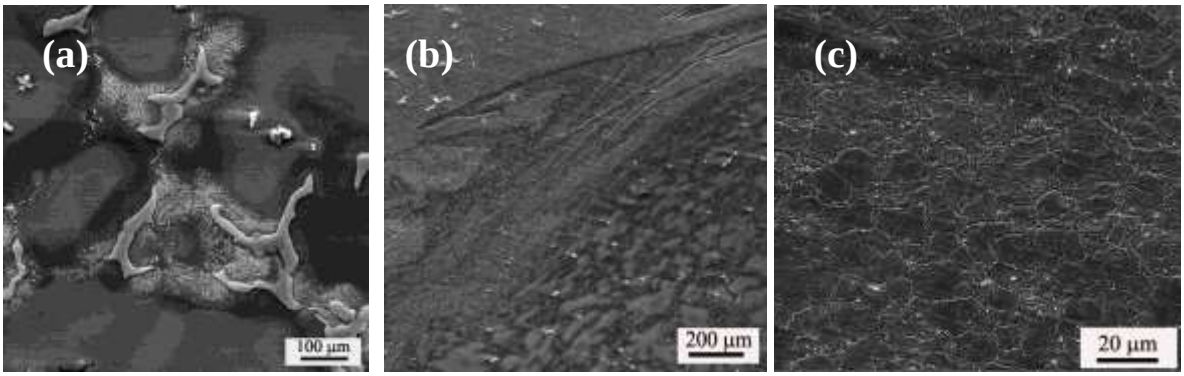

Figure 5.11 SEM micrographs of Mg AZ91D Mg alloy/AZ31C weldment of condition 1025 rpm, 75mm/min near the welds (a) HAZ, (b) TMAZ, (c) SZ.

The dendrite structure of base materials got completely disappeared in the stir zone. The stir zone underwent dynamic recrystallization (DRX). Fine grains and smaller network of in the nugget zone can be attributed to dynamic recrystallization as shown in the SZ. This is due to heat generated by friction between the material and tool and high strain rates applied to the material surface by the tool pin [111]. Significant grain refinement in stir zone was observed compared to parent metals due to dynamic recrystallization [115-117]. The presence of small particles of intermetallic $Mg_{17}Al_{12}$ within in stir zone indicates the higher level of material mixing of both the alloys. Increase in the rotational speed increases leads to increase in degree of deformation due to development of friction and hence the peak temperature increase. Increase in local temperature causes the grain coarsening, but the increase of the degree of deformation has the opposite effect

As a consequence, with decreasing traverse speed the heat input increases due to more contact time of the tool with work piece. This results in coarser grain size in the SZ. Figure 5.13 illustrates the XRD patterns of parent alloys (AZ91D Mg alloy and AZ31C) as well as FSW specimens, confirmed the presence of α-phase and Eutectic β ($Mg_{17}Al_{12}$) phase present is confirmed.

Figure 5.13 illustrates the XRD patterns of parent alloys (AZ91D Mg alloy and AZ31C) as well as FSW specimens, confirmed the presence of α-phase and Eutectic β ($Mg_{17}Al_{12}$) phase presence.

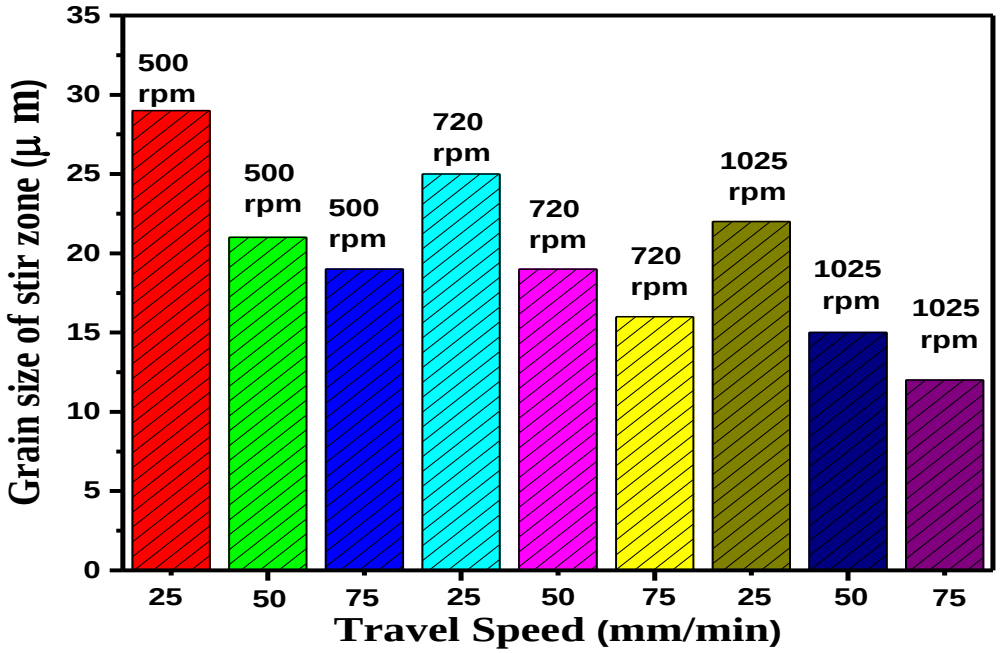

Figure 5.12 Grain size variations with varying welding speeds.

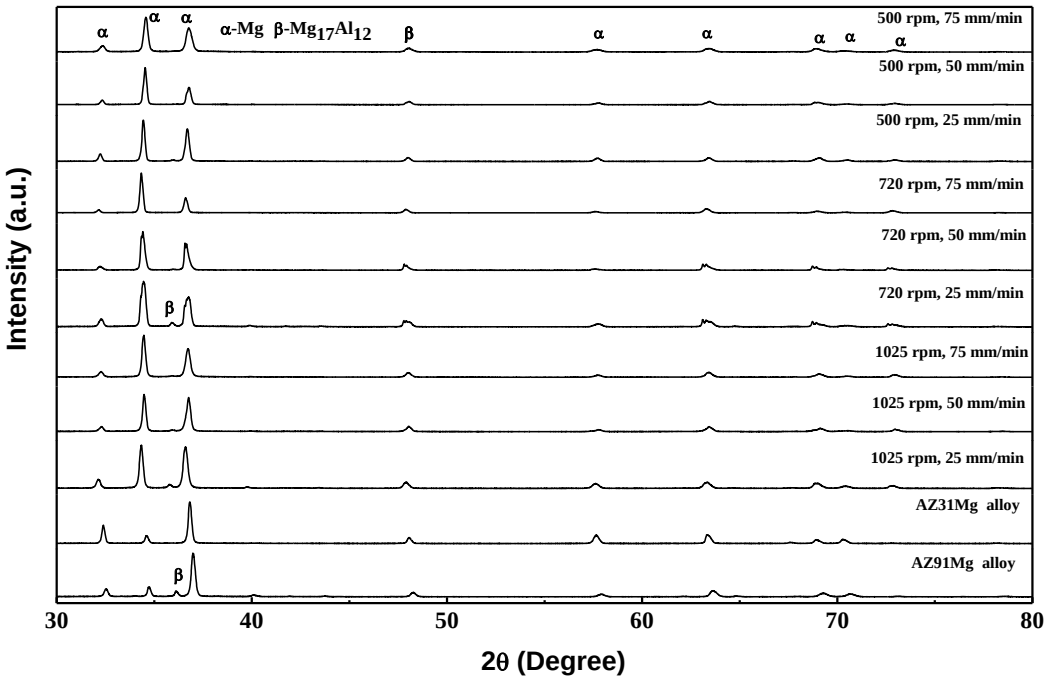

Figure 5.13 XRD patterns of (a) AZ91 Mg alloy (b) AZ31C Mg alloy and weldments.

5.2.3 Micro Hardness Measurements of Dissimilar Weldments

The base alloy hardness in the un-welded condition for AZ91 and AZ31 is 65. and 42 respectively. AZ91D alloy showed more harness than AZ31C due to high volume fraction of intermetallic β phase. Figure 5.14 shows micro hardness profile of welded specimens at transverse section from retreating side (AZ31 Mg alloy) to advancing side (AZ91 Mg alloy) for different welding conditions. It was observed that there was an increase in hardness in SZ, because of fine recrystallized grain structure and dissolution of aluminum content. The presence of $Al_{12}Mg_{17}$ is responsible for the same. The reason for hardness variation is due to the presence soft α which is a Mg solid solution and hard β intermetallic compound and its volume fraction.

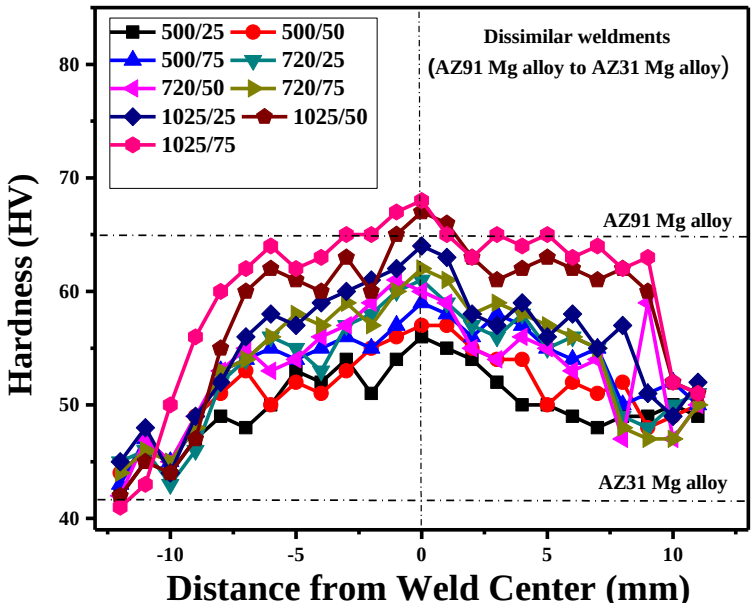

Figure 5.14 Hardness profiles of the dissimilar weldments (AZ91Mg alloy to AZ31Mg alloy) at various processing parameter

The hardness mainly depends upon the range of welding speeds. As welding speed increases, the hardness of the stir zone increases significantly due to grain refinement. However, at higher welding speeds, the hardness profile is non-uniform due to microstructural irregularity. Compared to the SZ the TMAZ and HAZ showed lower hardness. A gradual increase of hardness was found while taking measurements from retrieving side to advancing side across the weld cross section.

5.2.4 Tensile Properties of Dissimilar Weldments

Figure 5.15 and 5.16 shows the effect of welding speed on tensile strength and ductility of dissimilar FSWed AZ91D-AZ31C joint. The AZ91D Mg alloy in as cast conditions exhibited lower tensile strength of 109 MPa and elongation of 3 %. The AZ31 Mg alloy in as cast conditions exhibited tensile strength of 191 MPa and elongation of 10.75%. The friction stir welded plate which was processed at the welding speed of 25 mm/min, 1025 rpm showed maximum ultimate tensile strength of 166 MPa and higher elongation of 14.88 %. The tensile strength and ductility of friction stir welded plates processed at welding speed of 50 mm/min, 500 rpm is 123 MPa, and 10.12 % respectively. However, there was a significant improvement in tensile strength as a function of welding speed.

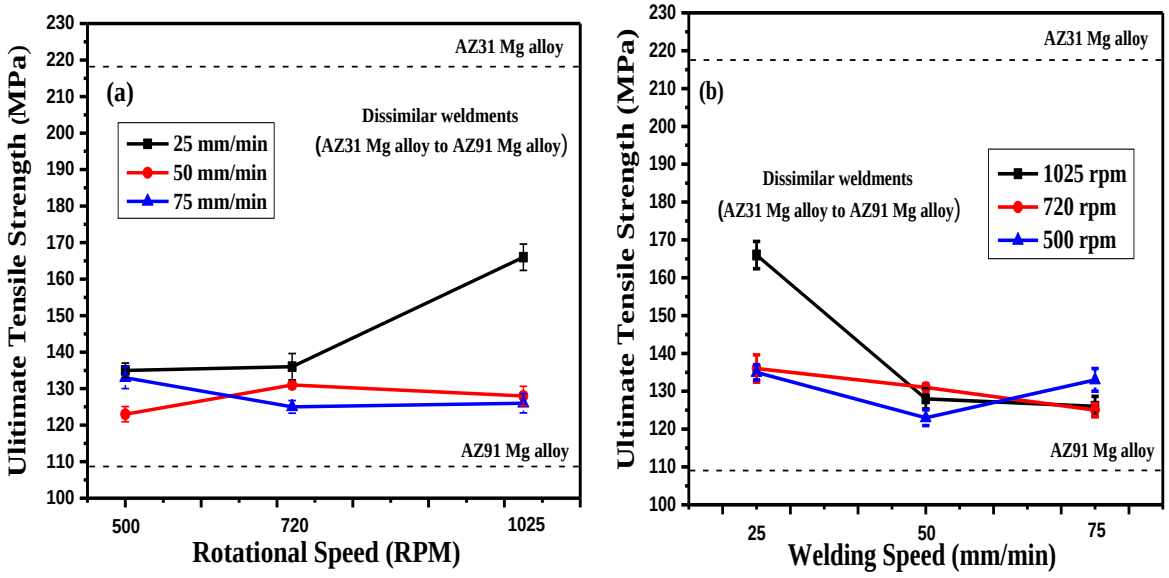

Figure 5.15 Effect of the rotation speed and welding speed on the tensile strength of dissimilar weldments.

The elongation noticeably changed as a function of the welding speed, although a maximum elongation of about 14.88 % was obtained at the welding speed of 25 mm/min. The friction stir welded plate processed at the welding speed of 25 mm/min, 1025 rpm showed higher tensile strength is attributed to the particle distribution and grain refinement. The welding speed of the process is responsible for the particle distribution and the grain refinement [108-110]. The other

hand friction stir welded plate processed at the welding speed of 50 mm/min, 500 rpm showed lower tensile strength due to the formation of brittle β ($Mg_{17}Al_{12}$) phase formation in the microstructure.

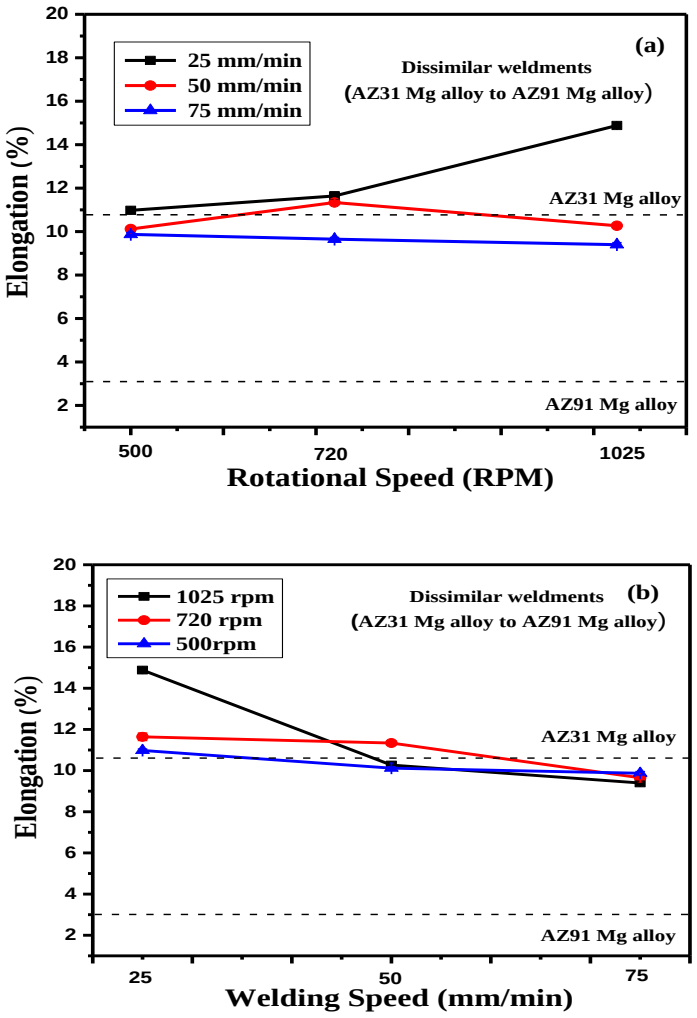

Figure 5.16. Effect of the rotation speed and welding speed on elongation of dissimilar weldments.

5.2.5 Fractographic Analysis of Dissimilar Weldments

Figure 5.17 show the SEM images of the fractured surface of the parental metal and dissimilar welded plates at different conditions. It was observed that fracture occurred at the weld interface.

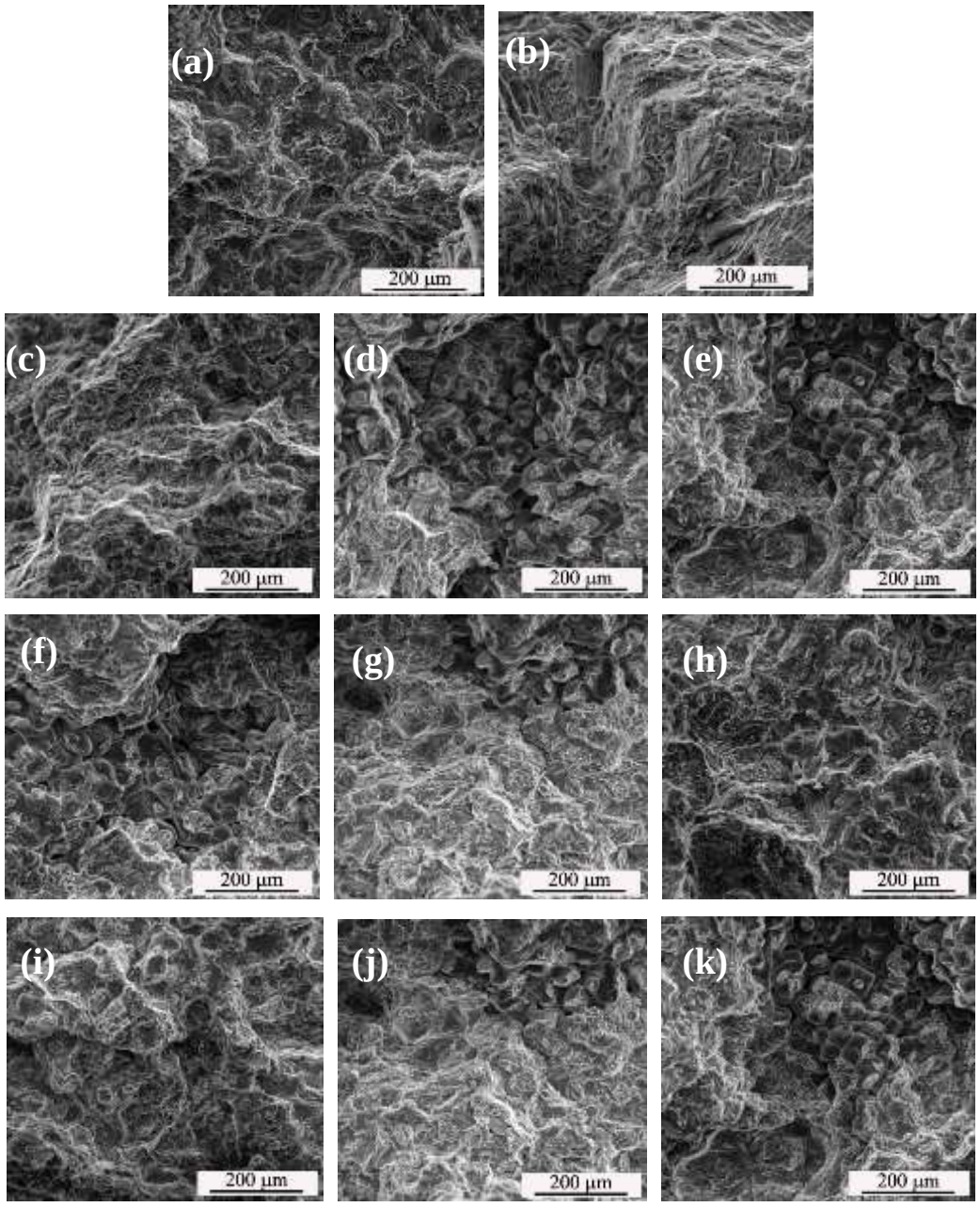

Figure 5.17 SEM images of fractured surface (a) AZ91D Mg alloy (b) AZ31 Mg alloy and Dissimilar weldments of different welding conditions at (c) 1025 rpm, 25 mm/min, (d) 1025 rpm, 50 mm/min, (e) 1025 rpm, 75 mm/min (f) 720 rpm, 25 mm/min, (g) 720 rpm, 50 mm/min (h) 720 rpm, 75 mm/min (i) 500 rpm, 25 mm/min (j) 500 rpm, 50 mm/min (k) 500 rpm, 75 mm/min showing brittle mode of fracture.

Absence of dimple morphology or presence of river pattern of the fractured surface clearly indicates that the mode of fracture is brittle in nature. The uneven distribution of eutectic β - $Al_{12}Mg_{17}$ and shrinkage defects acts as a nucleation site for the crack to initiate. Irrespective of the weld parameter fractured happened at interface of base metal and weldment. Some of the area revealed the quasi cleavage nature of the fracture due to the in homogeneity in the dilution at the interface.

5.2.6 Impact Properties of Dissimilar Weldments

The effect of welding speed and rotational speed on impact strength has been given in Figure 5.18 and Figure 5.19. It has been observed that the impact strength hasn't get affected much.

5.2.7 Optimization of Process Parameter Using Taguchi Method

The parent alloy's ultimate tensile strength (UTS), elongation percentage (percent EL), and impact strength (IS) of FSW joints of dissimilar welds were measured and displayed in Table 5.1. From the results it is noticed that the IS of the FSW joints is not significantly improved. The joint made at processing condition 500 rpm, 75 mm/min, 2.5^{o} resulted in higher impact strength relative to all other condition of joints. The tensile strength and percentage of elongation of the weldments significantly compared to parent AZ91 Mg alloy. The joint made at processing condition at processing condition 1025 rpm, 25 mm/min, 2.5^{o} exhibit significance tensile strength and percentage elongation compared to other joints processed at different condition. This is attributed to the development of fine grain structure that results in a more ductile nature relative to all other weldments.

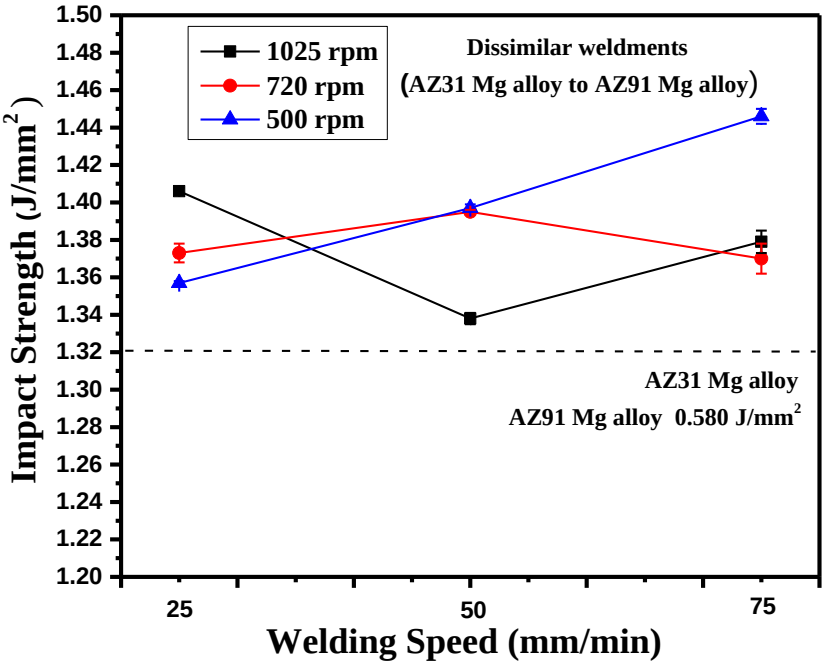

Figure 5.18 Influence of welding speed on the impact strength of dissimilar weldments

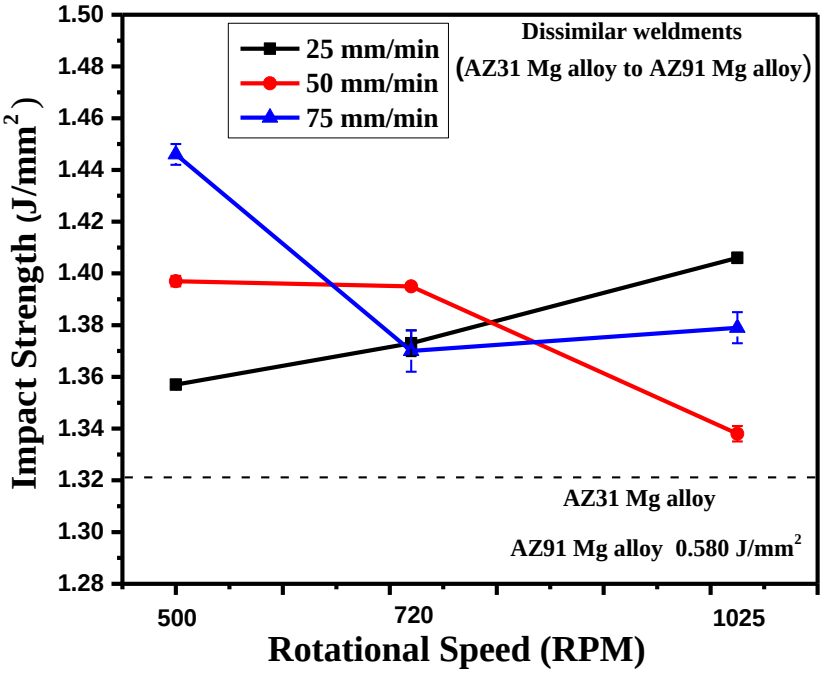

Figure 5.19 Influence of rotational speed on the impact strength of dissimilar weldments.

Table 5.1 Mechanical properties of dissimilar weldments (AZ31 to AZ91 Mg alloy) and Parent alloy.

Exp. No.	Welding Condition	UTS* (MPa)	% El*	Impact* strength (J/mm2)
1	500 rpm, 25 mm/min,1.5º	135	10.98	1.357
2	500 rpm, 50 mm/min,2º	123	10.12	1.397
3	500 rpm, 75 mm/min,1.5º	133	9.87	1.446
4	720 rpm, 25 mm/min,2º	136	11.64	1.373
5	720 rpm, 50 mm/min,2.5º	131	11.34	1.395
6	720 rpm, 75 mm/min,1.5º	125	9.65	1.370
7	1025 rpm, 25 mm/min, 2.5º	166	14.88	1.406
8	1025 rpm, 50 m/min, 1.5º	128	10.27	1.338
9	1025 rpm, 75 mm/min, 2º	126	9.40	1.379
AZ31Mg alloy (As received)		218	10.75	1.32435
AZ91Mg alloy (As received)		109	3.0483	0.580

* Average of three values

5.2.8 Ultimate Tensile Strength

The UTS of the dissimilar welds is measured to observe the effect of RS, TS and TTA. The main effects (mean and S/N ratio) are plotted in Figure 5.20 and Figure 5.21 respectively, for mean and S/N ratio.

It is obvious that a greater S/N ratio leads to characteristics of higher quality. Hence the optimal level of processing parameters is the maximum S/N ratio. The mean and S/N ratio values confirmed that the UTS is at highest for RS at level 3, TS at level 1 and TTA at level 2. That is, RS is 1025, TS is 25 and TTA is 2.5°.

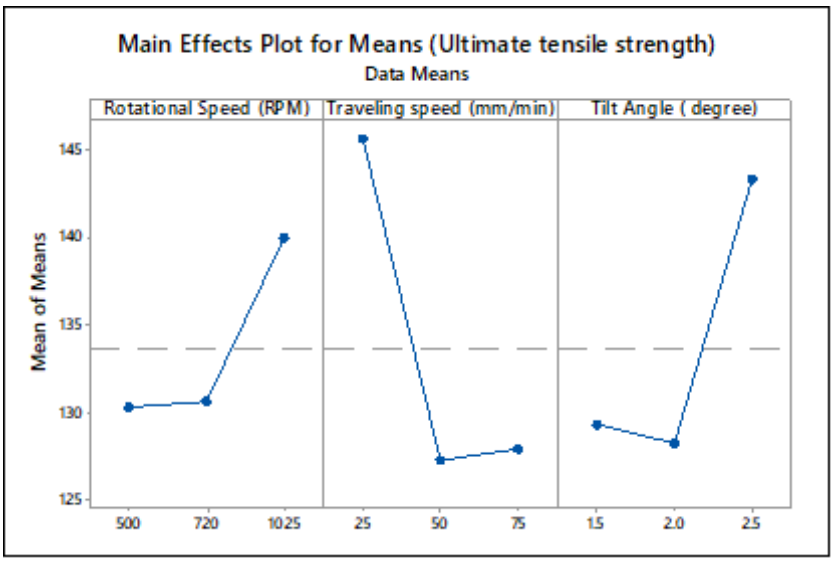

Figure 5.20 Effects plot for means of dissimilar weldments (UTS)

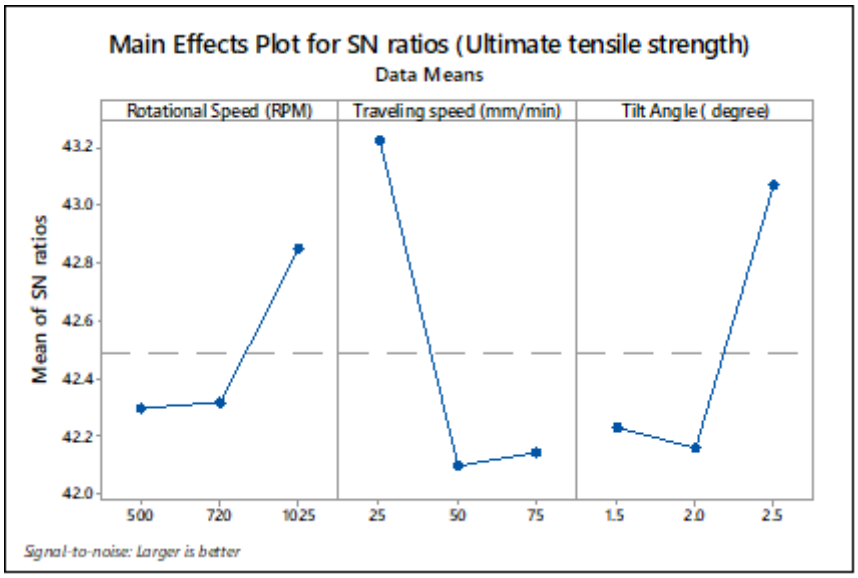

Figure 5.21 Effects plot for S/N ratio of dissimilar weldments (UTS)

5.2.9 Percentage Elongation

The Dissimilar welding %EL is evaluated to examine the influence of RS, TS, and TTA. The main effects are plotted in Figure 5.22 and Figure 5.23 respectively, for mean and S/N ratio.

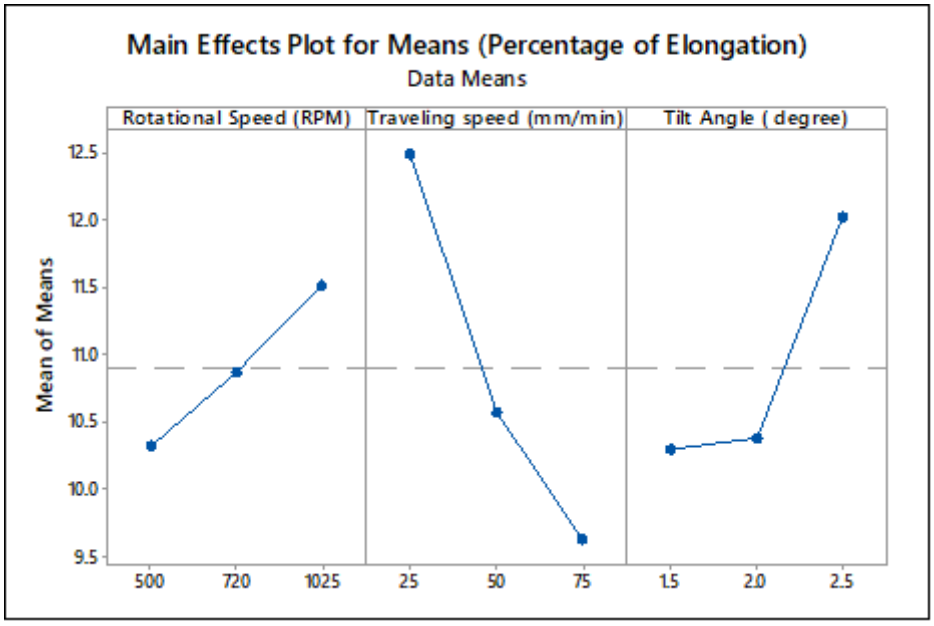

Figure 5.22 Effects plot for Mean of dissimilar weldments (%EL)

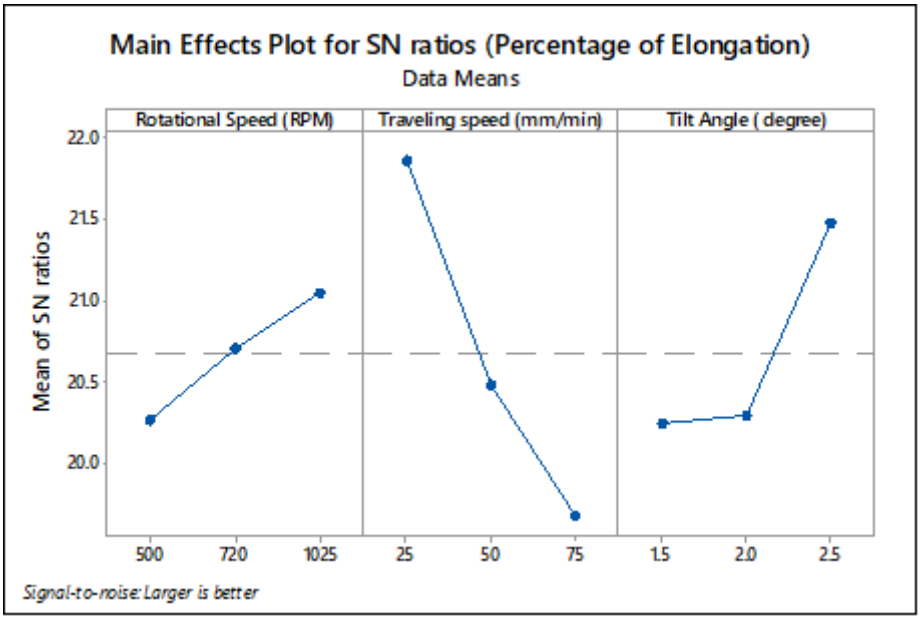

Figure 5.23 Effects plot for S/N ratio of dissimilar weldments (%EL)

The effect plot values indicated that the %EL is at highest for RS at level 3,TS at level 1 and TTA at level 2 i.e., RS is 1025, TS is 25 and TTA is 2.5°.

5.2.10 Impact Strength

The Impact Strength of dissimilar weldments are analyzed to examine the effect of RS, TS and TTA. The main effects are shown in Figure 5.24 and Figure 5.25 for mean and S/N ratio respectively.

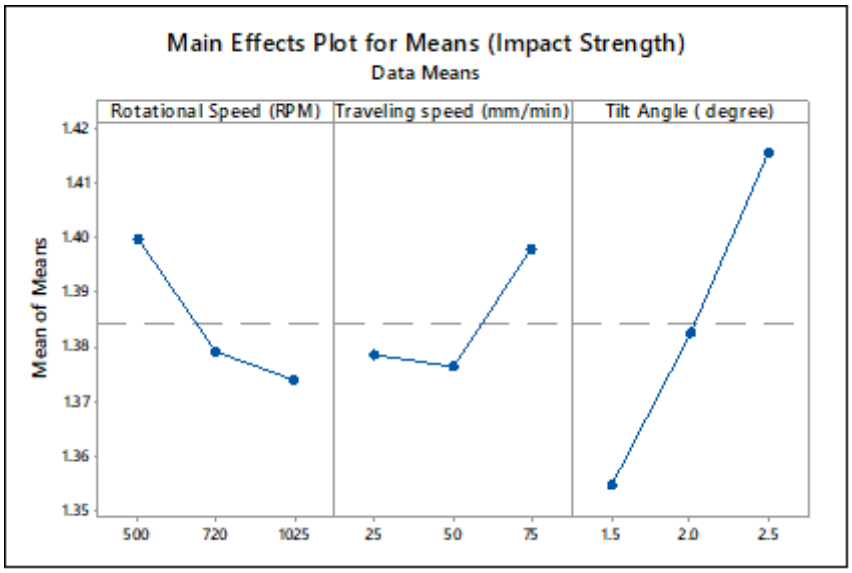

Figure 5.24 Effects plot for Mean of dissimilar weldments (IS)

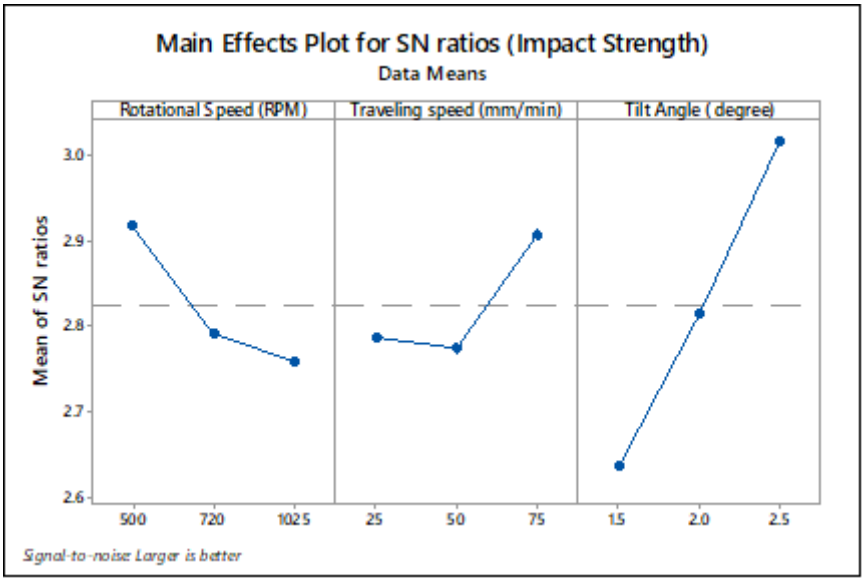

Figure 5.25 Effects plot for S/N ratio of dissimilar weldments (IS)

The effect plot results showed that the IS is at highest for RS at level 1, TS at level 3 and TTA at level 2. i.e., RS is 500, TS is 75 and TTA is 2.5°. Optimization of RS, TS and TTA using Taguchi method enables evaluation of the effects of individual elements on the quality characteristics found, i.e. UTS, % EL and IS, irrespective of other elements. The effect of each RS, TS and TTA can be calculated by measuring the S/N ratio for each factor at each level. The means and S/N ratios plots of various responses such as UTS, %EL and IS are shown in Figure 5.20 to Figure 5.25. The optimal parametric combinations for good mechanical properties are derived from the study of the means and S/N ratios plots and are summarized in Table 5.1.

Figure 5.20 to Figure 5.23 displays the means and S/N ratios plots for tensile properties such as UTS, and the % EL. The increase in UTS and %EL of the similar weldment was found at higher RS of 1025 rpm, and lower TS of 25 mm/min. The increased UTS of the dissimilar weldments is due to the grain refinement in the weld zone. The elongation at elevated temperature of the friction stir welded specimens was improved as compared to parent alloy is due to this reason.

Figure 5.24 shows the variation of the IS values with RS. It is observed that at lower RS the weldment exhibited higher IS compared to higher RS. At lower TS the heat input increases. The grain size is coarser at lower TS due to the enhancement of heat input, which promotes the growth of recrystallization of the grains [106].

At 2.5°tilt angle it was observed the UTS, %EL and Impact strength improved. It may be due to the influence of enough surface flash at TTA and in fact produces adequate material in the SZ [113].

5.2.11 Analysis of Variance (ANOVA) of Tensile and Impact Properties of Dissimilar Weldments

ANOVA is performed to find the effect of factors (or interactions) on various quality characteristics of dissimilar weldments, and the details are shown in Table 5.2.

Table 5.2 ANOVA results for various responses of the dissimilar weldments

Process Parameter	Degree of freedom (DF)	Adj. Sum of squares (ASS)	Adj Mean squares (AMS)	F-Value	P-Value	% of contribution
(a) Ultimate tensile strength						
RS	2	180.67	90.33	2.04	0.329	13.48284
TS	2	648.67	324.33	7.32	0.12	48.40821
TTA	2	422	211	4.76	0.174	31.49254
Error	2	88.67	44.33			6.617164
Total	8	1340				100
(b) Percentage of Elongation						
RS	2	2.144	1.0719	1.15	0.466	9.540337
TS	2	12.765	6.3823	6.82	0.128	56.8015
TTA	2	5.693	2.8467	3.04	0.247	25.6262
Error	2	1.872	0.9358			8.329996
Total	8	22.473				100
(c) Impact Strength						
RS	1	0.000921	0.000921	5.87	0.06	11.74146
TS	1	0.000568	0.000568	3.62	0.116	7.241203
TTA	1	0.005569	0.005569	35.19	0.002	70.99694
Error	5	0.000785	0.000157			10.00765
Total	8	0.007844				100

The percentage contribution of selected parameters such as RS, TS and %EL on the quality characteristics such as such as UTS, %EL and IS are shown in diagrams in Figure 5.25. Results of ANOVA revealed that the TS and TTA have a significant effect on UTS, %EL, whereas TS has less contribution percentage on impact strength compression to TTA and RS. It is observed that lower values are considered to be the R^2 values of all the built models. The calculated R^2 values for UTS, elongation and impact strength are 93.38, 91.67, and 89.99 % respectively for the developed models. The models built are therefore very adequate and are statistically valid at a 95 % confidence level. These equations have been used to estimate the UTS, %EL and IS, within the exploited factorial space. The correlation coefficients were presented in Table 5.3.

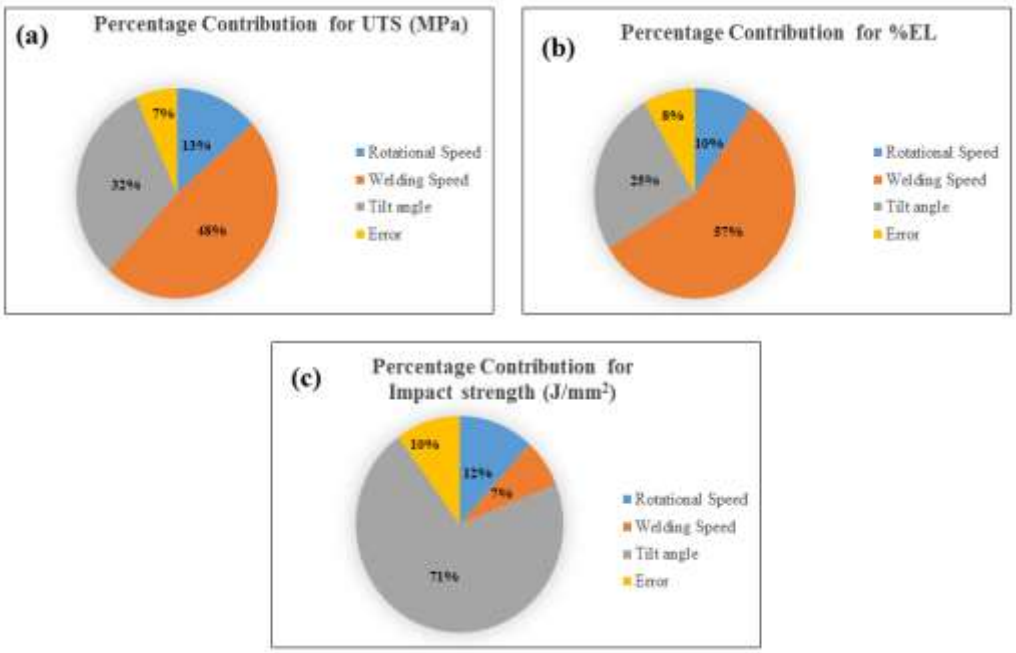

Figure 5.26. Percentage of contribution of selected parameter for (a) Ultimate tensile strength (b) percentage of elongation (c) Impact strength.

Table 5.3. Regression equations of the mechanical properties of the dissimilar weldments

Sl. No	Response	Regression equation	R-sq (%)
1.	UTS (MPa)	UTS = 109.0 + 0.0192 RS (RPM) - 0.353 TS (mm/min)+ 14.00 TTA (degree)	93.38
2.	%EL	% EL= 8.61 + 0.00226 RS (RPM) - 0.0572 TS (mm/min)	91.67
3.	IS (J/mm^2)	Impact Strength (J/mm^2) = 1.2781 - 0.000047 RS (RPM) + 0.000389 TS (mm/min) + 0.0609 TTA	89.99

5.2.12 Optimization and Validation of Selected Process Parameters on Quality Characteristics of Dissimilar Weldments

Confirmation test is the final step of designing the experimental process. For the justification of the optimum results obtained the conformation tests are conducted and results are presented in Table 5.4 and Table 5.5.

Table 5.4 Optimum conditions of the performance characteristics of dissimilar weldments

Sl. No.	Performance characteristics	Optimum condition	Optimum value
1.	UTS (MPa)	RS at 1025 rpm, TS at 25 mm/min, TTA at 2.5º	154.855
2.	%EL	RS at 1025 rpm, TS at 25 mm/min, TTA at 1.5º	13.819
3.	IS (J/mm^2)	RS at 500 rpm, TS at 75 mm/min, TTA at 2.5º	1.4360

Table 5.5 confirmation test results for validation of optimum values of dissimilar weldments

Sl. No.	Performance characteristics	Optimum condition	Optimum value	Conformation test results*
1.	UTS (MPa)	RS at 1025 rpm, TS at 25 mm/min, TTA at 2.5º	154.855	157.9521
2.	%EL	RS at 1025 rpm, TS at 25 mm/min, TTA at 1.5º	13.819	14.09538
3.	IS (J/mm^2)	RS at 500 rpm, TS at 75 mm/min, TTA at 2.5º	1.4360	1.316443

The obtained confirmation test results for tensile strength, traverse speed, and impact strength from regression equation were closer with least error ($\pm$6%). While the resulting equations produced are able to predict the mechanical properties to the acceptable level of accuracy.

5.3 Chapter Summary

In this chapter, the effect of FSW process parameters on the microstructure and mechanical properties of AZ31/AZ91 dissimilar weldments are summarized as follows:

i. The microstructure of the AZ91 Mg alloy and AZ31Mg alloy consisted of primary α-phase and lower volume fraction of β ($Mg_{17}Al_{12}$) phase in as-received condition which were verified by X-ray diffraction (XRD) analysis.
ii. Defect-free welds were produced for the dissimilar welding conditions of 25, 50, and 75mm/minute with varying tool rotational speed of 500, 720, 1025 rpm respectively.

iii. Hardness improved considerably at high rotational speeds (1025 RPM) as compared with lower rotational speeds due to more dynamic crystallization in the stir field. Compared to parent AZ31 Mg alloy and AZ91 Mg alloy, the average grain size of the SZ is substantially smaller regardless of the varying process parameters.

iv. The process parameter has significant effect on micro-structural, mechanical and corrosion properties of the dissimilar welds. The optimum condition obtained for ultimate tensile strength and percentage of elongation at rotational speed of 1025 rpm, traverse speed of 25 mm/minute, and tilt angle of 2.5°. The optimum conditions obtained for impact strength at rotational speed of 500 rpm, traverse speed of 75 mm/minute, and tilt angle of 2.5°. The results obtained agree well with the established theory.

v. ANOVA findings showed that traverse speed and tilt angle have a major effect on tensile strength, percentage of elongation, whereas traverse speed has less percentage of contribution on impact strength compared to tilt angle and rotational speed. It is observed that lower values are considered to be the R^2 values of all the built models. The calculated R^2 values for UTS, elongation and impact strength are 93.38, 91.67, and 89.99 % respectively for the developed models. The models built are therefore very adequate and are statistically valid at a 95 % confidence level.

CHAPTER − 6

CORROSION BEHAVIOR OF SIMILAR AZ91 / AZ91 AND DISSIMILAR AZ31 / AZ91 Mg ALLOY WELDMENTS

6. 1 Introduction

This chapter describes the corrosion behaviour of the as-prepared similar and dissimilar weldments in comparison to the respective parent alloys. The applications of Mg alloys are often challenged by their poor corrosion resistance in aqueous environments. As corrosion of a material is often influenced by its microstructure, which in turn is governed by the processing, corrosion study of reactive materials such as Mg alloys is therefore inevitable whenever new processing routes such as friction stir welding are used explored to process these alloys. Corrosion of Mg alloy in a given environment is found to be primarily governed by microstructure, alloying additions, particularly Fe, Ni, Cu, Si, and Co, and distribution and volume fraction of the constituent phases. Hence, the role of microstructure in the corrosion process has received great interest in assessing the microstructural impact on the corrosion characteristics of mg alloys, which further leads to alloy development through various casting and processing routes aimed at improving microstructure.

Corrosion of Mg-based weldments is invariably a cause for concern as the weldments are often different in microstructure (and composition in case of dissimilar welding). In particular, corrosion of Mg-based weldments is of particular interest as they are characterized by high chemical reactivity and low redox potentials in a wide range of environments. While

previous studies on FSW of Mg-based alloys reported on the microstructure and mechanical properties [119–123], there is no information on the corrosion behaviour of friction stir welded Mg alloy components. As corrosion of a given material in a given environment is primarily governed by its microstructure, which is in turn governed by the processing, it is necessary to understand the corrosion of friction stir welded components as FSW tends to produce a microstructure which is appreciably different from those that result from conventional welding methods. As the weldments are subjected to severe plastic deformation during FSW [124], it is interesting to study the effect of evolving microstructure on corrosion of Mg-based alloys considering the fact that their recrystallization temperatures are relatively low.

In this chapter, the influence of welding parameters on corrosion properties of Friction stir welded Magnesium based AZ91 Mg alloy, and AZ31 Mg alloy is reported. Similar AZ91 to AZ91 Mg alloy plates and dissimilar AZ91 to AZ31 Mg alloy plates of 130 mm long, 45 mm wide, and 3 mm thickness butt joints were produced using a commercially available automated vertical milling machine as shown in Figure 3.1 (Chapter 3). Taguchi method was used to obtain the optimum combinations of processing parameters such as rotational speed (RPM), welding speed (mm/min), and tilt angle (degree) for improving the microstructural and corrosion properties of weldments. This chapter explores the corrosion behaviour of the similar and dissimilar weldments obtained by FSW in 3.5 wt. % NaCl as a function of processing parameters and the resulting microstructure. The processing parameters included in this chapter are rotational speed (500 to 1025 RPM), tilt angle (1.5° to 2.5°), and weld speed (25 to 75mm/min). The potentiodynamic polarization was used to determine their corrosion behaviour in 3.5 wt.% NaCl. The corrosion of similar welds were compared to that of dissimilar welds.

6. 2 Results and Discussions

6. 2. 1 Corrosion Behaviour in 3.5 wt.% NaCl

6. 2. 1. 1. Potentiodynamic Polarization Measurements on Similar Weldments

Figure 6.1 presents the Tafel polarization in 3.5 wt% NaCl. The electrochemical corrosion parameters, namely E_{corr}, $i_{corr,}$ and Tafel slopes, were extracted from these Tafel plots and

tabulated in Table No. 6.1. It is evident from these Tafel plots and Table No. 6.1 that AZ31 Mg alloy was superior in corrosion resistance compared to AZ91 Mg alloy. The greater corrosion resistance of AZ31 Mg alloy (Figure 6.1) can be immediately ascribed to the smaller volume fraction of $Mg_{17}Al_{12}$ intermetallic phase (Refer chapter 5).

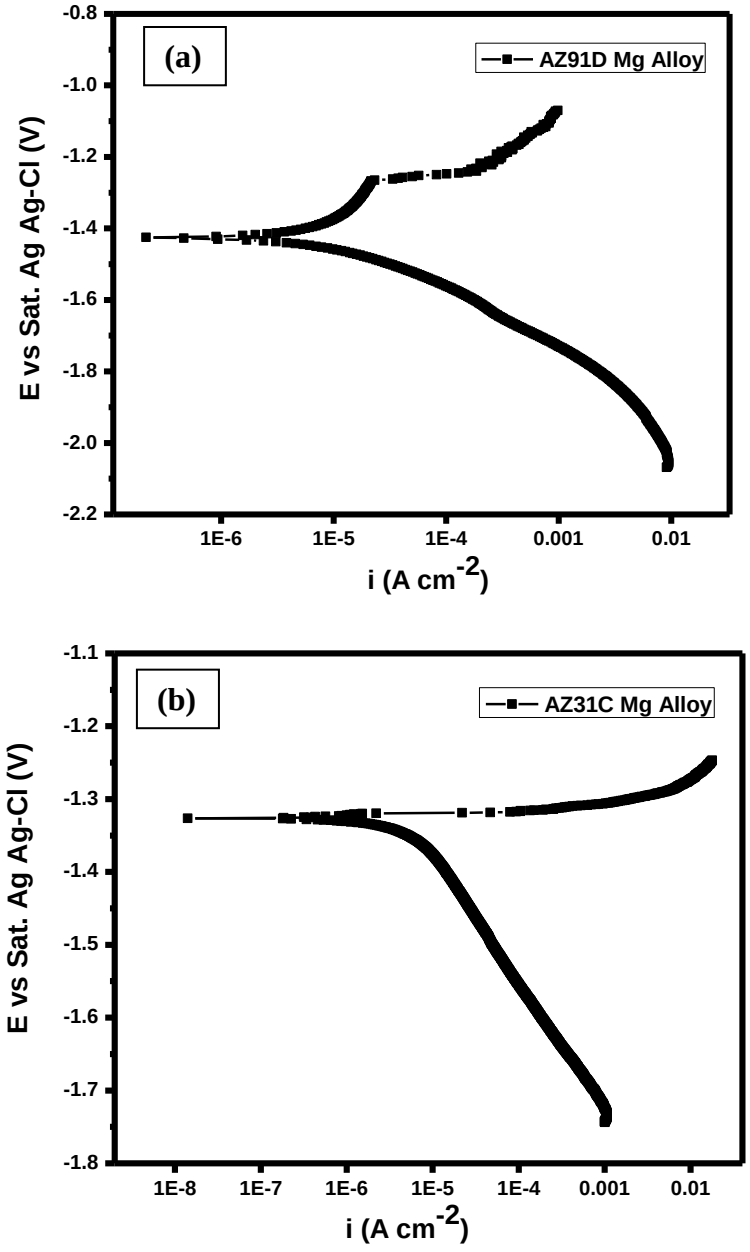

Figure 6.1 Anodic polarization curves of (a) AZ91Mg alloy (parental metal) and (b) AZ31 Mg alloy (parental alloy).

Table 6.1 Electrochemical data of AZ91Mg alloy and AZ31 Mg alloy.

Details	**AZ 91D Mg alloy (Base)**	**AZ31Mg alloy (Base)**
Corrosion rate (mpy)	12.137	5.520
E_{corr} (V vs Ag-AgCl)	-1.425	-1.326
i_{corr} ($\mu A/cm^2$)	13.687	5.822
β_a (mV/decade)	660.07	183.722
β_c (mV/decade)	147.155	65.556

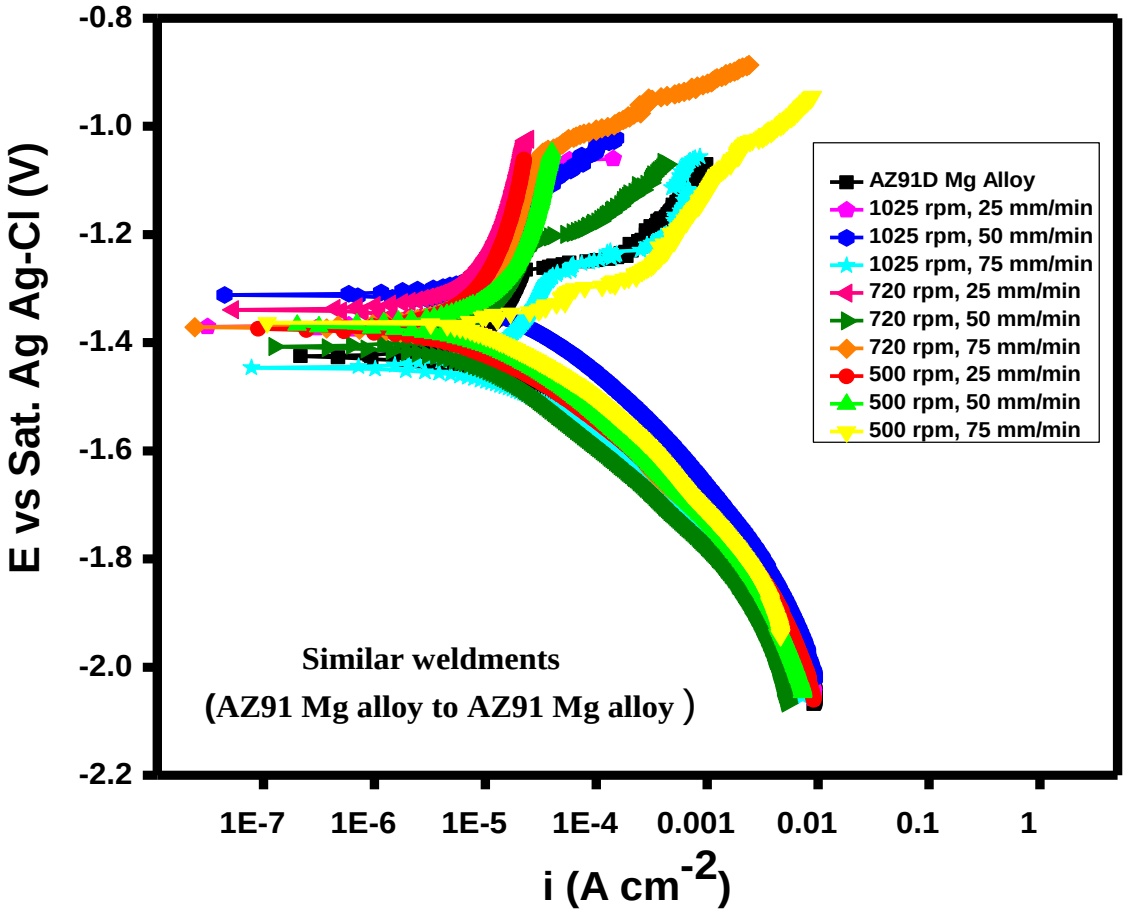

Figure 6.2. Consolidated Tafel curves of similar weldments (AZ91Mg Alloy) processed at different conditions in 3.5 % NaCl solution

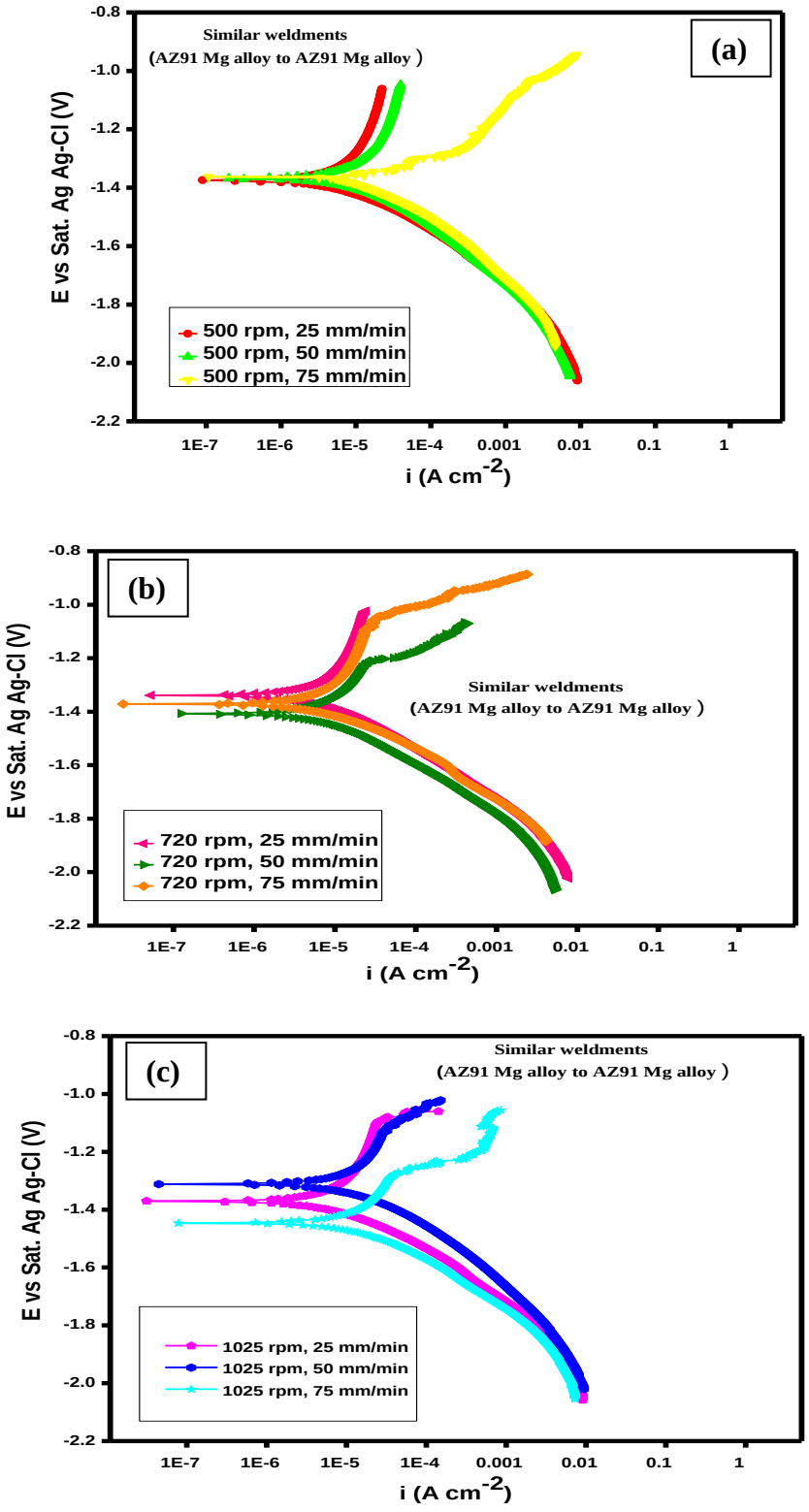

Figure 6.3 (a-c) Tafel curves of similar weldments as a function of rotational speed.

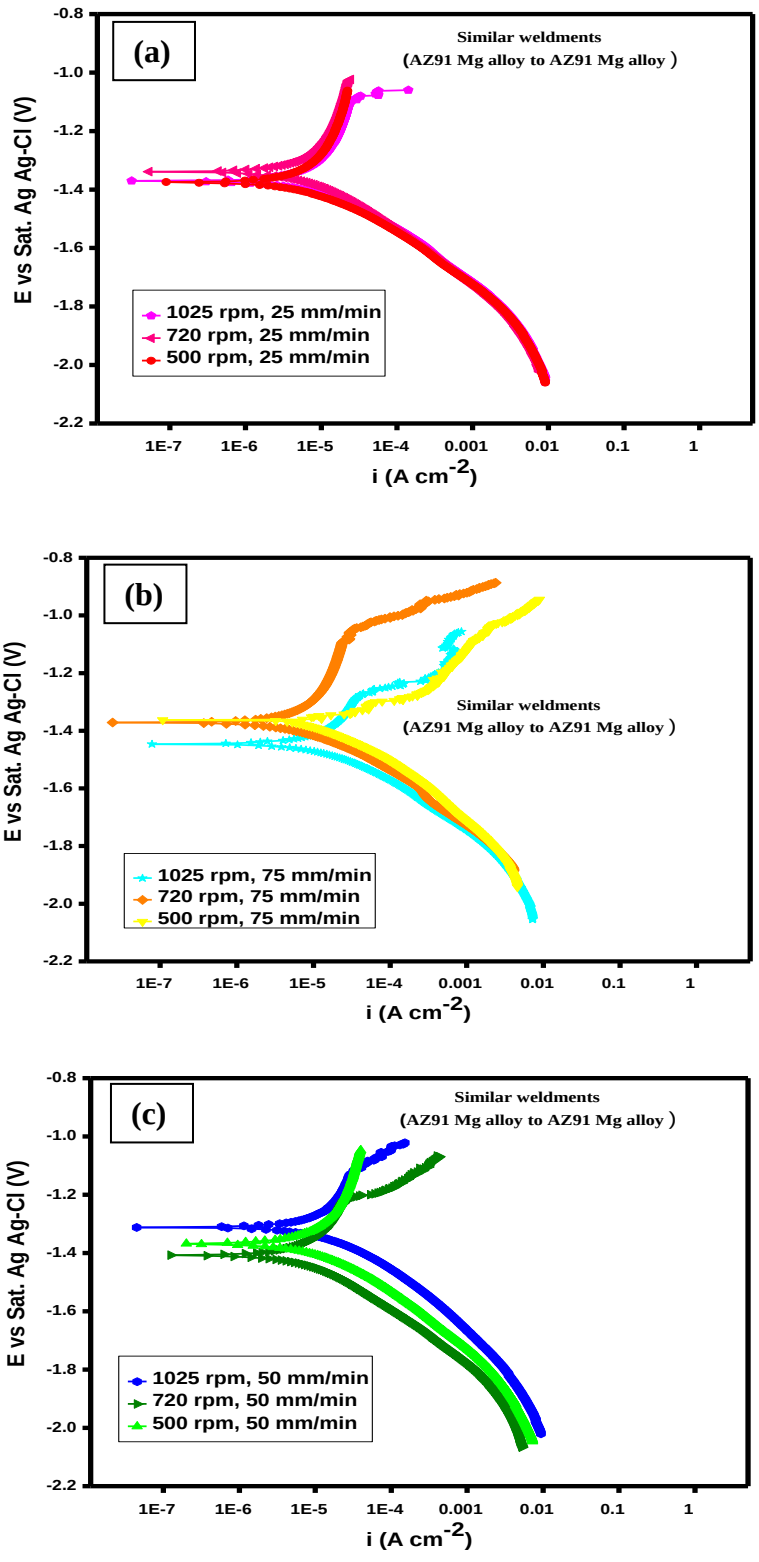

Figure 6.4 (a-c) Tafel curves of similar weldments as a function of traverse speed.

The corrosion rate (in mpy) was subsequently calculated using the following expression [125].

$$\text{Corrosion rate (mpy)} = \frac{0.13 \times i_{corr} \times W_{eq}}{A\rho} \quad (6.1)$$

Where 'W_e' is Equivalent weight (g), 'ρ' is density (g/cc), and 'A' is Area (cm^2). Accordingly, the corrosion rate of AZ91 Mg alloy and AZ31 Mg alloy was found to be 12.137 and 5.520 mpy, respectively.

Table 6.2 Electrochemical parameters of similar weldments (AZ91Mg alloy to AZ91Mg alloy) obtained from potentiodynamic polarization in 3.5% NaCl solution.

Details	1025 RPM, 25 mm/min	1025 RPM, 50 mm/min	1025 RPM, 75 mm/min	720 RPM, 25 mm/min	720 RPM, 50 mm/min	720 RPM, 75 mm/min	500 RPM, 25 mm/min	500 RPM, 50 mm/min	500 RPM, 75 mm/min
Corrosion rate (mil/ year)	8.965	19.406	17.065	8.909	14.21	9.743	8.075	13.869	29.943
E_{corr} (V vs Ag-AgCl)	-1.371	-1.311	-1.466	-1.339	-1.407	-1.371	-1.375	-1.368	-1.372
i_{corr} ($\mu A/cm^2$)	10.111	21.885	19.245	10.047	16.025	10.989	9.107	15.641	33.769
β_a (mV/ decade)	650.53	1092	517.45	793.12	1125	711.87	673.01	676.98	84.731
β_c (mV/ decade)	166.16	204.84	165.93	213.72	234.50	174.14	159.76	203.05	189.63

For the sake of coherent discussion, the Tafel curves from the similar weldments (shown in Figure 6.2) are presented in Figure 6.3 (a-c) and Figure 6.4 (a-c). Figure 6.3 (a-c) shows the Tafel curves of similar weldments as a function of RPM while Figure 6.4 (a-c) depict the Tafel behaviour of similar weldments as a function of traverse speed. Figure 6.2 shows the Tafel curves recorded on both parent alloys and similar weldments of AZ91 Mg alloy. The extracted electrochemical parameters are shown in Table 6.2. From the Tafel plots shown in Figure 6.2, Figure 6.3 (a-c), Figure 6.4 (a-c) and Table 6.2, it is evident that parent

metals and similar weldments (AZ91) showed different anodic polarization curves while their cathodic polarization segments were roughly similar. Between parent metals, AZ31 registered larger E_{corr} and smaller i_{corr} than AZ91, indicating lower corrosion resistance of AZ91. This can be attributed to the little or absence of matrix-Mg_{17} Al_{12} galvanic coupling. Mg_{17} Al_{12} becomes cathodic to the matrix, promoting galvanic corrosion. This is particularly true when the volume fraction of β (cathodic phase is very small compared to the matrix.

The corrosion resistance of similar weldments decreased in the following order: 500 RPM, 25 mm/min (i_{corr} 9.107) > 720 RPM, 25 mm/min (i_{corr} 10.047) > 1025 RPM, 25mm/min (i_{corr} 10.111)>720 RPM, 75 mm/min (i_{corr} 10.989)>AZ91 Mg alloy (i_{corr} 13.697)>500 RPM, 50 mm/min(i_{corr} 15.641)>720 RPM, 50 mm/min (i_{corr} 16.025)>1025 RPM, 75 mm/min (i_{corr} 19.245)>1025 RPM, 50 mm/min (i_{corr} 21.885)>500 RPM, 75 mm/min (i_{corr} 33.769). Weldments of Similar welding (AZ91 Mg alloy to AZ91 Mg alloy) of condition 500 RPM, 25 mm/min (i_{corr} 9.107), 720 RPM, 25mm/min (i_{corr} 10.047), 1025 RPM, 25mm/min (i_{corr} 10.111) and 720 RPM, 75 mm/min (i_{corr} 10.989) showed improved corrosion resistance compared to AZ91 Mg alloy ((i_{corr} 13.697) parent metal) after one hour immersion in 3.5% NaCl environment.

The observed negative E_{corr} values and high corrosion rates of alloys lower potential and exceptionally high reactivity of Mg Chloride environment [126]. Mg can be simply attributed to standard electrode. It is worth noting that pure Mg is prone to corrosion due to highly negative E_{corr} (-1.63 V vs SCE) value. The presence of salts such as Cl^- make them highly vulnerable to corrosion at all the pH values due to dissolution of MgO surface layer. Chloride ions generally promote local breakdown of the natural surface films $Mg(OH)_2$. The protective ability passive films depend largely on the environment, microstructure and impurities in the metallic material [127-129].

Between parent AZ91 and FSW AZ91, the latter demonstrated a superior electro chemical stability against Cl^- ions. While the parent metal (AZ91) showed a low passive film breakdown potential(of about -1.25 volts), the weldments obtained under tool rotation of 500 RPM and traverse speed of 25 mm/min were found to passive till -1.0 volts suggesting an improved stability of passive films. Such variations in the nature of surface films can offer result in changes in anodic polarizations. The weldments obtained under high rotation speed

and high traverse speed however were susceptible to passive film breakdown at potentials less than -1.0 volts. This led to formation of pits [130-133].

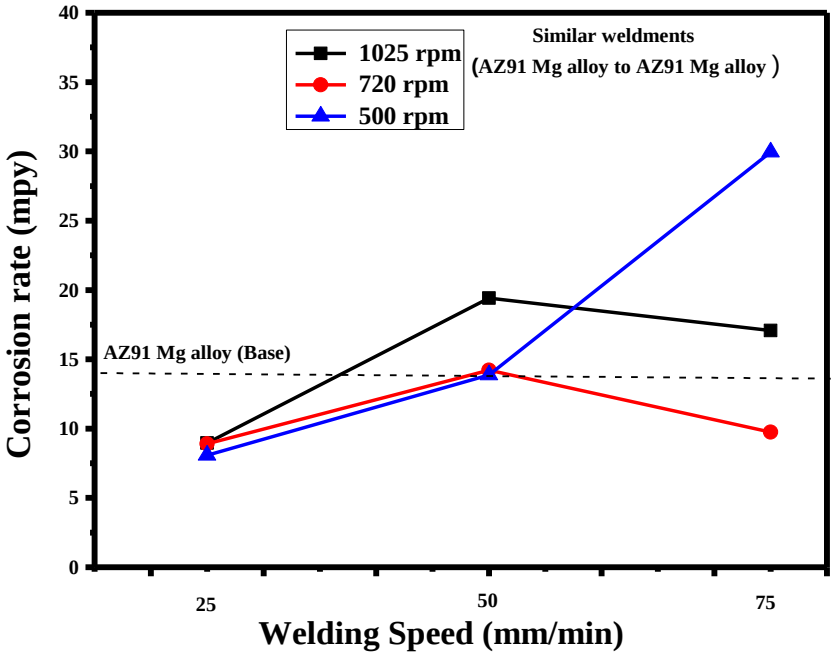

Figure 6.5 Schematic showing the corrosion rate of the parent alloys and similar weldments at different process parameters.

Corrosion behavior of Mg-Al alloys in Cl^- media is generally governed by the nature of surface passive films and the micro structure. The local anodic dissolution of these alloys is normally caused by galvanic coupling between the matrix-intermetallic phase, which act as anode and cathode respectively. The improved corrosion resistance offered by similar weldments can be attributed to reduced volume fraction of $Mg_{17}Al_{12}$ phase due to redissolution of fraction of this intermediate phase during FSW and grain refinement [Refer chapter 4]. The grain size normally place an indirect role in corrosion behaviour of these alloys. The observed increase in their corrosion resistance with reduction in grain size can be attributed to enhanced partial film formation it is worth noting has that smaller grains promote passive film formation due to increased surface film area. Also, the finer grains are expected to enhance the passivity due to increased Al content.

Also, compared to the parent alloy [AZ31 Mg alloy], the similar weldments obtained using 500 RPM and 25mm/minute registered a high passive breakdown potential suggesting

a relatively superior passive film stability in Cl^- used. On the other hand, the weldments obtained under high RPM and welding speed yielded less passive breakdown potentials (< -1.0 V) which consequently led to formation of pits. For the sake of simplicity the effect of welding parameters namely RPM and traverse speed on the corrosion rate is shown in Figure 6.5. From the closer examination of the Tafel results, it can be noticed that the lowest weld speed, namely 25 mm/minute yielded comparatively low corrosion rate irrespective of rotational speed.

6. 2. 1. 2.Potentiodynamic Polarization Measurements on Dissimilar Weldments

Figure 6.6 presents the Tafel polarization of dissimilar weldments in 3.5 wt% NaCl. The electrochemical corrosion parameters namely E_{corr}, i_{corr} and Tafel slopes were extracted from this Tafel plots and tabulated in Table 6.3. It is evident from the Tafel plots and table that dissimilar weldments was superior in corrosion resistance compared similar weldments. Greater corrosion resistance of dissimilar weldment (Figure 6.6) can be immediately ascribed to the smaller volume fraction of ascribed $Mg_{17}Al_{12}$ intermetallic phase [Chapter 5]. The Tafel curves of the dissimilar welds (shown in Figure 6.6) are shown in Figure 6.7 (a-c) and Figure 6.8 (a-c) for the sake of coherent discussion . Figure 6.7 (a-c) shows the Tafel curves of dissimilar weldments as a function of RPM while Figure 6.8 (a-c) depict the Tafel behaviour of dissimilar weldments as a function of traverse speed. In the dissimilar welding (AZ91 Mg alloy to AZ31 Mg alloy) the weldments of condition 1025 RPM, 50 mm/min(i_{corr} 2.457), 720 RPM, 25 mm/min(i_{corr} 3.577) showed improved corrosion resistance as compared to AZ91 Mg alloy ((i_{corr} 13.697) parental metal) and AZ31 Mg alloy ((i_{corr} 5.822) parental metal)). In addition, both these weldments displayed a comparatively high breakdown potentials, which clearly indicated superior passive film stability.

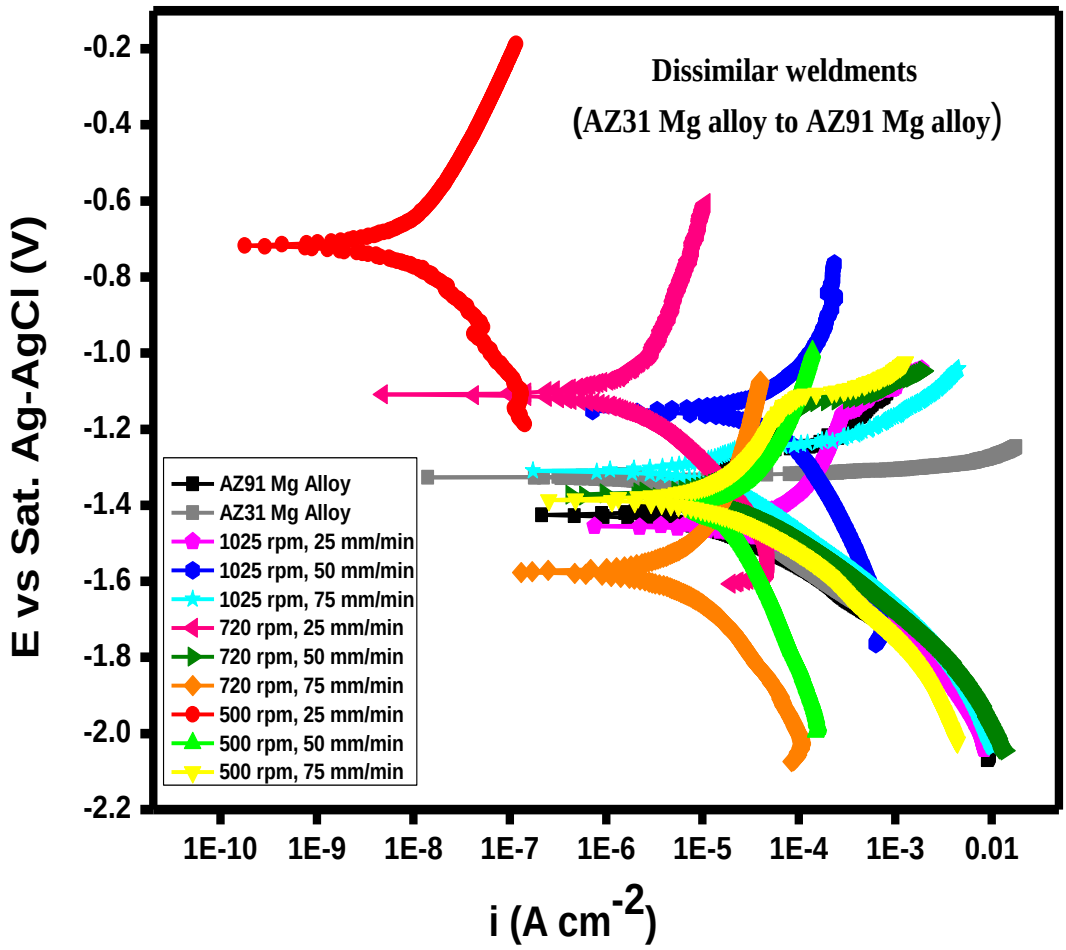

Figure 6.6. Consolidated Tafel curves of dissimilar weldments (AZ31Mg to Alloy AZ91Mg alloy) processed at different conditions in 3.5 % NaCl solution

Compared to similar weldments, dissimilar weldments produced relatively high corrosion rates, and showed no correlation with regard to processing parameters. Based on the above results on Tafel polarization, tool rotation speed in the range of 500 - 720 RPM and traverse speed in the range of 25 – 50 mm/min can be used to produce highly stable weldments for applications in aggressive environments such as NaCl. 3.5 wt.% NaCl constitutes a sufficiently large concentration of aggressive chloride ions that can weaken air-formed MgO passive films as widely reported in the literature [131]. However, a further study is necessary to understand the passive film stability as a function of microstructural changes caused by FSW.

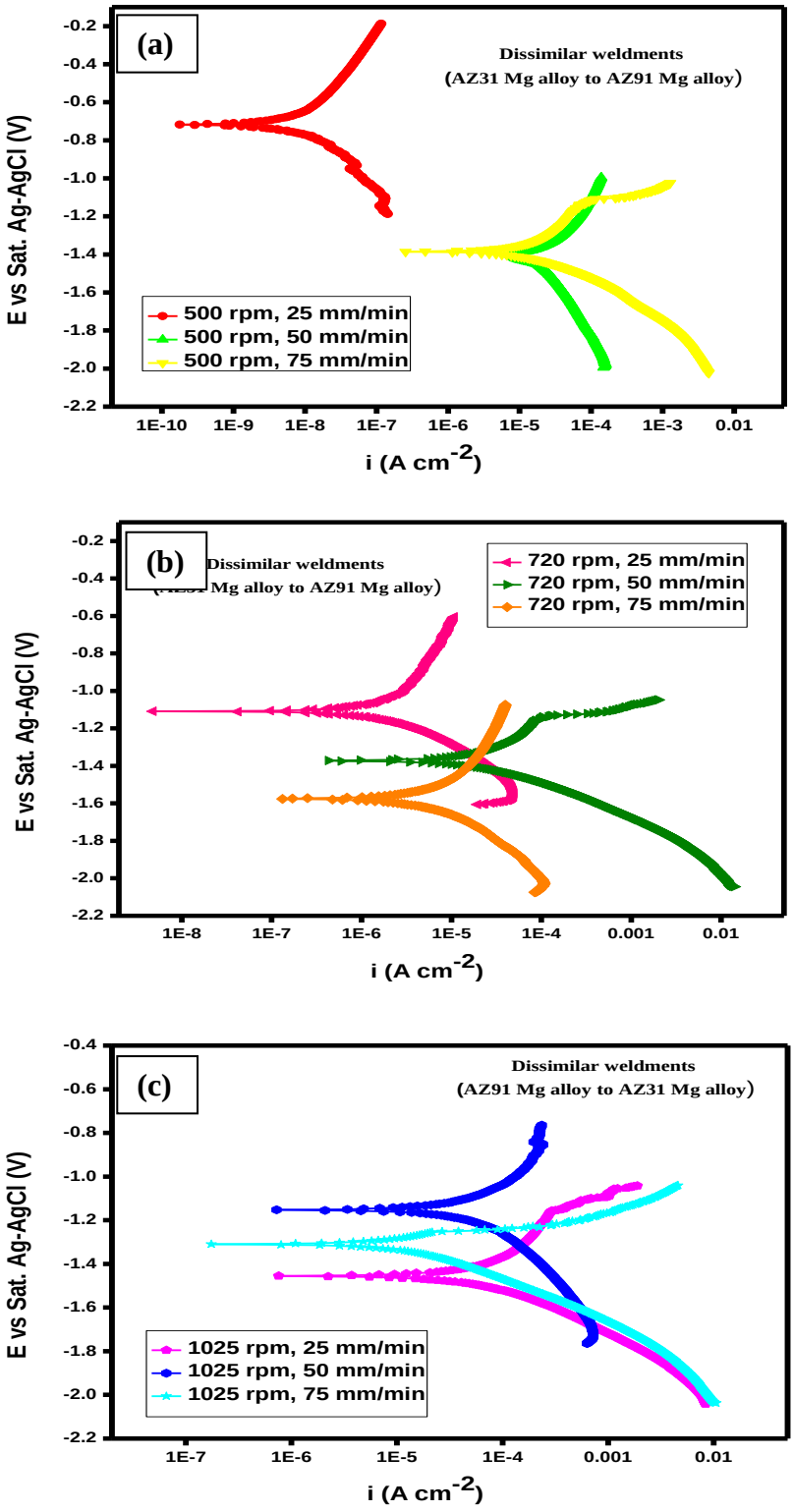

Figure 6.7 (a-c) Tafel curves of dissimilar weldments as a function of rotational speed.

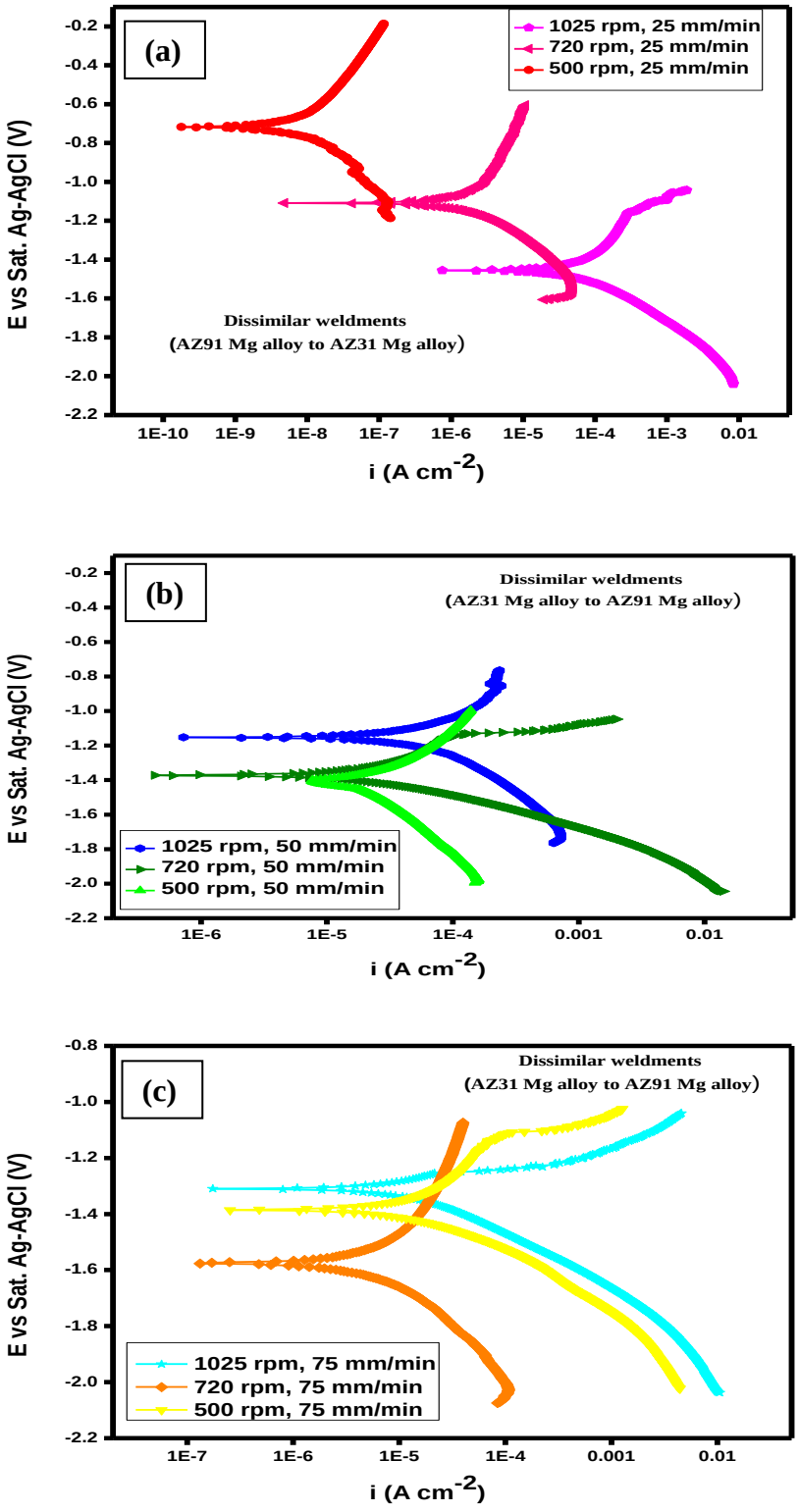

Figure 6.8 (a-c) Tafel curves of dissimilar weldments as a function of traverse speed.

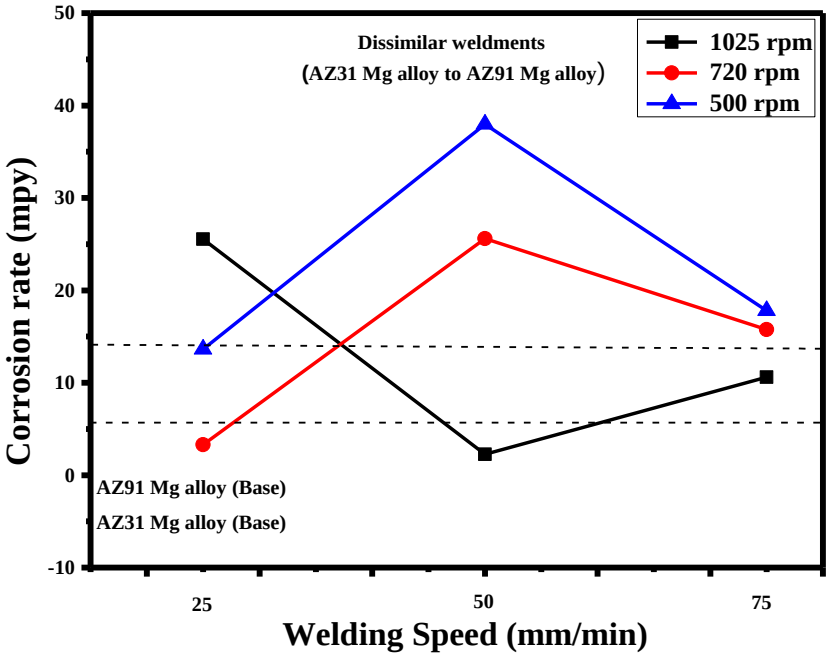

Figure 6.9 Schematic showing the corrosion rate of the parent alloys and dissimilar weldments at different process parameters.

Table 6.3 Electrochemical data of dissimilar weldments (AZ31Mg alloy to AZ91Mg alloy) obtained from potentiodynamic polarization in 3.5% NaCl solution.

Details	1025 RPM, 25 mm/min	1025 RPM, 50 mm/min	1025 RPM, 75 mm/min	720 RPM, 25 mm/min	720 RPM, 50 mm/min	720 RPM, 75 mm/min	500 RPM, 25 mm/min	500 RPM, 50 mm/min	500 RPM, 75 mm/min
Corrosion rate (mil/ year)	25.550	2.264	10.600	3.297	25.588	15.769	13.637	37.980	17.795
E_{corr} (V vs Ag-AgCl)	-1.455	-1.15	-1.304	-1.108	-1.373	-1.576	-713.55	-1.407	-1.385
i_{corr} ($\mu A/cm^2$)	27.713	2.457	11.5	3.577	27.76	17.108	14.795	41.203	19.305
β_a (mV/ decade)	111.875	26675	83471	1196	394627	1266	620.23	308.675	418.733
β_c (mV/ decade)	99.897	6690	187833	331.833	184.159	532.491	355.356	1356	190.21

6. 2. 2 Open Circuit Potential Behavior

6. 2. 2. 1. OCP Analysis of Similar Weldments

Compared to parent alloy, low and medium RPM produce adequately stable film compared to base metal. Similar weldments at low RPM and speed, the surface film were found to be adequately stable and intact as indicated by the little or minor fluctuations in OCP. The film for 720 RPM, was found to be reasonably stable compared to both 1025 RPM and low RPM as indicated by the high value of OCP. The results fairly agree with Tafel results as discussed above.

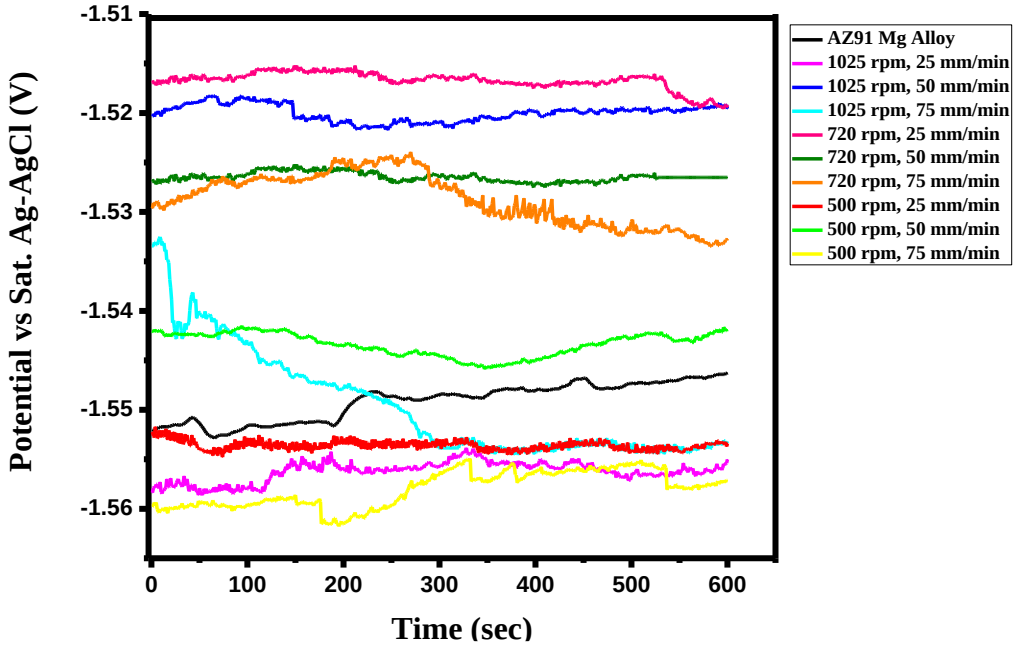

Figure 6.10 Variation in the evolution of open circuit potential (OCP) of AZ91 Mg alloy (Base) and similar weldments with exposure time.

6. 2. 2. 2. OCP Analysis of Dissimilar Weldments

Both base metals did not show any classic signature of localized film break down. The surface film on base metal are expected to be intact during the immersion period. OCP curves did not show any specific correlation with measured corrosion rates. This might be due to predominately effect of fairly complicated microstructure consisting of two matrix phases and

fragmented intermetallic particles. This could subsequently result in increased galvanic effect, and thus increased corrosion rates. Also, a close examination of the OCP curves shows in Figure 6.11 reveals that high rotational speed coupled with medium to high traverse speed could make the weldments more prone to localized corrosion.

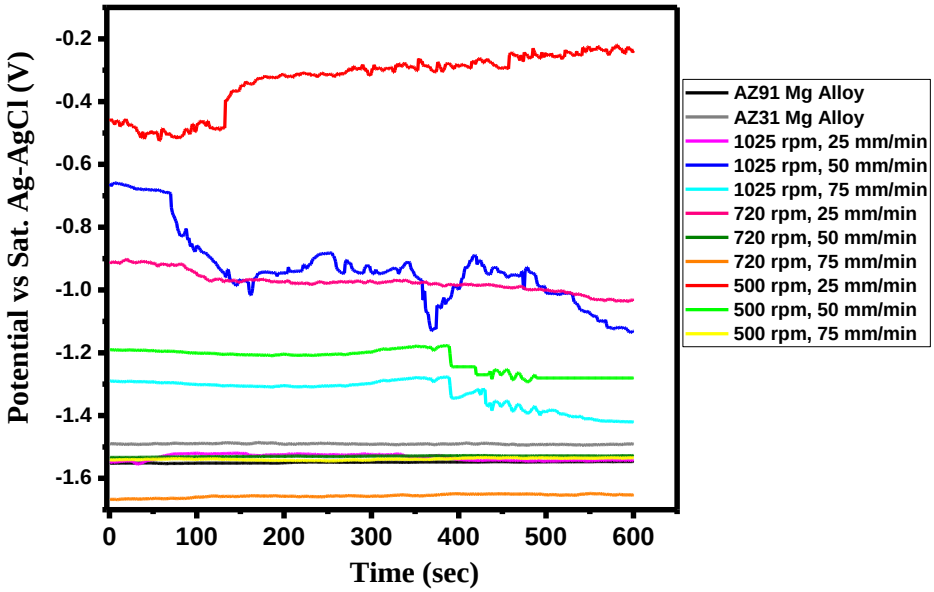

Figure 6.11 Variation in the evolution of open circuit potential (OCP) of AZ91 Mg alloy (Base alloy), AZ31 Mg alloy (Base alloy) and dissimilar weldments with exposure time.

6. 2. 3 Study of Surface Morphology After Corrosion Test

It is generally observed that Mg alloys are prone to formation of pits due to localized corrosion .The surface corrosion products often cover these pits which challenges the analysis of pit size

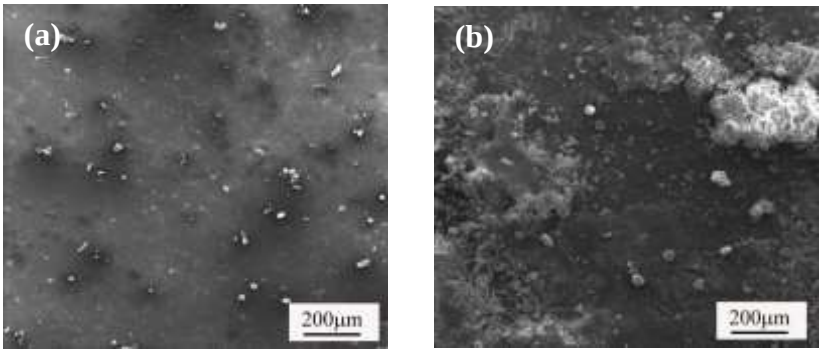

Figure 6.12 SEM surface morphologies of (a) AZ91 Mg alloy (b) AZ31 Mg alloy

and density. Detailed analysis of surface morphology after the corrosion tests revealed that these pits generally nucleate at matrix-$Mg_{17}Al_{12}$.

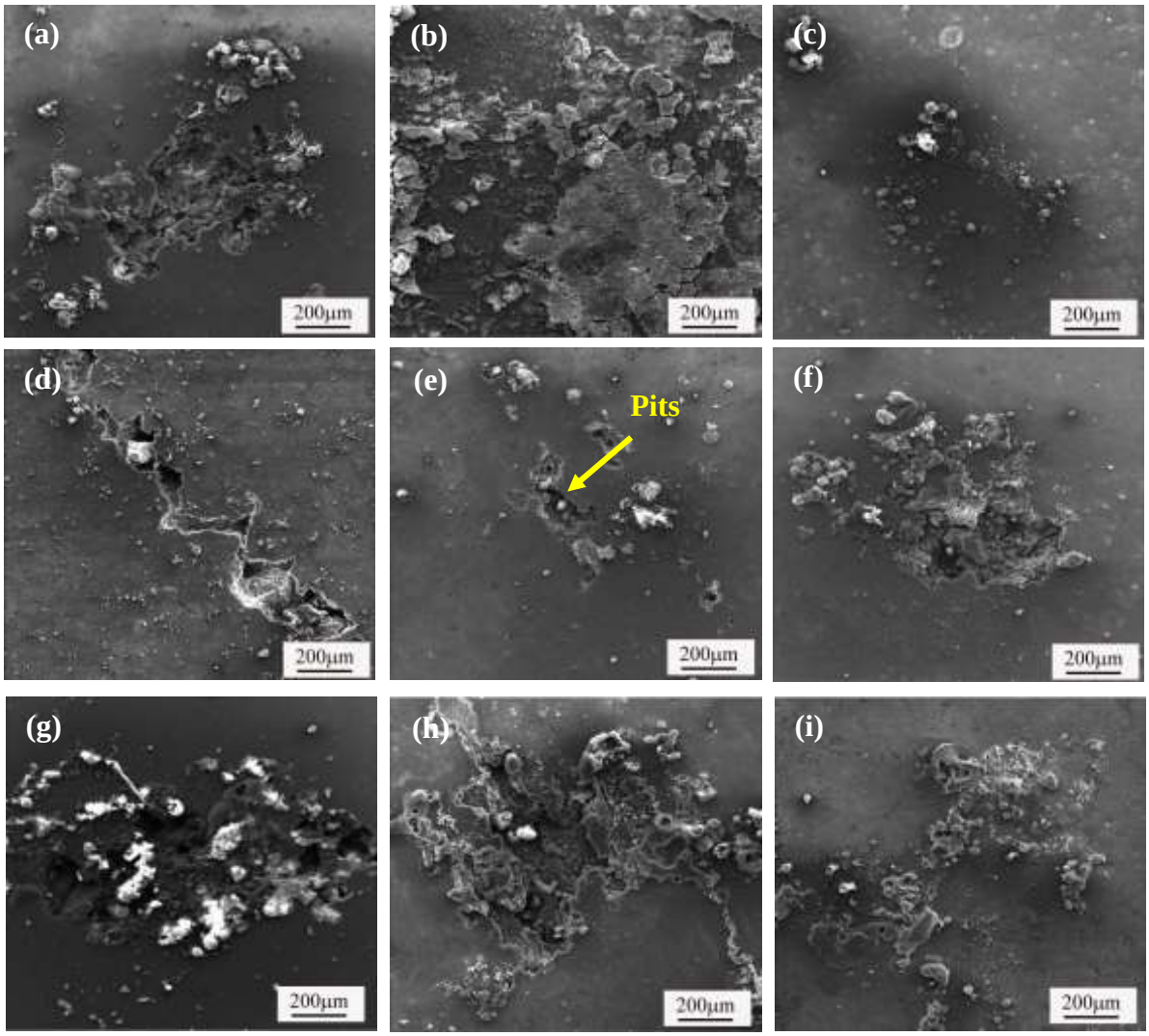

Figure 6.13 SEM surface morphologies of Similar Weldments(AZ91 Mg alloy to AZ91 Mg alloy) at different welding conditions, (a) 500 rpm, 25 mm/min, 1.5° (b) 500 rpm, 50 mm/min, 2° (c) 500 rpm, 75 mm/min, 2.5° (d)720 rpm, 25 mm/min, 2° (e) 720 rpm, 50 mm/min, 2.5° (f) 720 rpm, 75 mm/min, 1.5° (g) 1025 rpm, 25 mm/min, 2.5° (h)1025 rpm, 50 mm/min, 1.5°and (i) 1025 rpm, 75 mm/min , 2°.

The surface films on Mg alloys exposed to Cl^- media consist of a mixture of MgO and $Mg(OH)_2$. The chemical and electro chemical reactions between the Mg alloys and Cl^- media can be described has follows.

$$Mg \longrightarrow Mg^{2+} + 2e \qquad \text{-------(1)}$$

$$2H_2O + 2e \longrightarrow 2OH^- + H_2 \qquad \text{--------(2)}$$

$$Mg^{2+} + 2OH^- \longrightarrow Mg(OH)_2 \qquad \text{--------(3)}$$

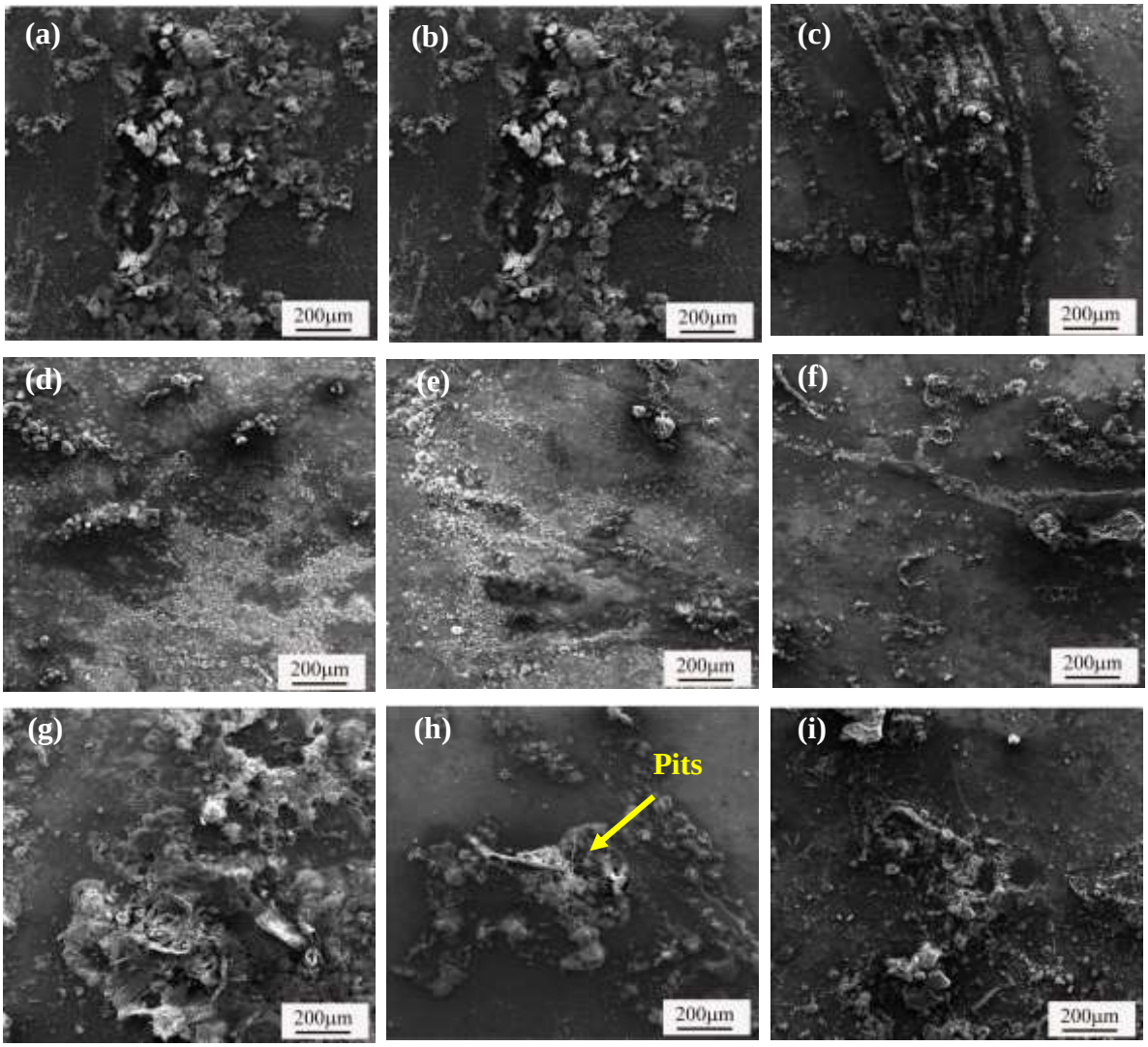

Figure 6.14 SEM surface morphologies of dissimilar Weldments(AZ31 Mg alloy to AZ91 Mg alloy) at different welding conditions, (a) 500 rpm, 25 mm/min, 1.5° (b) 500 rpm, 50 mm/min, 2° (c) 500 rpm, 75 mm/min, 2.5° (d)720 rpm, 25 mm/min, 2° (e) 720 rpm, 50 mm/min, 2.5° (f) 720 rpm, 75 mm/min, 1.5° (g) 1025 rpm, 25 mm/min, 2.5° (h)1025 rpm, 50 mm/min, 1.5°and (i) 1025 rpm, 75 mm/min , 2°.

Being a basic oxide, MgO is generally protective in alkaline environment. While it offers only limited or mild protection in acidic and neutral media. The presence of aggressive Cl^- in aqueous media make this Mg alloys even more susceptible to corrosion. Cl^- ions lead to local breakdown of the MgO surface film thereby promoting anodic dissolution of Mg according to the reaction (1).The released Mg^{2+} ions get precipitated as $Mg(OH)_2$ occurring to low solubility constant (Ksp = 5.61x10-12) [134]. The formation of $Mg(OH)_2$ resulting from local breakdown of the MgO film can be simply described as follows.

$MgO + H_2O \longrightarrow Mg(OH)_2$ -------(4)

The Cl^- ion concentration in 3.5 wt% NaCl solution is high enough to cause local surface film breakdown. The SEM-EDS composition analysis revealed the possible formation of MgO and $Mg(OH)_2$ (Figure 6.15 to Figure 6.18).

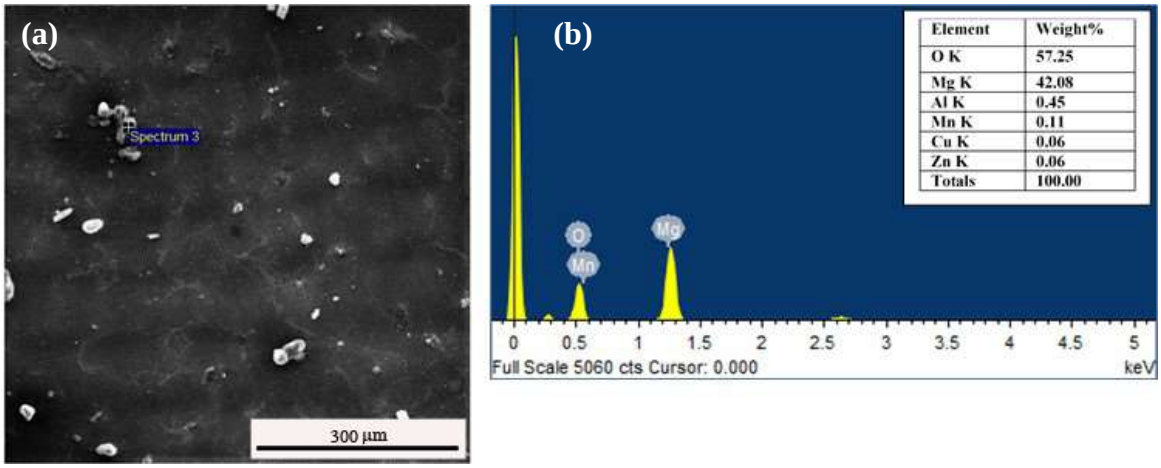

Figure 6.15 SEM-EDS analysis of (a) as received AZ91 Mg alloy (b) corresponds to spectrum and mass % of elements

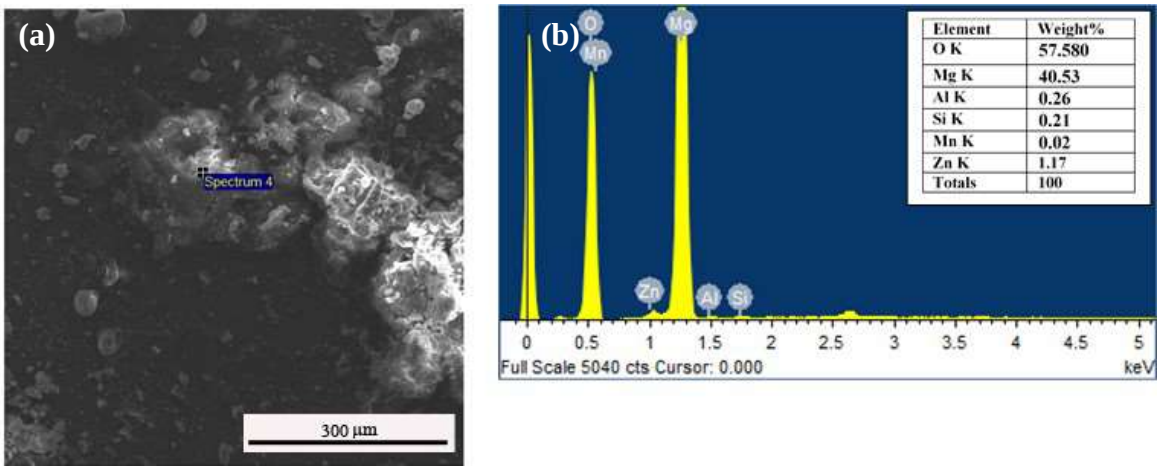

Figure 6.16 SEM-EDS analysis of (a) as received AZ31 Mg alloy (b) corresponds to spectrum and mass % of elements

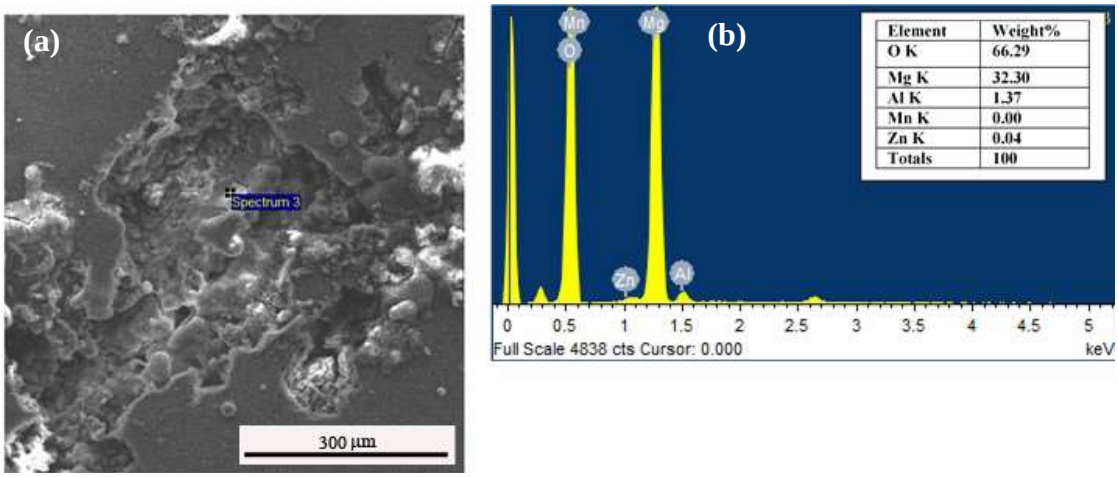

Figure 6.17 SEM-EDS analysis of (a) similar weldment (AZ91 Mg alloy to AZ91 Mg alloy) of condition 500 RPM, 25 mm/minute (b) corresponds to spectrum and mass % of elements.

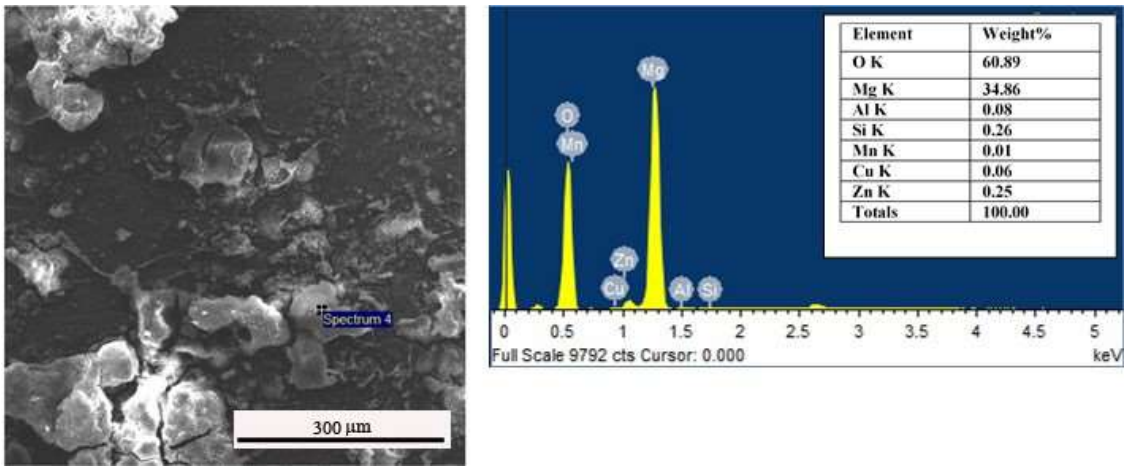

Figure 6.18 SEM-EDS analysis of (a) dissimilar weldment (AZ31 Mg alloy to AZ91 Mg alloy) of condition 1025 RPM, 50 mm/minute (b) corresponds to spectrum and mass % of elements.

Corrosion products were analyzed using SEM-EDS for parent alloys (AZ91 Mg alloy and AZ31 Mg alloy), similar and dissimilar weldments having high corrosion resistance. There is dominant amount of oxygen along with base metal, which indicates the possible formation of oxides like MgO, $Mg(OH)_2$.

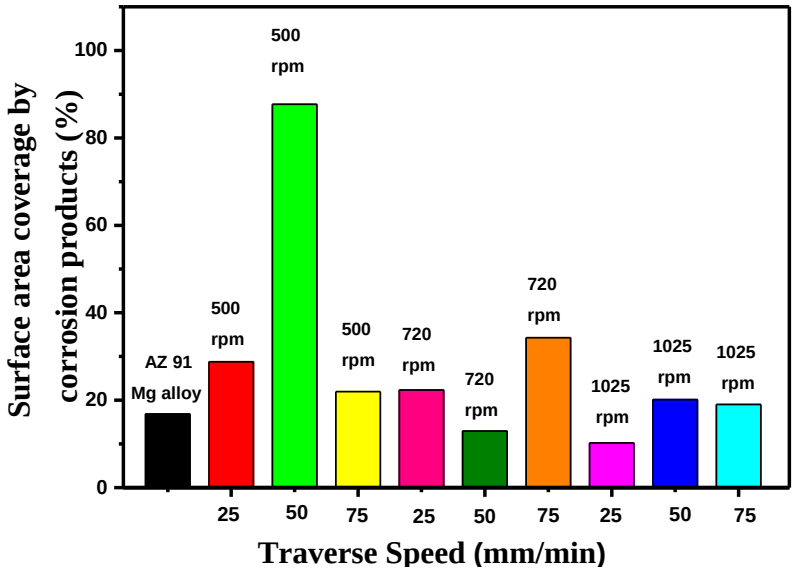

Figure 6.19 Percentage of surface covered by corrosion products on similar weldments.

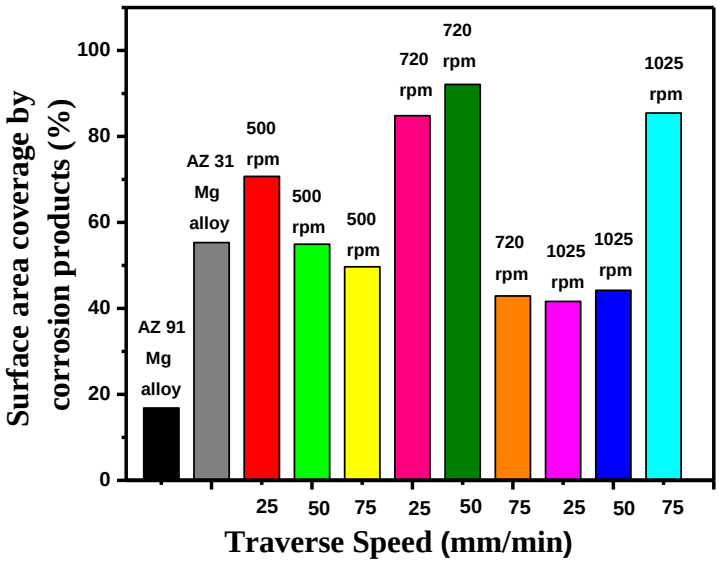

Figure 6.20 Percentage of surface covered by corrosion products on dissimilar weldments.

An attempt was made to relate the surface coverage by corrosion products to the corrosion behavior. Figure 6.19 and Figure 6.20 present the surface coverage by the corrosion products. Lack of such correlation can be traced back to the fact that most of the corrosion products forms during in immersion in chloride media. In other words, $Mg(OH)_2$ which is

predominantly in surface corrosion product forms prior to tafel polarization measurements. However, it is worth notify that surface coverage by corrosion products was more on dissimilar weldments than similar weldments. Which can be initially ascribed to the high corrosion rate of dissimilar weldments. Such increased corrosion and corrosion products, as already stated, can be attributed to enhanced galvanic effects as shown below.

(1) Matrix phase 1 - $Mg_{17}Al_{12}$ couple
(2) Matrix phase 2 - $Mg_{17}Al_{12}$ couple
(3) Matrix phase 1 - Matrix phase 2

6. 3 Chapter Summary

This chapter describes the effect of FSW processing parameters on corrosion, AZ91 D/AZ91D similar weldments and AZ31 /AZ91D dissimilar weldments in 3.5 wt. % NaCl. Careful analysis of corrosion results, and electrochemical morphology, microstructure and compositional analysis via XRD and SEM reveals that corrosion behavior can be related to the microstructure, particularly, grain size, β phase volume fraction and distribution.

i. Lack of proper correlation between the corrosion behaviour and processing parameters (traverse speed and rotational speed) can be somewhat attributed to changes in the tilt angle and highly unstable nature of surface passive films on this materials
ii. Corrosion of these alloys in Cl^- media was primarily caused by matrix - β phase galvanic coupling, distribution of β phase and local breakdown of surface passive films. Corrosion rates of dissimilar weldments was found to be greater than that of similar weldments, due to enhance galvanic effects caused by the presence of two phases and intermetallic phases. Al content, grain size and defect density can influence the corrosion by modifying the volume fraction, distribution of β phase and nature of surface passive films.
iii. Both parent metal (AZ91D and AZ31) and the weldments registered negative values of E_{corr} , indicating their high tendency to corrosion in chloride media. This can be easily ascribed to high reactivity of Mg alloys in Cl^- media.
iv. Compared to parent alloys, the weldments invariably showed high corrosion rates due to introduction of crystal defects particular dislocation during FSW. However, the

reduction of corrosion resistance was somewhat controlled by the fragmentation and uniform distribution of β phase. Corrosion of dissimilar weldments was found to be greater than that of similar weldments, due to the enhanced galvanic effects between two matrix phases and intermetallic phase.

v. While Tafel polarization studies reveled the kinetics of corrosion, OCP curves were found to be useful in qualitatively judging stability of the passive surface films on these alloys. Thus, overall corrosion behaviour of these alloys needs to be determined using both Tafel polarization and OCP measurements. In evaluating the overall corrosion behaviour of such alloys, the Tafel polarization studies are invariably complemented by OCP curves.

CHAPTER − 7

CONCLUSIONS & FUTURE SCOPE

7. 1 Introduction

AZ91D Magnesium alloy/AZ91Magnesium alloy sheets and AZ91D Magnesium alloy/AZ31Magnesium alloy sheets were successfully joined by friction stir welding at different process parameters. Welding has been performed at varying rotational speeds (500, 720, 1025rpm), welding speeds in three levels (25, 50, and 75mm/min), and tilt angles of 1.5º, 2º, 2.5º. The effect of FSW process parameters on the mechanical properties and microstructure and also on the corrosion properties have been studied, and based on the result, the following conclusions are drawn:

7. 2 Microstructural, Mechanical and Corrosion Properties of Similar and Dissimilar Weldments

i. The microstructure of the AZ91D Mg alloy (gravity die-cast) consists of the primary α-phase and intermetallic β ($Mg_{17}Al_{12}$) phase. AZ31C Mg alloy consists of primary α-phase and intermetallic phase β ($Mg_{17}Al_{12}$) phase in as-received condition (die-cast). AZ91D Mg alloy possessed more intermetallic β than AZ31C alloy. The weldments of both similar and dissimilar contain Mg solid solution α and β $Mg_{17}Al_{12}$ intermetallic phase. X-ray diffraction analysis had also confirmed the same.

ii. Defect-free welds were produced for the welding conditions (similar and dissimilar) of 25, 50, and 75mm/minute with varying tool rotational speed of 500, 720, 1025 rpm, respectively.

iii. There were small flaws that were generated in the advancing side of the stir zone called the tunnel defects. The tunnel defects were found in similar weldments when the tool rotational speed is greater than 1025 rpm. At different welding speeds (25, 50, and 75 mm/min respectively) at a fixed tool rotation speed, 1525 rpm.

iv. The original grain structure morphology got disappeared in the stir zone. It was replaced with fine α grains, and β intermetallic phase was dissolved due to frictional heat input produced by the tool. Fine grains and small $Mg_{17}Al_{12}$ particles were observed in the stir zone.

v. In the stir zone, grain refinement occurred due to dynamic recrystallisation (DRX), and the hardness found was maximum due to the presence of fine recrystallised grains and $Mg_{17}Al_{12}$ particles along with the solid solution strengthening.

vi. The recrystallized grain structure in the stir zone is formed due to severe plastic deformation taking place with the development of frictional heat during welding.

vii. At high rotational speeds (1025 rpm), mechanical properties such as hardness, tensile, and impact strength improved considerably when compared to lower rotational speeds due to more dynamic crystallization occurred in the stir zone.

viii. The mode of fracture in the similar and dissimilar weldments was observed to be brittle in nature.

ix. Corrosion of these alloys in Cl^- media was primarily caused by matrix - β phase galvanic coupling, distribution of β phase, and local breakdown of surface passive films. Corrosion rates of dissimilar weldments were found to be greater than that of similar weldments due to enhance galvanic effects caused by the presence of two phases and intermetallic phases. Al content, grain size, and defect density can influence the corrosion by modifying the volume fraction, distribution of the β phase, and nature of surface passive films.

x. Both parent metal (AZ91D and AZ31) and the weldments registered negative values of E_{corr} , indicating their high tendency to corrosion in chloride media. This can be easily ascribed to the high reactivity of Mg alloys in Cl^- media.

7. 3 Influence of FSW Process Parameters On Similar Weldments (AZ91 to AZ91 Mg Alloy)

The influence of process parameters such as rotational speed, traverse speed, and tilt angle on mechanical properties of similar weldments (AZ91 to AZ91 Mg alloy) joints fabricated via FSW were examined, and the following conclusions are obtained. The percentage contributions of each process parameters of similar weldments are determined.

i. The optimum condition was obtained for ultimate tensile strength and percentage of elongation at a rotational speed of 1025 RPM, transverse speed 75 mm/min, and tilt angle of 1.5^0.

ii. The optimum condition obtained for impact strength is at a rotational speed of 500 rpm, transverse speed of 75 mm/min, and tilt angle of 2.5^0.

iii. Regression models are established to calculate the quality characteristics (ultimate tensile strength, percentage of elongation, and impact strength) obtained within the working range of process parameters. The responses are authenticated through ANOVA analysis.

iv. The contribution of rotational speed and traverse speed is more (55%, 27%) and less contribution of tilt angle (9%) for tensile strength.

v. The rotational speed and traverse speed has more percentage of contribution of 54%, 21%, and tilt angle makes a contribution of 18% on elongation for elongation.

vi. The rotational speed and tilt angle have more percentage of contribution of 80%, 11%, and welding speed make a contribution of 2% on impact strength.

7. 4 Influence of Process Parameters on Dissimilar Weldments (AZ31 to AZ91 Mg Alloy)

The influence of process parameters such as rotational speed, welding speed, and tilt angle on mechanical properties of dissimilar weldments (AZ31 to AZ91 Mg alloy) joints fabricated via FSW was examined, and the following conclusions are obtained. The percentage contributions of each process parameters of dissimilar weldments are determined.

i. The optimum condition obtained for ultimate tensile strength and percentage of elongation at a rotational speed of 1025 rpm, traverse speed of 25 mm/min, and tilt angle of 2.5º.
ii. The optimum conditions were obtained for impact strength at a rotational speed of 500 rpm, traverse speed of 75 mm/min., and tilt angle of 2.5º.
iii. The welding speed and tilt angle have more percentage of contribution of 48%, 31%, and rotational speed make a contribution of 13% on tensile strength.
iv. The welding speed and tilt angle have more percentage of contribution of 56%, 25%, and rotational speed make a contribution of 9% on elongation.
v. The tilt angle has more percentage of contribution of 11% and rotational speed, and traverse speed contributes 11%, 7% respectively, on impact strength, respectively.

7. 5 Future Scope

The present study gives a clear understanding of the effect of process parameters on microstructural, mechanical, and corrosion properties of similar and different welds, and during this study, a few areas emerged which need further investigation as described below:

i. Studies related to the effect of process parameters on other mechanical properties such as fatigue crack growth rate and fracture toughness were not performed in this investigation. Hence, the studies may be conducted in detail.
ii. The Stress Corrosion Cracking (SCC) behaviour of AZ91 and AZ31 Mg alloy weldments can be studied.
iii. Predicting and measuring the generated forces, torques, and power while performing the FSW process and correlating them with the microstructure and mechanical properties of similar and dissimilar welded blanks and development of a related mathematical model.
iv. Microstructural investigation of friction stir welded magnesium-based alloys may be carried out using 3D tomography to examine the actual size and depth of the defects or flaws obtained during welding.
v. Texture studies on similar and dissimilar FSWed Magnesium alloys may be done.

vi. The effect of post-weld heat treatment on microstructural and mechanical properties of AZ91 and AZ31 magnesium alloy joints can be made.

vii. Similar and dissimilar Magnesium-based alloys can be joined by adopting friction stir spot welding (FSSW)

viii. The influence of surface coatings (MAO) on weldments and parent metals can be explored.

ix. The effect on corrosion resistance of weldments and parameters using EIS and potentiodynamic polarization technique in other electrolytes like sulfuric and chloride environments (0.5 H_2SO_4 and 0.5 M NaCl) can be investigated.

x. The effect of the electrochemical behaviour of weldments and parent metals in simulated body fluids (SBF) like 0.9% NaCl and Hank's Solution may be studied.

xi. Mass loss measurements (Immersion experiments) to study the corrosion rate/ to study the corrosion rate can be taken up.

xii. Different optimization techniques can be engaged to predict the best processing parameter conditions for FSW of AZ91 Mg alloy and AZ31 Mg alloy.

xiii. Friction stir processed surface composites of AZ91 and AZ31 Mg alloys can be fabricated by nano-sized reinforced particles and a combination of reinforced particles having better wear and mechanical properties.

REFERENCES

1. Mero, John L., The mineral resources of the sea, 1, Elsevier, 1965.
2. Friedrich, Horst E. and Barry L. Mordike., Magnesium Technology, 212, Springer-Verlag Berlin Heidelberg, 2006.
3. Polmear, I. J., Magnesium alloys and applications, Materials Science and Technology, 10, No. 1, 1-16, 1994.
4. Blawert, C., Hort, N. and Kainer, K. U., Automotive applications of magnesium and its alloys, Transactions of The Indian Institute of Metals, 57, No. 4, pp. 397-408, 2004.
5. Fojo Álvarez, Daniel., A C0 interior penalty method for 4th order PDE's, Master's thesis, Universitat Politècnica de Catalunya, 2019.
6. Kainer, K. U., Magnesium alloys and technology, John Wiley & Sons, 2003.
7. Luo, A. and Pekguleryuz, M. O., Cast magnesium alloys for elevated temperature applications, Journal of Materials Science 29, No. 20, pp. 5259-5271, 1994.
8. Masaki, K., Ochi,Y., Kakiuchi, T., Keiichi, K., Hirasawa, T., Matsumura, T., Takigawa, Y. and Higashi, K., High cycle fatigue property of extruded non-combustible Mg alloy AMCa602, Materials Transactions, 49, No. 5, pp. 1148-1156, 2008.
9. Fontana, M. G., Corrosion engineering, Tata McGraw-Hill Education, 2005.
10. Davis, J. R., Aluminum and aluminum alloys, ASM international, 1993.
11. Xunhong, W. and Kuaishe, W., Microstructure and properties of friction stir butt-welded AZ31 magnesium alloy, Materials Science and Engineering: A, 431, No. 1-2, pp. 114-117, 2006.
12. Marya, M., Edwards, G., Marya, S. and Olson, D. L., Fundamentals in the fusion welding of magnesium and its alloys, Proceedings of the seventh JWS international symposium, Kobe, pp. 597-602, 2001.
13. Kumbhar, N. T. and Bhanumurthy, K., Friction stir welding of Al 6061 alloy, Asian Journal of Experimental Sciences, 22, No. 2, pp. 63-74, 2008.

14. Thomas, W. M., Improvements relating to friction welding, European Patent Specifications 0615 48 B1, 1995.
15. Ouyang, J., Yarrapareddy, E. and Kovacevic, R., Microstructural evolution in the friction stir welded 6061 aluminum alloy (T6-temper condition) to copper, Journal of Materials Processing Technology, 172, No. 1, pp. 110-122, 2006.
16. Rajendra Prasad, S., Suvarna Raju, L. and Kumar, A., An overview of friction stir processing, National conference on Advances In Mechanical Engineering, Huzurabad, India, 2012.
17. Dawes, C. J., Woodward, R. and Leroy, C., Friction Stir Welding - Training in Aluminium Application Technologies, TALAT Lecture 4410, TWI, 1999.
18. Esmaeili, A., Besharati Givi, M.K. and Zareie Rajani, H. R., A metallurgical and mechanical study on dissimilar Friction Stir welding of aluminum 1050 to brass (CuZn30), Materials Science and Engineering: A, 528, No. 22-23, pp. 7093-7102, 2011.
19. Bakesh, H., Benjamin, D. and Kirkpatrick , C. W., Metals Handbook, 2, ASM Metals Park, OH, pp.3-23, 1979.
20. Kallee, S.W., Nicholas, E. D. and W. M. Thomas., Friction stir welding- invention, innovations and applications, 8th International Conference on Joints in Aluminium, INALCO 2001, March 2001.
21. Friction stir welding - A general introduction, High tech welding, website: http://www.frictionstirwelding.com.
22. Thomas, W. M., Friction stir welding and related friction process characteristics, Proccdings of 7th interntation conference on Joints in aluminium–INALCO, 98, pp. 157-174, 1998.
23. Xunhong, W. and Kuaishe, W., Microstructure and properties of friction stir butt-welded AZ31 magnesium alloy, Materials Science and Engineering: A, 431, No. 1-2, pp. 114-117, 2006.
24. Johnson, R., Friction stir welding of magnesium alloys, Indian Foundry Journal, 48, No. 3 pp. 36-37, 2002.
25. Johnson, R., Friction stir welding of magnesium alloys, Materials Science Forum, vol. 419, Trans Tech Publications Ltd., Zurich-Uetikon, Switzerland, pp. 365-370, 2003.

26. Esparza, J. A., Davis,W.C., Trillo, E. A. and Lawrence E. M., Friction-stir welding of magnesium alloy AZ31B, Journal of Materials Science Letters, 21, No. 12, pp. 917-920, 2002.
27. Esparza, J. A., Davis, W. C. and Murr, L. E., Microstructure-property studies in friction-stir welded, Thixomolded magnesium alloy AM60, Journal of Materials Science, 38, No. 5, pp. 941-952, 2003.
28. Zhang, H., Lin, S. B., Wu, L, Feng, J. C. and Ma, Sh. L., Defects formation procedure and mathematic model for defect free friction stir welding of magnesium alloy, Materials & Design, 27, No. 9, pp. 805-809, 2006.
29. Nakata, K., Kim, Y.G. and Ushio, M., Friction Stir Welding of Mg-Al-Zn alloys (Physics, Processes, Instruments & Measurements), Transactions of Joining and Welding Research Institute, 31, No. 2, pp. 141-146, 2002.
30. Lee, W. B., Yeon,Y. M., Kim, S. K, and Jung, S. B., Microstructure and mechanical properties of friction stir welded AZ31 Mg alloy, Proc. Magnesium Technology, pp. 17-21, 2002.
31. Zettler, R., Blanco, A. C., dos Santos, J. F. and Marya, S., Magnesium Technology, pp. 409-23, 2005.
32. Threadgill, P. L., Friction stir welds in aluminium alloys-preliminary microstructural assessment, TWI Bulletin, pp. 30-33, 1997.
33. Norman, A. F., Brough, I. and Prangnell, P. B, High resolution EBSD analysis of the grain structure in an AA2024 friction stir weld, Materials Science Forum, 331, pp. 1713-1718, 2000.
34. Karlsen, M., Tangen, S., Hjelen, J., Friggard, O. and Grong, O., Advances in FSW, Proceedings of III International Symposium on friction stir welding, Kobe, Japan, Sept 2001.
35. Lee, W. B., Kim, J. W., Yeon, Y, M. and Jung, S.B., The joint characteristics of friction stir welded AZ91D magnesium alloy, Materials Transactions, 44, No. 5, pp. 917-923, 2003.
36. Nakata,K., Inoki, S., Nagano, Y., Hashimoto T., Johgan, S. and Ushio, M., Friction Stir Welding of AZ91D Thixomolded Sheet, Proceedings of the Third International Symposium on Friction Stir Welding, Kobe, Japan, September 2001.

37. Lee, W. B., Yeon, Y. M. and Jung, S. B, Joint properties of friction stir welded AZ31B–H24 magnesium alloy, Materials Science and Technology, 19, No. 6, pp. 785-790, 2003.
38. Park, Seung Hwan C., Sato, Y. S. and Kokawa, H., Microstructural evolution and its effect on Hall-Petch relationship in friction stir welding of thixomolded Mg alloy AZ91D, Journal of Materials Science, 38, No. 21, pp. 4379-4383, 2003.
39. Hassan, K. A., Prangnell, P. B., Norman, A. F, Price, D. A. and Williams, S. W., Effect of welding parameters on nugget zone microstructure and properties in high strength aluminium alloy friction stir welds, Science and Technology of Welding and Joining, 8, No. 4, pp. 257-268, 2003.
40. Davenport, A. J., Ambat, R., Jariayaboon, M., Morgan, P.C., Price, D.A., Wescott, A. and Williams, S. W., Corrosion of Friction Stir Welds in High Strength Aluminium alloys, International Conferene on Corrosion in the 21st Century, 2003.
41. Lee, W.B., Kim, J.W., Yeon, Y.M. and Jung, S.B., The joint characteristics of friction stir welded AZ91D magnesium alloy. Materials Transactions, 44, No.6, pp.917-923, 2003.
42. Yan, J., Xu, Z.,Li, Z., Lei L. and Yang, S., Microstructure characteristics and performance of dissimilar welds between magnesium alloy and aluminum formed by friction stirring, Scripta Materialia, 53, No. 5, pp. 585-589, 2005.
43. Yang, Bangcheng, Junhui Y., Michael, A. S. and Anthony P. R., Residual Stress and Microstructure Effects on Fatigue Crack Growth in AA2050 Friction Stir Welds, Materials Science and Engineering: A, 364, No. 1-2, pp. 55, 2004.
44. Gharacheh, M. A, Kokabi, A. H., Daneshi, G. H, Shalchi, B. and R. Sarrafi., The influence of the ratio of rotational speed/traverse speed (ω/v) on mechanical properties of AZ31 friction stir welds, International Journal of Machine Tools and Manufacture, 46, No. 15, pp. 1983-1987, 2006.
45. Sanbao, L., Zhang H., Wu Lin, F. J. and Hongbin, D., Friction stir welding of AZ31 magnesium alloy, China Welding, 12, No. 2, pp. 137-141, 2007.
46. Guerra, M., McClure, J.C., Murr, L.E., Nunes, A.C., Jata, K.V., Mahoney, M.W., Mishra, R.S., Semiatin, S.L. and Filed, D.P., Friction Stir Welding and Processing, TMS, Warrendale, PA, USA, pp. 25, 2001.

47. Colligan. and Kevin., Dynamic material deformation during friction stir welding of aluminum, Proc. of 1st International Friction Stir Welding Symp. Oaks, CA, USA, pp. 14-16. 1999.
48. Colligan, K., Material flow behavior during friction welding of aluminum, Weld Journal, 75, No. 7, pp. 229-237, 1999.
49. Li, Y., Murr, L. E. and McClure, J. C., Solid-state flow visualization in the friction-stir welding of 2024 Al to 6061 Al, Scripta Materialia, 9, No. 40, pp. 1041-1046, 1999.
50. Li, Y., Murr L.E. and McClure, J.C., Flow visualization and residual microstructures associated with the friction-stir welding of 2024 aluminum to 6061 aluminum, Materials Science and Engineering: A, 271, No. 1-2, pp. 213-223, 1999.
51. Seidel, T. U. and Anthony P. R., Visualization of the material flow in AA2195 friction-stir welds using a marker insert technique, Metallurgical and Materials Transactions A, 32, No. 11, pp. 2879-2884, 2001.
52. Guerra, M., Schmidt, C., McClure, J. C., Murr, L. E, and Nunes, A. C., Flow patterns during friction stir welding, Materials characterization, 49, No. 2, pp. 95-101, 2002.
53. Norman, A.F., Brough, I. and Prangnell, P.B., High resolution EBSD analysis of the grain structure in an AA2024 friction stir weld, Materials Science Forum , 331, pp. 1713-1718, 2000.
54. Mishra, R. S. and Murray W. Mahoney., Friction stir welding and processing, ASM International, Material Park, Ohio, The Materials Information Society, 2007.
55. Fratini, L. and Gianluca B., CDRX modelling in friction stir welding of aluminium alloys, International Journal of Machine Tools and Manufacture, 45, No. 10, pp. 1188-1194, 2005.
56. Bird, C. R., The inspection of friction stir welded aluminium plant, Proceedings of the 5th international symposium on friction stir welding, TWI, 2004.
57. Guerra, M., C. Schmidt, McClure, J. C., Murr, L. E. and Nunes, A. C., Flow patterns during friction stir welding, Materials Characterization, 49, No. 2, pp. 95-101, 2002.
58. Hashimoto,T., Jyogan, S., Nakada, K., Kim, Y.G., Ushio, M., FSW joints of high strength aluminum alloy, Proceedings of the First International Symposium on Friction Stir Welding, CA, USA, TWI Ltd, Paper No. S9-P3, 1999.

59. Sato, Y, S., Urata, M. and Kokawa, H., Parameters controlling microstructure and hardness during friction-stir welding of precipitation-hardenable aluminum alloy 6063, Metallurgical and Materials Transactions A, 33, No. 3, pp. 625-635, 2002.
60. A. J. and Lockyer, S. A., Flaws in friction stir welds, 4th international symposium on friction stir welding, 16, USA, 2003.
61. Christner, B. K. and Sylva., G. D., Friction stir weld development for aerospace applications, Proceedings of ICAWT, pp. 311-320, 1996.
62. Dickerson, T., Shi, Q. and Shercliff, H. R., Validation of friction stir welding process models, 4th international symposium on friction stir welding, 16, USA, 2003.
63. Okamura, H., K. Aota, M., Sakamoto, M. E. and Ikeuchi, K, Behaviour of oxides during friction stir welding of aluminium alloy and their effect on its mechanical properties, Welding International, 16, No. 4, pp. 266-275, 2002.
64. Palm, F., Henneboehle, U., Erofeev,V., Karpuchin, E., and Zaitzev, O., Improved verification of FSW-process modelling relating to the origin of material plasticity, 4th international symposium on friction stir welding, TWI Ltd., Metz, France, 2004.
65. Zhou, C., Yang, X. and Luan, G., Effect of oxide array on the fatigue property of friction stir welds, Scripta Materialia, 54, No. 8, pp. 1515-1520, 2006.
66. Lemos, G. V. B., Hanke, S., Dos Santos, J. F, L. Reguly, B, A. and Strohaecker, T. R., Progress in friction stir welding of Ni alloys, Science and Technology of Welding and Joining, 22, No. 8, pp. 643-657, 2017.
67. Johnson, R., Further assessment of the friction stir welding of magnesium alloys, The welding institute, 2003.
68. Sato, Y. S., Park, S. H. C., Michiuchi, M. and Hiroyuki Kokawa., Constitutional liquation during dissimilar friction stir welding of Al and Mg alloys, Scripta Materialia, 50, No. 9, pp. 1233-1236, 2004.
69. Shreir, L. L., Jarman, R. A. and Burstein, G. T., Corrosion: corrosion control, 2, Butterworth-Heinemann, 1994.
70. Song, G. and Andrej A., Understanding magnesium corrosion—a framework for improved alloy performance, Advanced Engineering Materials, 5, No. 12, pp. 837-858, 2003.

71. Yang, J., Kuwabara,M., Liu, Z., Asano, T. and Sano, M., ASM Special Handbook, Magnesium and Magnesium alloys, 8, 1999.
72. Li, G., Zhou, L., Luo, S., Dong, F. and Guo, N., Microstructure and mechanical properties of bobbin tool friction stir welded ZK60 magnesium alloy, Materials Science and Engineering: A, 776, pp.138953, 2020.
73. Weng, F., Liu, Y., Chew, Y., Lee, B. Y., Ng, F. L. and Bi, G., Double-side friction stir welding of thick magnesium alloy: microstructure and mechanical properties, Science and Technology of Welding and Joining, pp. 1-10, 2020.
74. Zheng, Y., Pan, X., Ma,Y., Liu,S., Zang, L. and Chen, Y., Microstructure and corrosion behavior of friction stir-welded 6061 Al/AZ31 Mg joints with a Zr interlayer, Materials, 12, No. 7, pp.1115, 2019.
75. Singh, K., Singh,G. and Singh, H., Investigation of microstructure and mechanical properties of friction stir welded AZ61 magnesium alloy joint, Journal of Magnesium and alloys, 6, No. 3, pp. 292-298, 2018.
76. Templeman, Y., Hamu, G. B. and Meshi, L., Friction stir welded AM50 and AZ31 Mg alloys: Microstructural evolution and improved corrosion resistance, Materials Characterization, 126, pp. 86-95, 2017.
77. Ji, S., Meng, X., Liu,Z., Huang, R. and Li, Z., Dissimilar friction stir welding of 6061 aluminum alloy and AZ31 magnesium alloy assisted with ultrasonic, Materials Letters, 201, pp. 173-176, 2017.
78. Çay, V. V., Nida, K. A, Ozan,S. and Veysel, V., Investigation of effects of different parameters on mechanical properties in friction stir welding of AZ 31B magnesium alloy, European Journal of Technique, 7, No. 1, pp. 49-59, 2017.
79. Mironov, S., Onuma, T., Sato, Y. S., Yoneyama, S. and Kokawa, H., Tensile behavior of friction-stir welded AZ31 magnesium alloy, Materials Science and Engineering: A, 679 pp. 272-281, 2017.
80. Luo, C., Li, X., Song, D., Zhou, N., Li, Y. and Qi, W., Microstructure evolution and mechanical properties of friction stir welded dissimilar joints of Mg–Zn–Gd and Mg–Al–Zn alloys, Materials Science and Engineering: A, 664, pp. 103-113, 2016.

81. Patel, N., Bhatt, K. D. and Mehta, V., Influence of tool pin profile and welding parameter on tensile strength of magnesium alloy AZ91 during FSW, Procedia Technology, 23, pp. 558-565, 2016.
82. Wang, W., Dean D., Mao, Z., Tong, Y. and Ran, Y., Influence of tool rotation rates on temperature profiles and mechanical properties of friction stir welded AZ31 magnesium alloy, The International Journal of Advanced Manufacturing Technology, 88, pp. 2191-2200, 2017.
83. Ugender, S., Kumar, A. and Somi Reddy, A., Influence of tool material and rotational speed on mechanical properties of friction stir welded AZ31B magnesium alloy, Journal of Magnesium and alloys, 3, No. 4, pp. 335-344, 2015.
84. Rouhi, S., Mostafapour,A. and Ashjari, A., Effects of welding environment on microstructure and mechanical properties of friction stir welded AZ91C magnesium alloy joints, Science and Technology of Welding and Joining, 21, No. 1, pp. 25-31, 2016.
85. Tabasi, M., Farahani,M., Besharati Givi, M.K., Farzami, M. and A. Moharami., Dissimilar friction stir welding of 7075 aluminum alloy to AZ31 magnesium alloy using SiC nanoparticles, The International Journal of Advanced Manufacturing Technology, 86, No. 1-4, pp. 705-715, 2016.
86. Ratna Sunil, B., Pradeep Kumar Reddy, G., Mounika, A. S. N., Navya Sree, P., Rama Pinneswari,P., Ambica, I., Ajay Babu, R. and P. Amarnadh., Joining of AZ31 and AZ91 Mg alloys by friction stir welding, Journal of Magnesium and alloys, 3, No. 4, 330-334, 2015.
87. Masoudian, A., Tahaei, A., Shakiba, A., Sharifianjazi, F. and Mohandesi, J. A. Microstructure and mechanical properties of friction stir weld of dissimilar AZ31-O magnesium alloy to 6061-T6 aluminum alloy, Transactions of Nonferrous Metals Society of China, 24, No. 5, pp. 1317-1322, 2014.
88. Sevvel, P. and Jaiganesh, V., Characterization of mechanical properties and microstructural analysis of friction stir welded AZ31B Mg alloy thorough optimized process parameters, Procedia Engineering, 97, pp. 741-751, 2014.

89. Ugender, S., Kumar, A. and Somi Reddy, A., Experimental investigation of tool geometry on mechanical properties of friction stir welding of AA 2014 aluminium alloy, Procedia Materials Science, 5, pp. 824-831, 2014.
90. Singh, I., Cheema G.S. and Kang, A. S, An experimental approach to study the effect of welding parameters on similar friction stir welded joints of AZ31B-O Mg alloy, Procedia Engineering, 97, pp. 837-846, 2014.
91. Sevvel, P. and Jaiganesh, V., Improving the mechanical properties of friction stir welded AZ31B magnesium alloy flat plates through axial force investigation, Applied Mechanics and Materials, 591, pp. 11-14, 2014.
92. Naik, B. S., Chen, D. L, Cao, X. and Wanjara, P., Microstructure and fatigue properties of a friction stir lap welded magnesium alloy, Metallurgical and Materials Transactions A, 44, No. 8, pp. 3732-3746, 2013.
93. Pourahmad, P. and Abbasi, M., Materials flow and phase transformation in friction stir welding of Al 6013/Mg, Transactions of Nonferrous Metals Society of China, 23, No. 5, pp.1253-126, 2013.
94. Venkateswaran, P. and Reynolds, A. P., Factors affecting the properties of Friction Stir Welds between aluminum and magnesium alloys, Materials Science and Engineering: A, 545, pp. 26-37, 2012.
95. Lin, Y.C., Ju-Jen Liu,en-Yuan L., Chun-Ming, L. and Hsien-Lung, T, Effects of process parameters on strength of Mg alloy AZ61 friction stir spot welds, Materials & Design, 35, pp. 350-357, 2012.
96. Cao, X. and Jahazi, M., Effect of tool rotational speed and probe length on lap joint quality of a friction stir welded magnesium alloy, Materials & Design, 32, No. 1, pp. 1-11, 2011.
97. Rose, A. R, Manisekar, K. and Balasubramanian, V., Effect of axial force on microstructure and tensile properties of friction stir welded AZ61A magnesium alloy, Transactions of Nonferrous Metals Society of China, 21, No. 5, pp. 974-984, 2011.
98. Cao, X. and Jahazi, M., Effect of welding speed on lap joint quality of friction stir welded AZ31 magnesium alloy, Trends in Welding Research: Proceedings of the 8th International Conference, June 1-6, 2008, USA, ASM international, 1, pp. 72. 2009.

99. Cao, X. and Jahazi, M., Effect of tool rotational speed and probe length on lap joint quality of a friction stir welded magnesium alloy, Materials & Design, 32, No. 1, pp.1-11, 2011.
100. Commin, L., Dumont, M., Masse, J. E. and Barrallier, L., Friction stir welding of AZ31 magnesium alloy rolled sheets: Influence of processing parameters, Acta Materialia, 57, No. 2, pp. 326-334, 2009.
101. Padmanaban, G. and Balasubramanian, V., Selection of FSW tool pin profile, shoulder diameter and material for joining AZ31B magnesium alloy–an experimental approach, Materials & Design, 30, No. 7, pp. 2647-2656, 2009.
102. Koneshlou, M., Kaveh Meshinchi, A. and Khomamizadeh, F., Effect of cryogenic treatment on microstructure, mechanical and wear behaviors of AISI H13 hot work tool steel, Cryogenics, 51, No. 1, pp. 55-61, 2011.
103. Taguchi, G., Chowdhury, S. and Wu, Y., Taguchi's quality engineering handbook, Wiley, 2005.
104. Colligan, K. J., The friction stir welding process: an overview, Friction stir welding, Woodhead Publishing, pp. 15-41, 2010.
105. Phadke, M.S., Quality engineering using robust design, Prentice Hall PTR, 1995.
106. Williamson, G. K. and Hall, W. H., X-ray line broadening from filed aluminium and wolfram, Acta Metallurgica, 1, No. 1, pp. 22-31, 1953.
107. Patel, N., Bhatt, K. D. and Mehta,V., Influence of tool pin profile and welding parameter on tensile strength of magnesium alloy AZ91 during FSW, Procedia Technology, 23, pp. 558-565, 2016.
108. Heidarzadeh, A. and Saeid, T., Correlation between process parameters, grain size and hardness of friction-stir-welded Cu–Zn alloys, Rare Metals, 37, No. 5 , pp. 388-398, 2018.
109. Chang, C.I., Lee, C.J. and Huang, J.C., Relationship between grain size and Zener–Holloman parameter during friction stir processing in AZ31 Mg alloys, Scripta Materialia, 51, pp.509-514, 2004.
110. Wang, Y. N., Chang, C. I., Lee, C. J., Lin, H. K. and Huang, J. C., Texture and weak grain size dependence in friction stir processed Mg–Al–Zn alloy, Scripta Materialia, 55, No. 7, pp. 637-640, 2006.

111. Mishra, R. S. and Ma, Z. Y., Friction stir welding and processing, Materials science and engineering: R: reports, 50, pp.1-78, 2005.
112. Kumar, K. S. V. K. and Kailas, S.V, The role of friction stir welding tool on material flow and weld formation, Materials Science and Engineering: A, 485, pp. 367-374, 2008.
113. Thomas, W. M., Nicholas, E. D., Needham, J. C., Murch, M. G., Temple-Smith, P. and Dawes, C. J., The Welding Institute, Improvements relating to friction welding, European Patent Specification 615, B1, 1992.
114. Lombard, H., Optimized fatigue and fracture performance of friction stir welded aluminium plate: A study of the inter-relationship between process parameters, TMAZ, microstructure, defect population and performance, Thesis, University of Plymouth, 2007.
115. Mishra, R. S, De, P.S. and Kumar, N., Friction stir processing, Friction stir welding and processing, Springer, Cham, pp. 259-296, 2014.
116. Liu, D., Xin, R., Zheng, X., Zhou, Z. and Liu, Q., Microstructure and mechanical properties of friction stir welded dissimilar Mg alloys of ZK60–AZ31, Materials Science and Engineering: A, 561, pp.419-426, 2013.
117. Asadi, P., Givi, M.K.B. and Akbari, M., Simulation of dynamic recrystallization process during friction stir welding of AZ91 magnesium alloy, The International Journal of Advanced Manufacturing Technology, 83, pp.301-311, 2016.
118. Mirzaei, M., Asadi, P. and Fazli, A., Effect of Tool Pin Profile on Material Flow in Double Shoulder Friction Stir Welding of AZ91 Magnesium Alloy, International Journal of Mechanical Sciences, pp.105775, 2020.
119. Woo W, Choo H, Prime, M.B., Feng, Z. and Clausen B., Microstructure, texture and residual stress in a friction-stir-processed AZ31B magnesium alloy. Acta Materialia, 56, pp.1701–1711, 2008.
120. Fu, R.D., Ji, H.S., Li, Y, J. and Liu, L., Effect of weld conditions on microstructures and mechanical properties of friction stir welded joints on AZ31B magnesium alloys. Science and Technology of Welding and Joining, 17, pp. 174–179, 2012.

121. Xin, R., Liu, D., Xu, Z., Li ,B. and Liu, Q., Changes in texture and microstructure of friction stir welded Mg alloy during post-rolling and their effects on mechanical properties, Material Scince and Engineering A, 582, pp.178–187, 2013.
122. Liu, G., Xin, R., Li, J., Liu, D. and Liu, Q., Fracture localization in retreating side of friction stir welded magnesium alloy, Science and Technology of welding and Joining, 20, pp. 378–384, 2015.
123. Liu, Z., Liu, D., Xu, J., Zheng, X., Liu, Q. and Xin, R., Microstructural investigation and mechanical properties of dissimilar friction stir welded magnesium alloys. Scinece and Technology of welding and Joining, 20, pp. 264–270, 2015.
124. Mishra, R. S. and Ma, Z. Y., Friction stir welding and processing, Materials Science and Engineering: R: reports, 50, pp. 1-78, 2005.
125. Raghupathy, Y., Kamboj, A., Rekha, M. Y., Rao, N. and Srivastava, C., Copper-graphene oxide composite coatings for corrosion protection of mild steel in 3.5% NaCl, Thin Solid Films, 636, pp. 107-115, 2017.
126. Liu, C., Chen, D.L., Bhole, S., Cao, X. and Jahazi, M., Polishing-assisted galvanic corrosion in the dissimilar friction stir welded joint of AZ31 magnesium alloy to 2024 aluminum alloy, Materials Characterization , 60, pp. 370-376, 2009.
127. Zeng, R.C., Zhang, J., Huang, W.J., Dietzel, W., Kainer, K. U., Blawert, C. and Wei, K. E., Review of studies on corrosion of magnesium alloys, Transactions of Nonferrous Metals Society of China, 16, pp. 763-771, 2006.
128. Ramalingam, V.V., Ramasamy, P., Mohan Das, K. and Govindaraju, M., Research and development in magnesium alloys for industrial and biomedical applications: a review, Metals and Materials International, pp. 1-22, 2019.
129. Hu, H., Nie, X. and Ma,Y., Corrosion and surface treatment of magnesium alloys, Magnesium Alloys-Properties in Solid and Liquid States, pp. 67-108, 2014.
130. Song, Y., Han, E.H., Shan, D., Yim,C. D. and You, B. S. The role of second phases in the corrosion behavior of Mg–5Zn alloy, Corrosion Science, 60, pp. 238-245, 2012.
131. Hara, N., Kobayashi, Y., Kagaya, D. and Akao, N., Formation and breakdown of surface films on magnesium and its alloys in aqueous solutions, Corrosion Science, 49, pp. 166-175, 2007.

132. Wang, L., Zhang, B. P. and Shinohara, T., Corrosion behavior of AZ91 magnesium alloy in dilute NaCl solutions, Materials & Design, 31, pp. 857-863, 2010.
133. Vignesh, R.V., Padmanaban, R. and Govindaraju, M., Investigations on the surface topography, corrosion behavior, and biocompatibility of friction stir processed magnesium alloy AZ91D, Surface Topography: Metrology and Properties, 7, pp.025020, 2019.
134. Ghosh, A., Textbook of Materials and Metallurgical thermodynamic, PHI Learning Pvt. Ltd., 2002.

LIST OF PUBLICATIONS BASED ON THIS THESIS

Publications in Journals:

1. Kadigithala Nagabhushan Kumar, and C. Vanitha. "Microstructural developments and mechanical properties of friction stir welding of AZ91D magnesium alloy plates." Metallurgical and Materials Engineering, 23, No. 2, pp.119-130, 2017.
2. Kadigithala Nagabhushan Kumar, and C. Vanitha. "Investigation on the Microstructure and Mechanical Properties of AZ91D Magnesium Alloy Plates Joined by Friction Stir Welding." Lecture notes in Mechanical Engineering, pp. 1021-1030, 2020.
3. Kadigithala Nagabhushan Kumar, and C. Vanitha. "Effects of welding speeds on the microstructural and mechanical properties of AZ91D Mg alloy by friction stir welding." International Journal of Structural Integrity, 11, No. 6, pp. 769-782, 2020.

Papers Presented in Conferences:

1. K.N.B.Kumar, C.Vanitha, Vivek Pancholi,“Microstructure and mechanical properties of AZ91D Magnesium Alloy sheets jointed by friction stir welding” Presented and Published in the NMD ATM2014,November 12^{th} to 15^{th},College of Engineering, Pune, 2014.
2. K.N.B.Kumar, C.Vanitha,“Effect of welding parameters of Friction stir butt welding of AZ91D Magnesium Alloy on Microrostructural developments and mechanical properties” Presented and Published in the NCAMPC 2016,January 4^{th} to 6^{th} , N.I.T, Warangal, 2016.

Metallurgical and Materials Engineering
Association of Metallurgical Engineers of Serbia AMES

Scientific paper
UDC: 669.721:621.791

MICROSTRUCTURAL DEVELOPMENTS AND MECHANICAL PROPERTIES OF FRICTION STIR WELDING OF AZ91D MAGNESIUM ALLOY PLATES

K. N. B.Kumar[*], *C. Vanitha*

Department of Metallurgical and Materials Engineering,
National institute of Technology, Warangal, India.

Received 01.09.2016
Accepted 21.06.2017

Abstract

Friction stir welding (FSW) is an efficient technique which can be used particularly for magnesium and aluminum alloys that are difficult to fusion weld. In this work AZ91D Mg alloy plates 3mm thick were friction stir welded at different process variables such as rotational speed and welding speed. The range of rotational speeds varied from 1025 to 1525 rpm, and the welding speed varied from 25 to 75 mm/min. Good quality welds were obtained under 1025 rpm of rotational speed with the welding speeds range from 25 to 75 mm/min. The microstructure of the AZ91D alloy consists of primary α-phase, eutectic α-phase and eutectic β ($Mg_{17}Al_{12}$) phase in the received condition (gravity die cast). The original dendrite grain structure completely disappeared and was transformed to fine equiaxed grains in stir zone (SZ). It was observed that there was a slight increase in hardness in SZ, because of fine recrystallized grain structure. The transverse tensile test results of weld specimens indicated constant strength irrespective of traveling speed. Fractrographic analysis of the friction stir welded specimens showed the brittle failure.

Key words: *Magnesium based alloys; AZ91D Mg Alloy; Friction stir welding; Dynamic recrystallization.*

Introduction

Magnesium based alloys are emerging as an essential engineering materials, especially in the automobile and aerospace sectors, because of their high damping capacity and recyclability, high strength-to-weight ratio, low density [1]. These alloys, having a density of about two-thirds of Al alloys, are the promising engineering materials to boost fuel economy especially for the automotive industry [2, 3]. At present magnesium based alloys are mainly used to develop cast based products. Their utility in

[*] Corresponding author: K. N. B Kumar: *knbkumar@nitw.ac.in*

Investigation on the Microstructure and Mechanical Properties of AZ91D Magnesium Alloy Plates Joined by Friction Stir Welding

Nagabhushan Kumar Kadigithala and C. Vanitha

Abstract Friction stir welding (FSW) is an effective technique to join magnesium-based alloys which are difficult to fusion weld. In this work, similar AZ91D Mg alloy sheet of 3 mm thick butt joint was produced via friction stir welding at welding parameters such as rotational speed, welding speed, and tilt angle. The rotational speed was kept constant of 720 rpm, the welding speed varied from 25 to 75 mm/min, and tilt angle from 1.5° to 2.5°. Defect-free weld was obtained under 75 mm/min welding speed and tilt angle of 1.5°. The microstructure of the parent alloy consists of phases, namely primary α and eutectic β ($Mg_{17}Al_{12}$) in the as-received condition (gravity die-cast) which was confirmed by X-ray diffraction (XRD) analysis. Microscopic studies, tensile tests, hardness test, and fractographic studies were conducted. Metallographic studies revealed different features in each zone depending on their thermomechanical condition. A significant increase in hardness was observed in the stir zone of weldment compared to parent alloy due to the recrystallized grain structure. The dendrite grain structure present in weldment was completely disappeared and was transformed to fine grains in stir zone (SZ). The transverse tensile test result of the weld specimen indicated that weldment was about 44.9% higher than the parent alloy. Fractographic analysis of the friction stir welded specimen indicated that the weld specimen failed through the brittle failure.

Keywords AZ91 D mg alloy · Friction stir welding · Microstructure · Dynamic recrystallization

N. K. Kadigithala (✉) · C. Vanitha
Department of Metallurgical and Materials Engineering, National Institute of Technology, Warangal, Warangal 506004, Telangana State, India
e-mail: knbkumar.ind@gmail.com

H. K. Voruganti et al. (eds.), *Advances in Applied Mechanical Engineering*,
Lecture Notes in Mechanical Engineering,
https://doi.org/10.1007/978-981-15-1201-8_109

Effects of welding speeds on the microstructural and mechanical properties of AZ91D Mg alloy by friction stir welding

Nagabhushan Kumar Kadigithala and Vanitha C
Department of Metallurgical and Materials Engineering, National Institute of Technology, Warangal, India

Received 5 December 2019
Revised 6 December 2019
Accepted 6 December 2019

Abstract

Purpose – The main purpose of the present work is to evaluate, the microstructural and mechanical properties of friction stir welded plates of AZ91D magnesium alloy with 3 mm thickness, and to determine the optimum range of welding conditions.

Design/methodology/approach – Microstructure and fractographic studies were carried out using scanning electron microscopy (SEM). Vickers micro hardness test was performed to evaluate the hardness profile in the region of the weld area. The phases in the material were confirmed by X-Ray diffraction (XRD) analysis. Transverse tensile tests were conducted using universal testing machine (UTM) to examine the joint strength of the weldments at different parameters.

Findings – Metallographic studies revealed that each zone shown different lineaments depending on the mechanical and thermal conditions. Significant improvement in the hardness was observed between the base material and weldments. Transverse tensile test results of weldments had shown almost similar strength that of base material regardless of welding speed. Fractographic examination indicated that the welded specimens failed due to brittle mode fracture. Through these studies it was confirmed that friction stir welding (FSW) can be used for the welding of AZ91D magnesium alloy.

Research limitations/implications – In the present study, the welding speed varied from 25 mm/min to 75 mm/min, tilt angle varied from 1.5 to 2.5 and constant rotational speed of 500 rpm.

Practical implications – Magnesium and aluminum based alloys which are having high strength and low density, used in automotive and aerospace applications can be successfully joined using FSW technique. The fusion welding defects can be eliminated by adopting this technique.

Originality/value – Limited work had been carried out on the FSW of magnesium based alloys over aluminum based alloys. Furthermore, this paper analyses the influence of welding parameters over the microstructural and mechanical properties.

Keywords AZ91D magnesium alloy, Microstructure, Friction stir welding, Micro hardness, Tensile strength

Paper type Research paper

1. Introduction

Today's interest in magnesium based alloys for automotive and aerospace applications is based on the combination of low density and high strength properties (Blawert *et al.*, 2004). Due to this reason magnesium alloys are attractive as structural materials where weight reductions are of great concern. In automotive and aerospace applications reduction in weights will enhance the performance of the vehicle by reducing the energy of acceleration and rolling resistance, thus reducing the consumption of fuel and reduction of the CO_2 (greenhouse gas) can be achieved.

However selection of materials is influenced by economic issues as much as by components and material properties and characteristics. From the economical point of view increasing percentage of magnesium reduces the cost per ton, which makes it more

The authors would like to thank MHRD, Govt. of India and Director, N.I.T, Warangal for funding support to this research work.

International Journal of Structural Integrity

1757-9864
DOI 10.1108/IJSI-12-2019-0131